Accessibility studies of ionic and non-ionic fluorophores embedded in sol-gel materials and new functionalised polyhedral silsesquioxanes

Zugänglichkeitsstudien über in Sol-Gel-Materialien eingebundene ionische und nichtionische Fluorophore sowie neue funktionalisierte polyhedrale Silsesquioxane

DISSERTATION

der Fakultät für Chemie und Pharmazie
der Eberhard-Karls-Universität Tübingen

zur Erlangung des Grades eines Doktors
der Naturwissenschaften

2008

vorgelegt von
David Ruiz Abad

Tag der mündlichen Prüfung: 3. November 2008

Dekan: Professor Dr. Lars Wesemann

1. Berichterstatter: Professor Dr. Hermann A. Mayer

2. Berichterstatter: Privatdozent Dr. Hans-Joachim Egelhaaf

To my parents

Die vorliegende Arbeit wurde am Institut für Anorganische Chemie der Eberhard-Karls-Universität Tübingen unter Anleitung von Herrn Prof. Dr. Hermann A. Mayer angefertigt.

Sincere thanks are due to my supervisor Prof. Dr. Hermann A. Mayer for providing invaluable guidance and discussions about sol-gel process and polyhedral silsesquioxanes.
I would like to acknowledge as well PD. Dr. H-J. Egelhaaf for his helpful discussions and supervision for the luminescence spectroscopy.

I also wish to thanks the Deutsche Forschung Gemeinachaft (DFG), and the Graduiertenkolleg “Chemie in Interphasen” for the financial support.

My special thanks to:

Prof. Dr. E. Lindner for the opportunity provided to develope this research within the framework of the Chemistry in Interphases.

Special thanks deserve Prof. Dr. Christoph Schüth and Annegret Walz for their support for BET measurement and provided assistance in questionings.

I would like to thank Dr. K. Eichele for his solid state NMR spectroscopy measurements, discussions and help interpreting the results.

Michael Marzini, Flor Toledo Rodríguez, and Nicolas Plumeré for their commitment in collaborations and interdisciplinary work to my research.

My special thanks to my working colleagues in the A.K. Mayer for the nice working environment and their helpful advice.

1. CONTENTS

1. **CONTENTS** I

2. **LISTS OF ABBREVIATIONS, UNITS and PREFIXES** 1

2.1 LIST OF ABBREVIATIONS 1
2.2 LIST OF UNITS 3
2.3 LIST OF PREFIXES 4

3. **INTRODUCTION** 5

4. **GENERAL SECTION** 9

4.1 SOL-GEL PROCESS 9
4.2 NANOPARTICLES AND STÖBER PROCESS 13
4.3 POLYHEDRAL OLIGOMERIC SILSESQUIOXANES (POSS) 15
4.4 LUMINESCENCE 17

5. **RESULTS AND DISCUSSION** 19

5.1 SYNTHESIS, CHARACTERISATION AND LUMINESCENCE SPECTROSCOPIC ACCESSIBILITY STUDIES OF FLUOROPHORE CONTAINING SOL-GEL MATRICES AND NANOPARTICLES 19
5.1.1 Introduction 19
5.1.2 Synthesis of fluorophores 1 and 2 21
5.1.3 Synthesis and characterization of the sol-gel materials A-D 22
5.1.4 Synthesis of the nanoparticles 26
5.1.5 Luminescence spectroscopic investigations 28
5.1.5.1 Luminescence and luminescence excitation spectra of **1** in different materials 28

5.1.5.2 Luminescence and luminescence excitation spectra of **2** in different materials 29
5.1.5.3 Kinetic analysis of luminescence decay curves 32
5.1.5.4 Luminescence decay curves of **1** in different matrices without quencher 35
5.1.5.5 Luminescence decay curves of **1** in different matrices in the presence of oxygen 35
5.1.5.6 Luminescence decay curves of **1** in different matrices in the presence of anthracene 38
5.1.5.7 Luminescence decay curves of **2** in different matrices without quencher 40
5.1.5.8 Luminescence decay curves of **2** in different matrices in the presence of oxygen 41
5.1.5.9 Luminescence decay curves of **2** in different matrices in the presence of N,N-diethylaniline 43
5.1.6 Conclusions 45

5.2 SYNTHESIS AND CHARACTERISATION OF FUNCTIONALISED POLYHEDRAL SILSESQUIOXANES (FPOSS) 48
5.2.1 Introduction 48
5.2.2 Synthesis of octa(3-(ethylmercapto)-propionic acid) silsesquioxane (6) 50
5.2.3 Synthesis of octa(3-(ethylmercapto)-propionacyl chloro) silsesquioxane (7) 51
5.2.4 Synthesis of octa(ethylbromo) silsesquioxane (8) 52
5.2.5 Synthesis of octa(ethyliodo) silsesquioxane (9) 52
5.2.6 Synthesis of ferrocenyl functionalised silsesquioxane (10) 53
5.2.7 Synthesis of SCS-pincer complex functionalised silsesquioxanes (12, 14) 54
5.2.8 Characterization of the silsesquioxanes 6 – 10, 12, 14 56
5.2.9 Conclusions 64

6. **EXPERIMENTAL SECTION** 65

6.1 GENERAL ASPECTS AND STARTING MATERIALS 65
6.2 STEADY STATE MEASUREMENTS 66
6.3 DECAY TIME MEASUREMENTS 66
6.4 BRUNAUER-EMMETT-TELLER (BET) MEASUREMENTS 67
6.5 NUCLEAR MAGNETIC RESONANCE (NMR) SPECTROSCOPY 67
6.6 SYNTHESES 68
6.6.1 Synthesis of triethoxysilylfunctionalised (1-pyrenyl)-methanol (2) 68
6.6.2 Preparation of sol-gel materials 68
6.6.3 Preparation of nanoparticles 69
6.6.4 Synthesis of octa(3-(ethylmercapto)-propionic acid) silsesquioxane (6) 69
6.6.5 Synthesis of octa(3-(ethylmercapto)-propionacyl chloro) silsesquioxane (7) 70
6.6.6 Synthesis of octa(ethylbromo) silsesquioxane (8) 71
6.6.7 Synthesis of octa(ethyliodo) silsesquioxane (9) 71
6.6.8 Synthesis of ferrocenyl functionalised silsesquioxane (10) 72
6.6.9 Synthesis of SCS-pincer complex functionalised silsesquioxanes (12, 14) 72

7. **REFERENCES** 74
8. **SUMMARY** 82

2. LISTS OF ABBREVIATIONS, UNITS and PREFIXES

2.1 LIST OF ABBREVIATIONS

AIBN	2,2'-Azo-bis-isobutyronitrile
ANT	anthracene
BET	Brunauer-Emmet-Teller
BJH	Barett-Joyner-Halenda
bpy	bipyridine
c	concentration
C_s	symmetry group
D	diffusion
DCM	dichloromethane
DEA	N,N-diethylaniline
dec.	decomposition
DIPEA	N,N-Diisopropylethylamine
DMF	dimethylformamide
DMSO	dimethylsulfoxide
DRIFT	diffuse reflectance infrared fourier transform spectroscopy
D_{trans}	diffusion translational
D_{2h}	symmetry group
EA	elemental analysis
ET	energy transfer
F_0	luminescence intensity in the absence of a quencher
F	luminescence intensity in the presence of a quencher
FAB	fast-atom bombardment (mass spectroscopy)
FPOSS	functionalised polyhedral oligomeric silsesquioxanes
HPDEC	high power decoupling
HR ESI	high-resolution electron-spray ionisation (mass spectroscopy)
IR	infrared
k	Stern-Volmer quenching constant
k_{abs}	absorption rate constant
k_d	diffusion rate constant
k_f	fluorescence rate constant

k_{isc}	intersystem crossing rate constant
k_{nr}	non-radiative rate constant
k_q	quenching process rate constant
k_r	photoreactive processes rate constant
k_{SV}	Stern-Volmer rate constant
k_1	spontaneous deactivation rate constant
k_2	quenching rate constant
L	luminescence
LE	luminescence excitation
MAS	magic angle spinning
MeCN	acetonitrile
MeOH	methanol
MLCT	metal to ligand charge transfer
m.p.	melting point
MS	mass spectroscopy
N_A	Avogadro number
NMR	nuclear magnetic resonance
P	product
POSS	polyhedral oligomeric silsesquioxanes
Q	Q type silicon atom (four oxygen neighbour)
Q	quantum yield
RT	room temperature
[S]	quencher concentration
SEM	scanning electron microscope
S_o	ground state
S_1	singlet excited state
t	time
T	T type silicon atom (three oxygen neighbour)
TEOS	tetraethoxysilane
t_{gel}	gelation time
THF	tetrahydrofuran
TMEDA	N,N,N',N'-tetramethyl-ethylendiamide
TMOS	tetramethoxysilane
TMS	tetramethylsilane

T_1	triplet excited state
T_1	spin-lattice relaxation time
T_2	spin-spin relaxation time
UV	ultraviolet
α	accessibility
δ	chemical shift
υ	frequency
τ_n	intrinsic or natural fluorescence lifetime
τ_0	unquenched lifetime
τ	fluorescence lifetime
$\tilde{\upsilon}$	wave number
λ_{em}	emission wave length
λ_{ex}	excitation wave length

2.2 LIST OF UNITS

^oC	centigrade
g	gram
h	hour
Hz	Hertz
K	Kelvin
l	litre
m	meter
M	molar
ppm	parts per million
rpm	revolutions per minute
s	second

2.3 LIST OF PREFIXES

M	mega (10^{6})
k	kilo (10^{3})
c	centi (10^{-2})
m	milli (10^{-3})
μ	micro (10^{-6})
n	nano (10^{-9})

3. INTRODUCTION

There is increased recognition by the world's scientific, industrial, and political communities that the concentrations of greenhouse gases in the earth's atmosphere are accumulating. To provoke a reduction of these gases the dependence of the economy on the fossil energy sources must be decreased and the efficiency of our energy production and consumption processes must be significantly improved. Moreover this must be reached without compromising the economy growth and the quality of life.[1]

In this aspect, the chemical industry has played a contradictory role. Although it represents one of the most successful sectors of manufacture, it produces huge amounts of pollutants and requires an elevated quantity of energy. In order to save energy and thus decrease the amount of greenhouse gases and other pollutants it is mandatory to develope new synthetic pathways. In these pathways more favourable conditions should be employed, which include the use of less contaminant solvents and highly efficient catalysts to reduce energy consumption and pollutant side products. Thus the development of new catalysts is nowadays one of the most important goals.[2]

The catalysts can be divided into homogeneous and heterogeneous.[3-5] The homogeneous catalysts have the advantage of leading to high and reproducible selectivity and the drawback to need enormous time and energy consuming processes to separate the catalyst from the reaction mixture.[2;6] The heterogeneous catalysts are easily removable from the reaction mixture by means of filtration but they have the disadvantage of a poor chemoselectivity which again requires energy consuming separation processes.[7;8]

For the combination of the advantages of homogeneous and heterogeneous catalysis, several concepts have been established. With the aim to develop high-performance heterogenised catalysts, the idea of chemistry in interphases has recently been introduced.[9] Major drawbacks of conventional supported catalysts can be overcome with this principle. "An interphase is defined as a region within a material in which a stationary and mobile component penetrate each other on a molecular level. The stationary phase is composed of an inert matrix, a flexible spacer, and an active center, whereas the mobile phase consists of a solvent or a gaseous, liquid, or dissolved reactant. In an ideal interphase, the reactive center is

uniform, well-defined, and highly mobile. Therefore, an interphase is able to simulate homogeneous reaction conditions, and at the same time it has the advantage of a heterogeneous catalyst".[6;10]

Basically, one way to heterogenise catalysts, is through the anchor of a homogeneous catalyst to a solid matrix[2;6] and the sol-gel process is an appropriate technique.[11] These hybrid catalysts have several disadvantages, like the chemical stability and the accessibility of the actives centers.[8] In addition, the knowledge about the nature of reactive centers is mostly empirical.[6] The first drawback can be corrected by increasing the crosslinking of the sol-gel material, but doing that, the accessibility of the active centers decreases.[3;11;12] To solve this problem, hybrid polymers were used instead of pure polysiloxanes.[11;13-15] The organic part of the hybrid polymers provides swelling abilities and the inorganic part crosslinking.[3;11;16;17] This leads to thermally inert inorganic-organic hybrid polymers with excellent swelling abilities and moderate accessibility.[2;12;18] When the polymer is swollen in solvents, an interphase is formed, in which the liquid and solid phase interpenetrate on a molecular level without forming a homogeneous phase.[2;6-8;11;12] In spite of that the catalytic activity of such materials is still strongly reduced compared to that in homogenous solutions. This might be due to a reduced diffusion of the educts and products in these hybrid materials.

The diffusion in micro- and mesopores in porous polysiloxanes restricts the mass transfer and reaction rates of the materials. The accessibility and reactivity in these porous domains should be a function of the pore sizes as well as pore polarities. Educts and products of a reaction may show different polarities resulting in a distribution of diffusivities with an impact on overall reaction rates.

The catalysts can exist in one or more environment within the matrix: in the liquid–filled pore, the interfacial region between the liquid and the pore wall, linked on the pore wall or within a channel between pores.[16;19] In order to improve the hybrid catalysts the knowledge about the location of the active side and its accessibility to reactants is of importance. It has been demonstrated that luminescence methods can help to answer some of these questions.[10]

The photochemistry of ruthenium polypyridyl complexes has been numerously times studied in recent years due to their strong luminescence, their stability and the long excited state lifetimes, which can be quenched by energy transfer, complex formation and electron transfer processes.[11;20-33] The luminescent excited state is

assigned to the MLCT (metal to ligand charge transfer) state whose properties are strongly dependent on the polarity and the viscosity of the environment.[34;35] These properties make the ruthenium polypyridyl complexes ideal for optical sensors and for solar energy conversion.[22;24;34;36-38] Numerous reports exist on encapsulation of ruthenium(II) polypyridyl complexes in SiO_2 gels and glasses.[24;34;39;40] It has been demonstrated that the dopant retains its properties in the matrices as in the solution states.[24]

Pyrene derived molecules are useful due to their vibronic structure fluorescence that is sensitive to changes of the polarity of its molecular environment.[41;41-43] In pyrene doped amorphous silica glasses prepared by the sol-gel method, pyrene molecules can be dispersed in these glasses[32;44-46] even at higher concentration than in solution without the formation of excimers.[47] Kaufman and Avnir have used this method to investigate the development from sol to gel and xerogel transition to take advantage of the sensibility of the fluorescence with the environment.[43;48]

In this study, the catalysts were replaced by fluorophores, a non ionic triethoxysilylfunctionalised pyrenemethanol and an ionic triethoxysilylfunctionalised ruthenium complex. The choice of fluorophores to characterise sol-gel materials is an important factor to determine their position, accessibility and microenvironment through luminescence.[14;49-53] These fluorophores were attached on the surface of nanoparticles and in sol-gel materials. Studying the accessibility on the nanoparticles, - where the dopants are on the surface -, and the fluorophores in solution, -where no sterical influence takes place -, it is possible to obtain information about where the fluorophores are distributed in the sol-gel materials.[41;54;55]

Years after the synthesis of the first polyhedral oligomeric silsesquioxanes (POSS),[56;57] they have attracted again the attention of the scientific community due to their ability to be functionalised and subsequently combined with catalysts and other molecules.[56;58-66] Additionally, these materials are used as model systems to gain more insight at a molecular level into the interaction of catalyst precursors with the surface of silica matrices and the structure and reactivity of the heterogeneous catalyst.[67] Their use as model systems can be explained due to their easier characterisation than further complicated matrices like nanoparticles or sol-gel materials. Thanks to this property, the synthesis of POSS can be followed by

techniques like NMR spectroscopy and the results can be applied to other silica matrices.

Another project of this work was the synthesis of new functionalised polyhedral oligomeric silsesquioxanes and the improvement of the methods of already synthesised silsesquioxanes. Additionally, diverse molecules like ferrocene and Pd-SCS pincer complexes were covalently attached to POSS.

4. GENERAL SECTION

4.1 SOL-GEL PROCESS

The sol-gel process can be described as the creation of an oxide network by progressive polycondensation reactions of molecular precursors in liquid medium. Compared to the transition metals, silicon is less electropositive and therefore it is not very susceptible for a nucleophilic attack. This makes silicon compounds quite stable and easy to handle. Sol-gel processing proceeds in several steps:[68-70]

1. Hydrolysis and condensation of the molecular precursors and formation of sols
2. Gelation (sol-gel transition)
3. Aging
4. Drying

1. Hydrolysis and condensation: The basic principle behind sol-gel processing is the transformation of Si-OR and Si-OH containing species to siloxane compounds (Scheme 1). The sol-gel process can proceed under acidic and basic conditions.[69] Parameters which influence the hydrolysis and condensation are: (1) kind of precursor, (2) the alkoxy group to water ratio, (3) kind of catalyst, (4) kind of solvent, (5) temperature, (6) pH, (7) relative and absolute concentration of the components in the precursor mixture.[70-72]

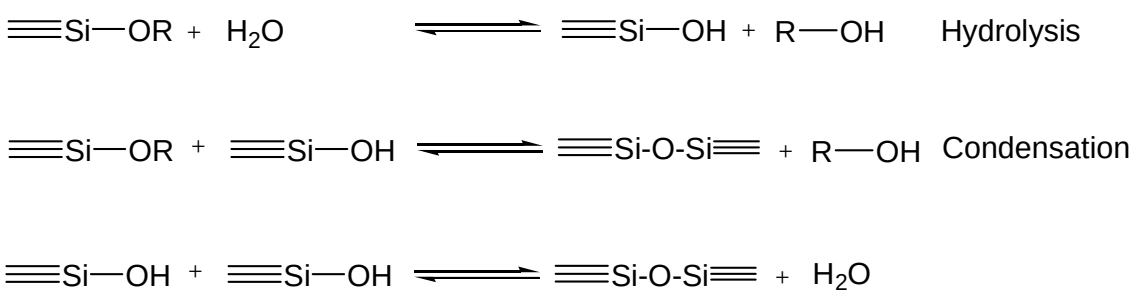

Scheme 1. Hydrolysis and condensation

Moreover due to several factors that have an influence on the hydrolysis and condensation, the control of the sol-gel process is difficult, as at the same time a mixture of different intermediates are produced (Figure 1).

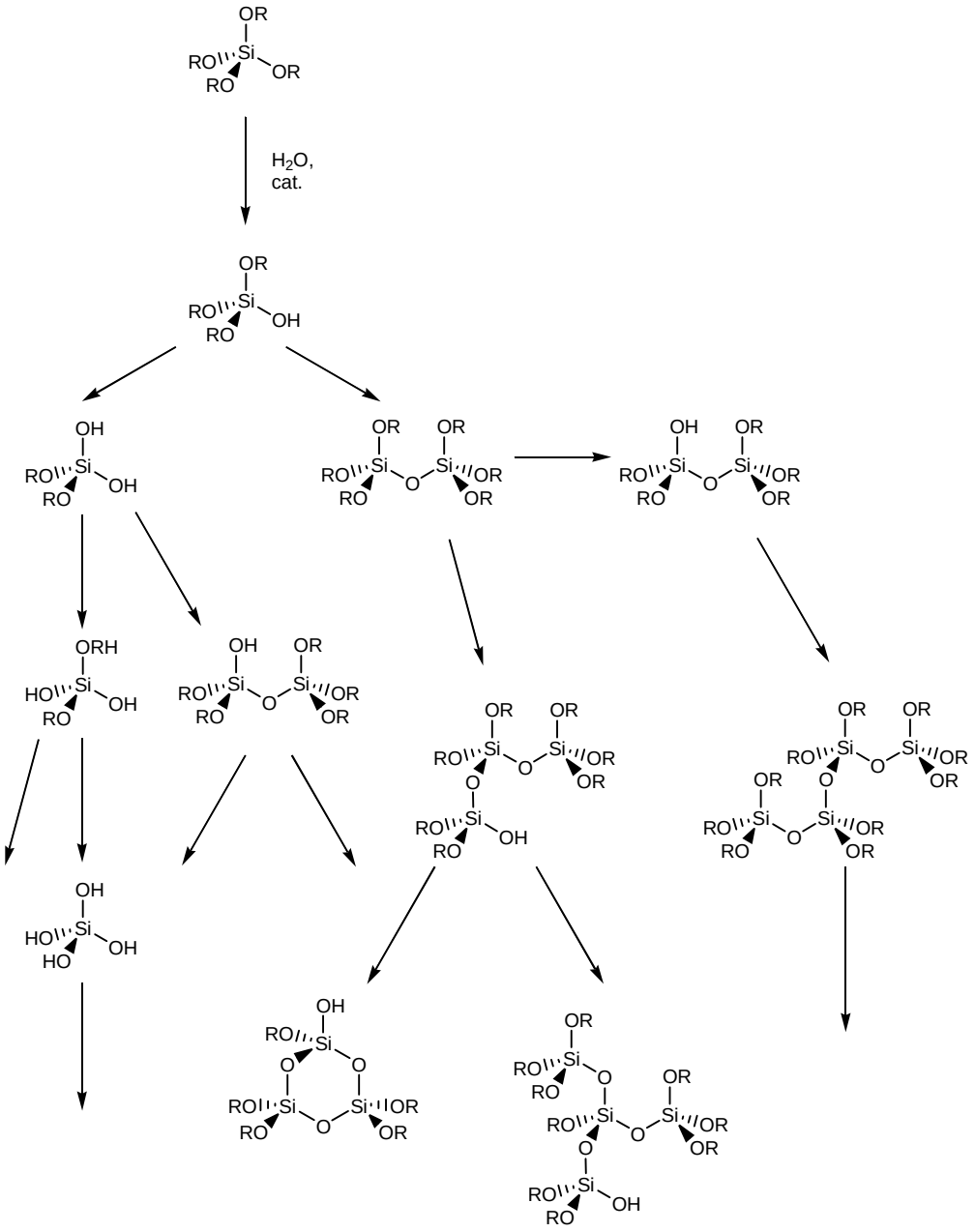

Figure 1. Initial intermediates during the sol-gel process

The sol gel process reactions may be acid or base catalysed. In both cases the reactions (hydrolysis and condensation) proceed via a rapid formation of a charged intermediate by reaction with the proton or hydroxide ion (Scheme 2).

Hydrolysis:

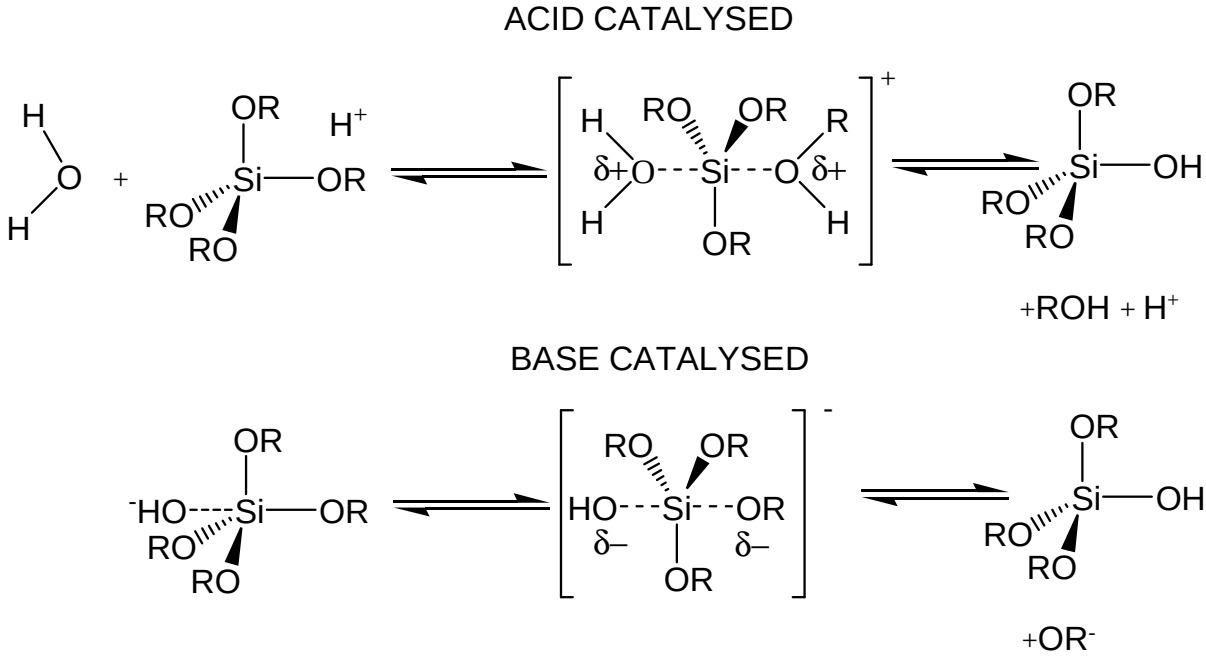

Condensation:

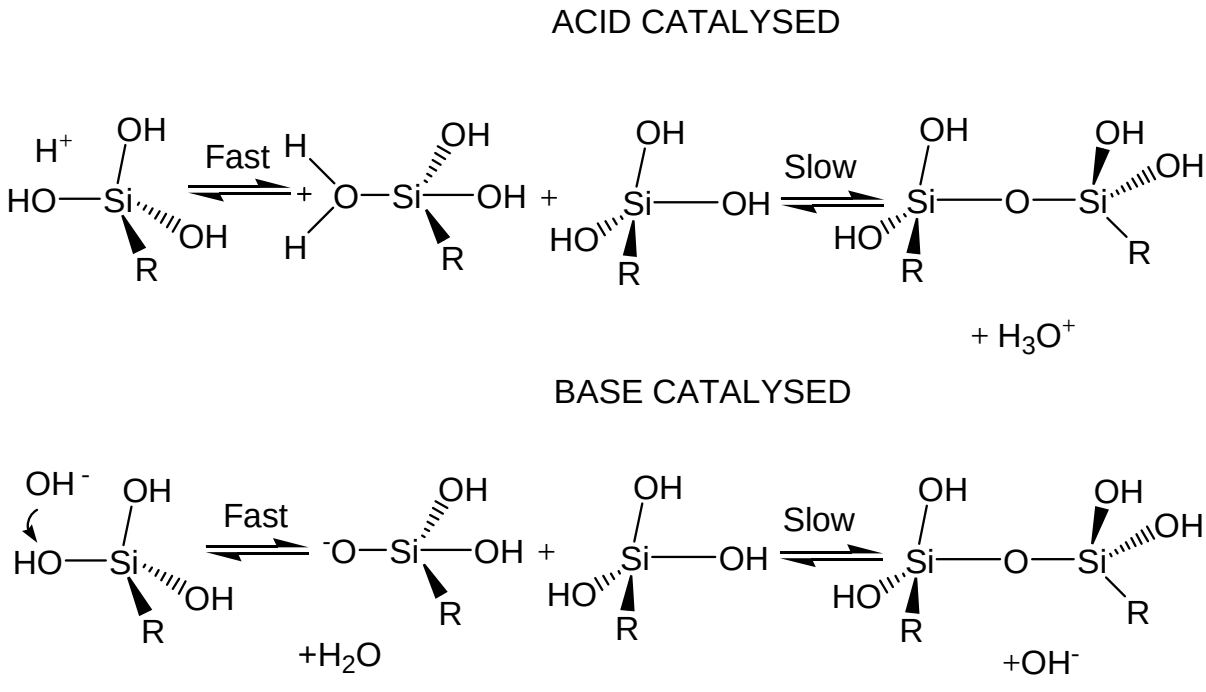

Scheme 2. Mechanisms of hydrolysis and condensation

For acid catalysed reactions, the first step of the hydrolysis is the fastest, thus the $(RO)_3SiOH$ is the most abundant species. This species goes as well in the fastest condensation. Consequently an open network structure is formed. In base catalysed reactions the successive hydrolysis steps occur increasingly fast, hence the totally

hydrolysed species $Si(OH)_4$ is the most abundant and the one that suffers the fastest condensation. As a consequence, highly crosslinked clusters are reached with the base catalysed reactions.

Interestingly, during the sol gel process the pH changes as the higher oligomers become more acidic. This in turn changes hydrolysis and condensation conditions during the sol-gel process which leads to amorphous materials with a broad distribution of e.g. pore sizes.[73]

2. Gelation: It occurs when links between silica sol particles, produced by hydrolysis and condensation, are generated, creating a spanning cluster which reaches across the containing vessel.[70] The sol-gel transition is reached when a continuous network is formed. One important parameter is t_{gel} which is the time at which the gel point is reached after starting hydrolysis and condensation reactions.[45] The t_{gel} is smaller by all the parameters that increase the rate of condensation reactions.[69]

3. Aging: The structure of the material that is obtained after gelation may change appreciably with time, depending on the temperature, solvent or pH conditions. This phenomenon increases the stiffness of the gels. Four processes can occur, singly or simultaneously, during aging. These processes are polycondensation (cross-linking), syneresis, coarsening and phase transformation.[45;69;70]

- The gel network still contains a continuous liquid phase that contains condensable particles. These particles can condense to the existing network.
- The polycondensation provokes shrinkage of the gel and the resulting expulsion of liquid from the pores.
- Since convex surfaces are more soluble than concave surfaces, dissolved material will tend to precipitate into regions of negative curves. This leads to an increase in the average pore sizes of the gel and decrease in the surface area.
- When the gelation was very fast, it can occur that isolated regions contain unreacted precursors. This material can react giving inclusions of material of different structure and composition.

4. Drying: The evaporation of the liquid from the wet gel proceeds in a very complex way in which three stages can be distinguished:

- Initially a gel will shrink by an amount equal to the volume of water or other liquid which has evaporated. This phase can only occur in gels which are still very flexible and compliant, and able to adjust to the reduced volume.[70] Upon shrinkage, OH groups at the inner surface approach at each other and can react with each other. As drying proceeds, the network becomes increasingly stiffer and the pore radii become smaller.[69]
- As the gel dries and shrinks, its more compact structure and associated additional cross-linking lead to increased stiffness. At the critical point the gel becomes sufficiently stiff to resist further shrinkage as liquid continues to evaporate. At the point the liquid begins to recede into the porous structure of the gel. Very large pressures are generated across the curved interphases of the liquid menisci in the pores. Unless the gel has been very carefully prepared it will crack due to this capillary stress.[70] Nevertheless, a continuous funicular film remains at the pores walls.[69]
- Here, the liquid film is raptured. Eventually, there is only liquid in isolated pockets which can leave the network only by diffusion via the gas phase.[69]

Two processes are important for the collapse of the network. First, the slower shrinkage of the network in the interior of the gel body results in a pressure gradient which causes cracks. Second, larger pores will empty faster than smaller during drying process. The walls between pores of different size are therefore subjected to uneven stress and crack.[69]

4.2 NANOPARTICLES AND STÖBER PROCESS

The Stöber process is a technique widely used to prepare silica particles controlling the size and obtaining narrow size distributions and smooth spherical particles (Figure 2).[74-77]

By means of addition of ammonia the sol-gel process proceeds as base catalysed (Figure 3). Important parameters in the control of the size of nanoparticles are temperature, the water and ammonia concentration and the type of alcohol.[78] Using shorter chain alcohols, more water, less ammonia and tetraalkoxysilane concentrations and low temperatures, smaller nanoparticles are synthesized.

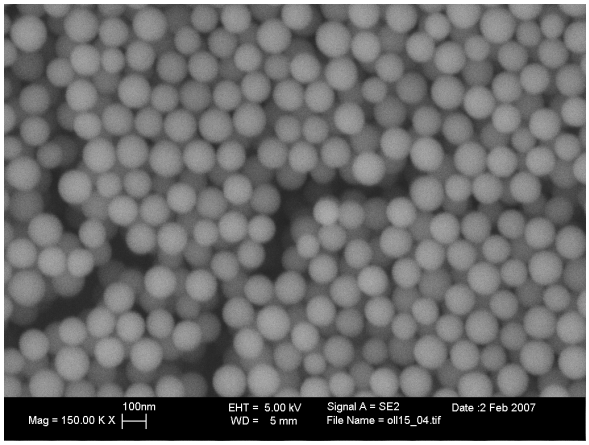

Figure 2. SEM picture of typical Stöber particles

Two models, controlled aggregation[75;79-81] and monomer addition[79;82-84] have been proposed to elucidate the chemical and/or physical growth mechanism of nanoparticles. The first model considered the nucleation and growth of silica as an aggregation process of small subparticles several nanometers in size. The second model proposed that particle nucleation is the result of the reaction between two hydrolysed monomers, such that the particles grow only by a molecular addition mechanism.

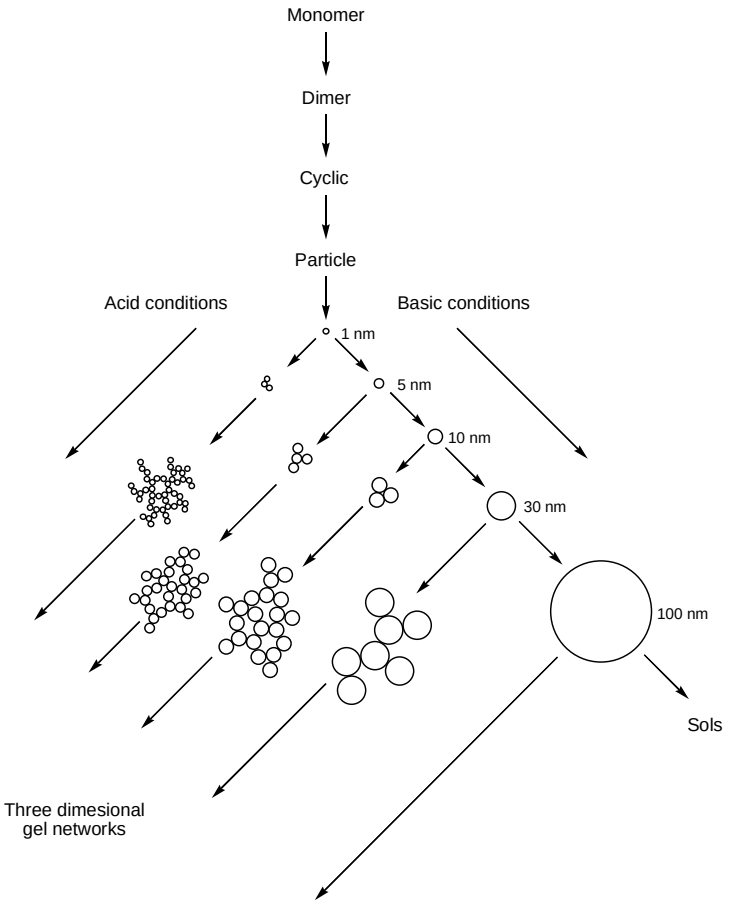

Figure 3. Structural development of silica gels

4.3 POLYHEDRAL OLIGOMERIC SILSESQUIOXANES (POSS)

The silsesquioxanes are organic-inorganic hybrid compounds in polymeric or in cyclic forms as shown in Figure 4. The materials with these cyclic structures are called POSS (Polyhedral Oligomeric Silsesquioxanes).[85-90]

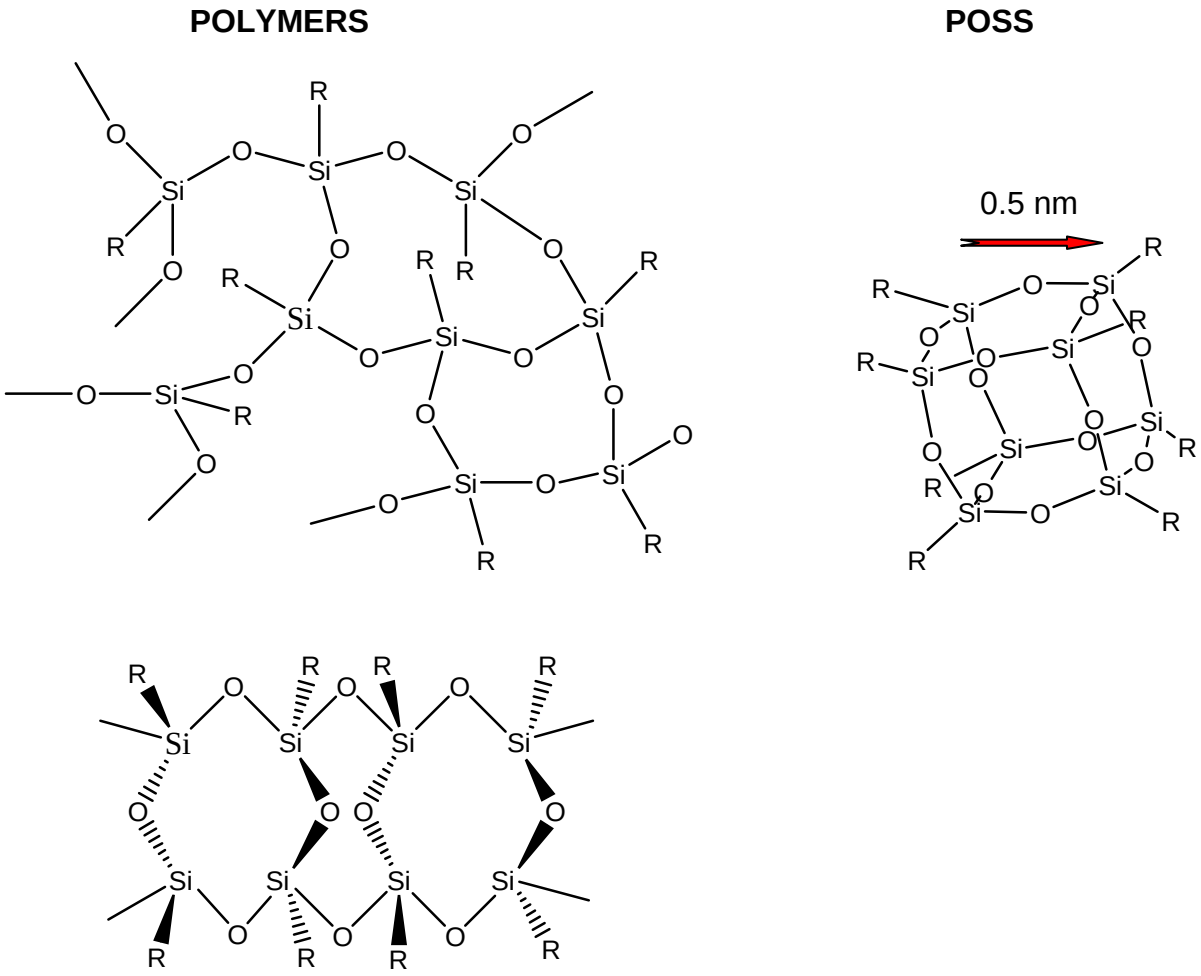

Figure 4. Structure of silsesquioxanes

POSS materials are synthesised through the hydrolysis and condensation of silanes ($RSiX_3$) where X is a halide or an alkoxy group.The general formula of these POSS materials can be reduced to $(RSiO_{3/2})_n$ where R is an organic group, a hydrogen or a halide. These materials can have different polyhedral structures, and can be divided into fully and partially condensed silsesquioxanes. The most characteristic materials are represented in Figure 5.[64;91-94]

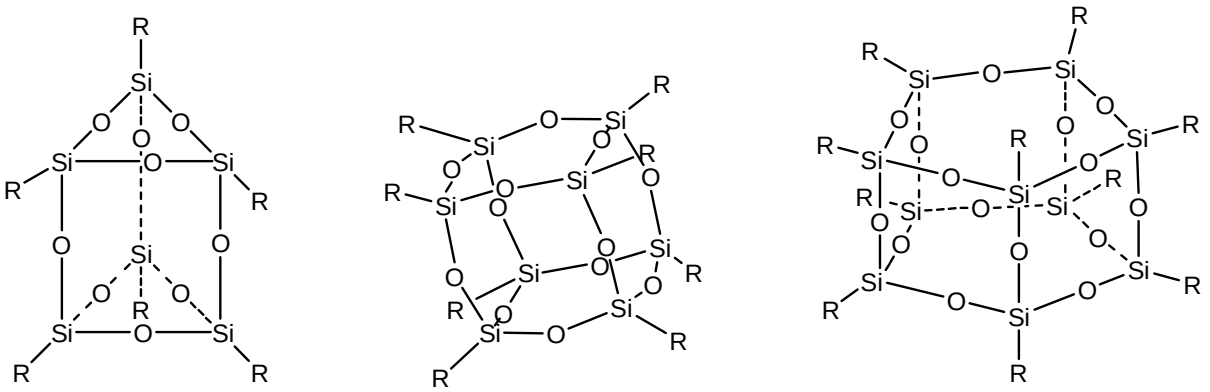

T_6 **T_8** **T_{10}**

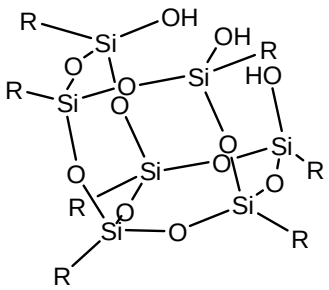

$T_7(OH)_3$

Figure 5. Structure of fully and partially condensed POSS

The nomenclature used for the fully condensed POSS is T_n. Where n correspond to the number of silicon atoms and T is the type of silicon atoms (unit where the silicon is connected to three oxygens).[95] Moreover partially open POSS have been as well synthesised which are ideal to condense metals in the cage. Many factors are known to influence the hydrolytic condensation of $RSiX_3$, determining which structures are formed and in which ratios:[96;97]

- Nature of the X groups: If X is a halide the hydrolysis is higher than if it is an alkoxy. Moreover, their hydrolysis produces acids (HX) which can catalyse the condensation reaction.
- Nature of the R groups: The experience shows that the sterical effects of the R group determine the condensation ratio in the products.[93;95;98-100] Additionally, together with the solvent, the nature of the R group determines the solubility of the products, controlling the rate of the condensation reaction.
- Solvent: Polar solvent molecules can form hydrogen bonds with the silanol groups and therefore stabilise the partially condensed silsesquioxanes.[64;101]

- Concentration of the silane: The concentration influences the reaction kinetics. Although it has been not possible to obtain a kinetic equation for the synthesis of the POSS, it is suggested that the higher the concentration, the most probable polymer silsesquioxanes are achieved.[96]
- Rate of addition and quantity of water: It influences the hydrolytic condensation.
- Temperature: Polymeric silsesquioxanes are formed when the temperature is higher.[97]
- pH: Polymeric silsesquioxanes are formed when the pH is higher due to the sensitivity of the Si-O-Si bonds with respect to pH.[99;102]

4.4 LUMINESCENCE

Luminescence is the emission of light from any substance and occurs from electronically excited states. Luminescence is formally divided into two categories, fluorescence and phosphorescence, depending on the nature of the excited state. In the singlet states the electrons in the excited orbital is paired to the second electron in the ground state orbital. Consequently, return to the ground state is spin allowed. Phosphorescence is emission of light from triplet excited states, in which the electron has the spin orientation as the ground state electron (Scheme 3).[103-105]

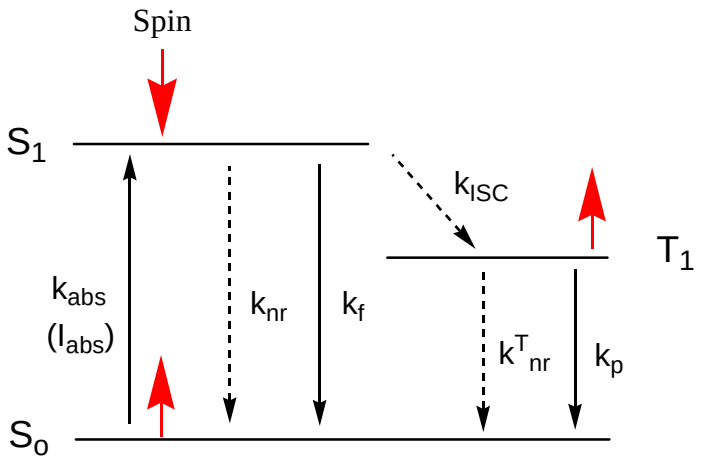

Scheme 3. Jabłoński diagram with theoretical excitations and emissions

k_{abs}, k_f, k_{isc}, k_{nr} and k_r are the rate constants for absorption, fluorescence, intersystem crossing, non-radiative and photoreactive processes. S_o is the ground state and S_1 (singlet) and T_1 (triplet) excited states.[103]

It should be noted that the distinction between fluorescence and phosphorescence is not always clear. Transition metal to ligand complexes which contain a metal and one or more organic ligands, display mixed singlet-triplet states.[103]

The fluorescence lifetime (τ) and quantum yield (Q) are perhaps the most important characteristics of a fluorophore. The quantum yield is the number of emitted photons relative to the number of absorbed photons. The lifetime is defined by the average time the molecule spends in the excited state prior to return to the ground state.

$$Q = \frac{k_f}{k_f + k_{nr}} \tag{1}$$

$$\tau = \frac{1}{k_f + k_{nr}} \tag{2}$$

The lifetime in absence of non-radiative processes is called intrinsic or natural lifetimes (τ_n).

$$\tau_n = \frac{1}{k_f} = \frac{\tau}{Q} \tag{3}$$

The lifetime determines the time available for the fluorophore to interact with or diffuse in its environment.

The intensity of the fluorescence can be decreased by a wide variety of processes. Collisional quenching occurs when the excited state of the fluorophore is deactivated upon contact with some other molecule in solution which is called quencher. The molecules are not chemically altered in the process. For collisional quenching the decrease in intensity is described by the well known Stern-Volmer equation.

$$\frac{F_0}{F} = 1 + k[S] = 1 + k_q \tau_0 [S] \tag{4}$$

k is the Stern-Volmer quenching constant, k_q the bimolecular quenching constant, τ_0 the unquenched lifetime and [S] the quencher concentration.

The bimolecular quenching constant gives important information. It reflects the efficiency of quenching or the accessibility of the fluorophores to the quencher. Smaller values of k_q can result from sterical shielding of the fluorophore and larger values usually indicate some type of binding interaction.

5. RESULTS AND DISCUSSIONS

5.1 SYNTHESIS, CHARACTERISATION AND LUMINESCENCE SPECTROSCOPIC ACCESSIBILITY STUDIES OF FLUOROPHORE CONTAINING SOL-GEL MATRICES AND NANOPARTICLES

5.1.1 Introduction

With the luminescence properties of the ionic triethoxysilylfunctionalised modified $[Ru(bpy)_3]^{2+}$ (**1**) and the non-ionic triethoxysilylfunctionalised pyrenemethanol (**2**) one is able to compare the accessibilities of both fluorophores in condensed silica materials, on nanoparticles and in solution. Moreover, the choice of an ionic and non-ionic fluorophore allows investigating the dependence of the accessibility on the polarity of the active centres, the solvent and the surface of the material. In Scheme 4 the mechanism of the luminescence quenching of **1** and **2** by anthracene (ANT) and N,N-diethylaniline (DEA), respectively, as well as dioxygen is depicted. Light absorption by **1** results in a Franck-Condon singlet metal to ligand charge transfer (^{1}MLCT) excited state which goes via intersystem crossing to a long lived ^{3}MLCT excited state. The triplet state decays by non-radiative deactivation and luminescence. Due to the long lifetimes, ^{3}MLCT are quenched efficiently if they are in close contact with a quencher molecule to which an energy transfer takes place by a electron exchange, according to the reactions:[11;34]

$$^3\mathbf{1}^* + {}^1anthracene \rightarrow {}^1\mathbf{1} + {}^3anthracene^*$$
$$^3\mathbf{1}^* + {}^3O_2 \rightarrow {}^1\mathbf{1} + {}^1O_2{}^*$$

The quenching of **2** is carried out through exciplex formation between the fluorophore and the quenchers, according to the reactions:

$$^1\mathbf{2}^* + {}^1DEA \rightarrow {}^1(\mathbf{2},\ DEA)^* \rightarrow {}^1\mathbf{2} + {}^1\mathrm{DEA}$$
$$^1\mathbf{2}^* + {}^3O_2 \rightarrow {}^3\mathbf{2} + {}^1O_2{}^*$$

where ^{1}(**2,** *DEA*)***** represent the exciplexes.

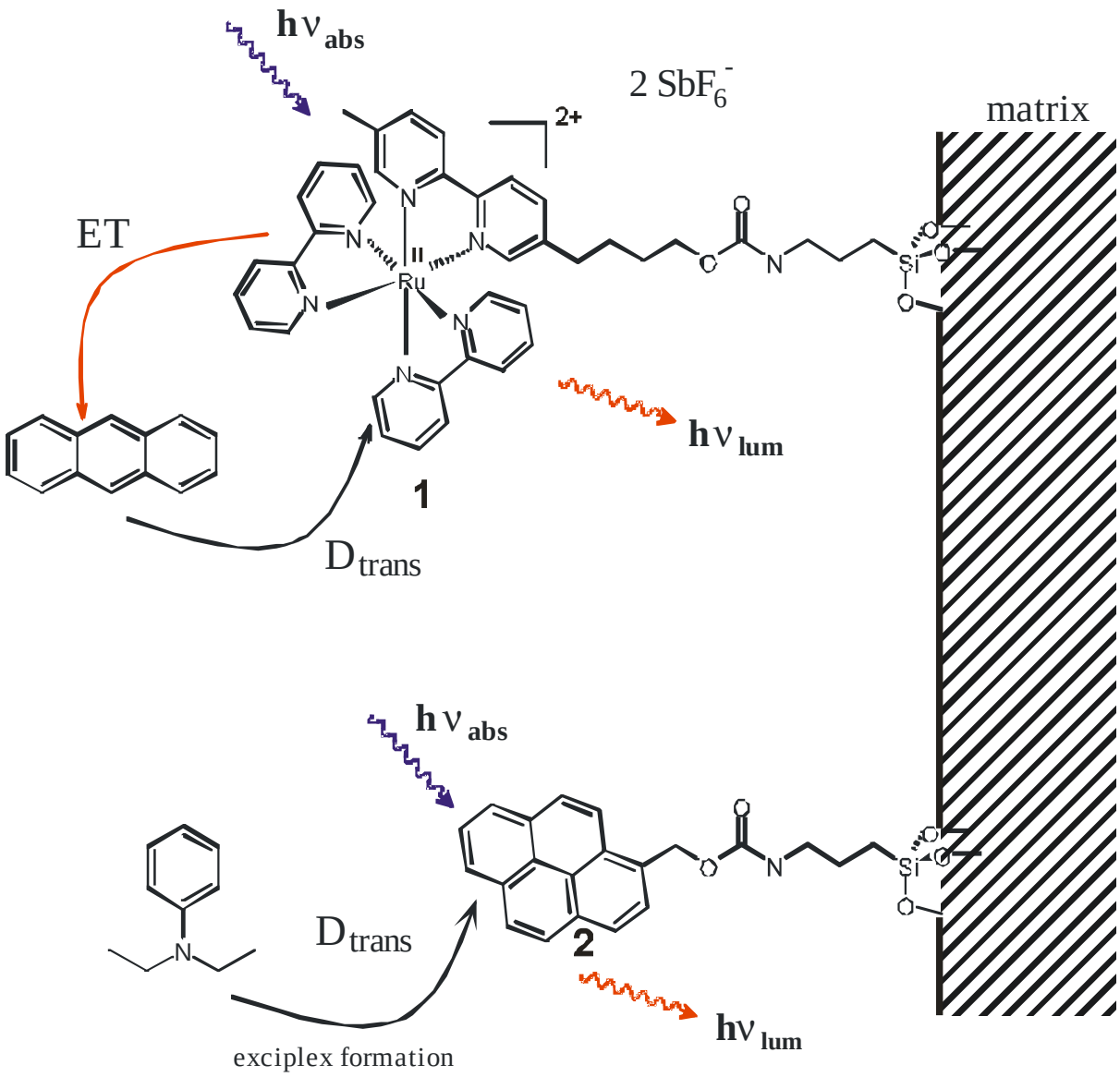

Scheme 4. Mechanisms of quenching of **1** and **2** in a matrix

Because both mechanisms require a close contact of the quencher molecule with the active centre this luminescence quenching is ideally suited to investigate the accessibility of active centres which are incorporated in different sol-gel materials or attached on nanoparticle surfaces. The results of this investigation can be useful for the future design of sol-gel materials which incorporate catalysts of different ionic nature.

5.1.2 Synthesis of fluorophores 1 and 2

In order to anchor the modified $Ru(bpy)_3^{2+}$ complex and the commercially available pyrenemethanol to different silica matrices they have to be functionalised with a hydrolysable triethoxysilane according to Schemes 5 and 6. The compounds **1** and **2** have been fully characterised by ^1H, ^{13}C NMR and IR spectroscopy.[10;106-108]

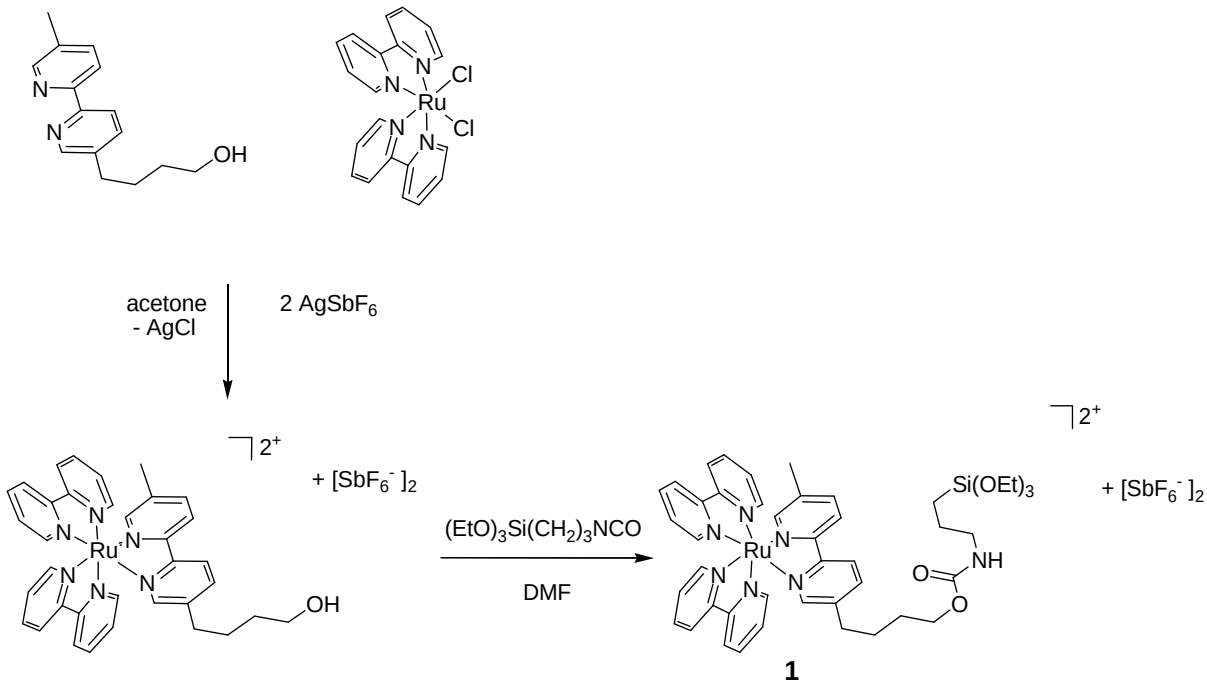

Scheme 5. Synthesis of **1**

The ruthenium complex **1** (red orange) is soluble in polar solvents like alcohols and acetone while **2** (bright yellow) dissolves in polar and non polar organic solvents quite well.

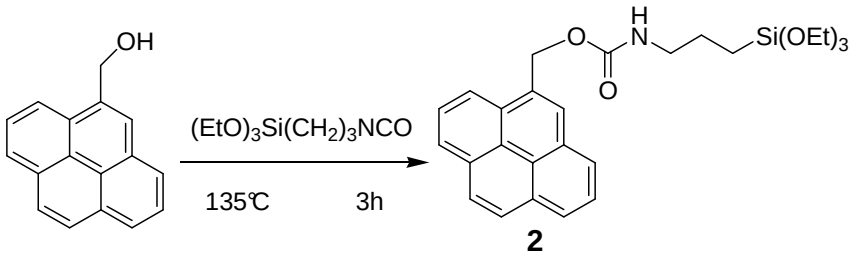

Scheme 6. Synthesis of **2**

5.1.3 Synthesis and characterisation of the sol-gel materials A - D

The incorporation of the two fluorophores **1** and **2** into a polysiloxane network is best achieved via a sol-gel process. Therefore both fluorophores **1** and **2** (0.2 mmol each) were added to a reaction mixture containing tetramethoxysilane (TMOS), ethanol and a sodium acetate/acetic acid water buffer in the ratio of 1:10:33. The buffer provides a constant pH at approximately 4.8 and thus controls the kinetics of the hydrolysis and condensation processes. At pH 4.8 the hydrolysis and condensation are well balanced so that small clusters are produced which upon gelation lead to porous materials. Moreover the constant pH ensures that the formed clusters are approximately the same size which should lead to a narrow pore size distribution.[73;109] It is crucial to use only small amounts of fluorophores to avoid excimer formation in the sol-gel materials. After three days of gelation, the sol-gel material containing the two fluorophores was divided into four parts and each one was dried in a different way: In vacuo (**A**), in a water atmosphere at 40℃ (**B**), under reduced pressure (**C**) and in air (**D**). The various drying procedures were chosen to study their influence on the pore sizes and pore size distribution of the four sol-gel materials. The dry materials were obtained as orange glassy solids. The colour is a strong indication that the ruthenium complexes are incorporated successfully into the polymer network. The sol-gel and drying conditions were chosen to assure that for all materials an open network structure is obtained.

Table 1. Relative amounts of Q^2, Q^3 and Q^4 groups derived from ^{29}Si HPDEC NMR spectroscopy of the materials **A** - **D**

Material	Q^2 [ppm] (%)[1]	Q^3 [ppm] (%)[1]	Q^4 [ppm] (%)[1]	Degree of Condensation (%)[1]
A	-91.24 (6.8)	-100.97 (34.2)	-110.22 (58.9)	87.95
B	-89.34 (4.2)	-98.99 (27.7)	-109.22 (68.1)	90.97
C	-90.96 (5.2)	-101.18 (31.7)	-110.59 (63.1)	89.47
D	-91.75 (4.1)	-101.81 (34.8)	-110.70 (61.1)	89.25
E[10]	---	*-101*	*-110*	

[1] Relative quantity of Q groups.

^{29}Si solid state NMR spectroscopy measurements revealed that the materials **A** - **D** are dominated by the polymeric nature of the Q-groups (Figure 6). No ^{29}Si NMR signals for polycondensed trifunctionalised silanes (T-groups) attached to the fluorophores are observed. This is due to the quantity relationship between TMOS and fluorophores ($1:2\cdot10^{-4}$). From the data in Table 1 it can be appreciated that the materials **A** - **D** are highly condensed with only minor differences among the materials which might be due to the different drying procedures.

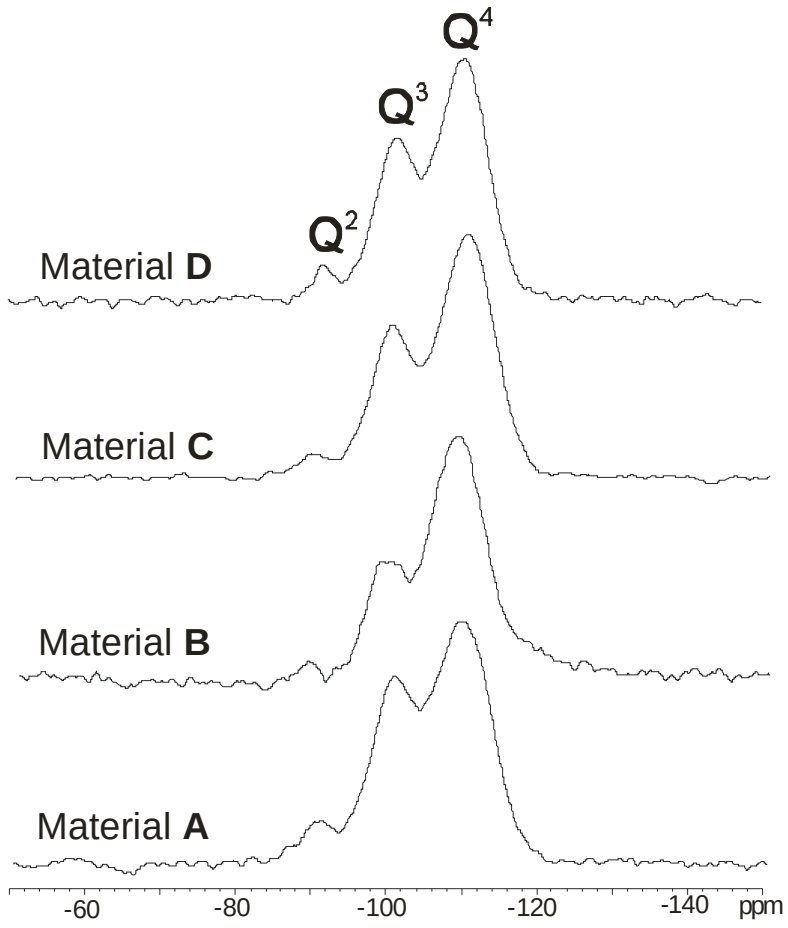

Figure 6. Solid state ^{29}Si MAS NMR spectrum for the materials **A** - **D**

Pore sizes, pore volumes and surface areas of the sol-gel materials **A** - **D** were calculated from data obtained by nitrogen absorption/desorption experiments applying the Brunauer-Emmet-Teller (BET) and Barett-Joyner-Halenda (BJH) models (Table 2).[110-112]

Table 2. BET surface area, pore area and pore radii of the materials **A** - **D**

Material	A_{BET} (m^2/g)[a)]	A_{BJH} (m^2/g)[a)]	$A_{Micropore}$ (m^2/g)[b)]	BET pore size (nm)[a)]	BJH pore size (nm)[c)]	BET total pore volume (cm^3/g)[a)]	BJH total pore volume (cm^3/g)[c)]
A	769.1	419.7	127.40	1.19	1.36	0.45	0.29
B	586.0	568.7	21.56	2.35	2.13	0.69	0.72
C	690.2	670.9	14.95	2.65	2.46	0.91	0.95
D	709.9	587.1	29.44	1.64	1.61	0.58	0.53
E	4.9		--	--	--	--	--

[a)] Calculated by BET,[b)] Obtained by t-plots,[c)] Fraction of pores open in both sides is 0.

From the BET model surface areas, pore volumes and pore sizes over the whole range were calculated. In contrast the BJH method provides pore volumes and sizes in the range of 0.85 to 150 nm. Additionally in the BJH model the fraction of the pores which are opened on both sides is considered to be zero. In general BET isotherms are categorized in different types depending on the shape of the curves.

The nitrogen absorption/desorption experiments exhibited a combination between isotherms of types I and IV for **A** and **D** (Figure 7 and 10) which are characteristic for microporous (pore size smaller than 2 nm) and mesoporous materials (between 2 and 50 nm), whereas silicas **B** and **C** showed pure type IV isotherms (Figure 8 and 9) attributed to materials with a high predominance of mesopores.

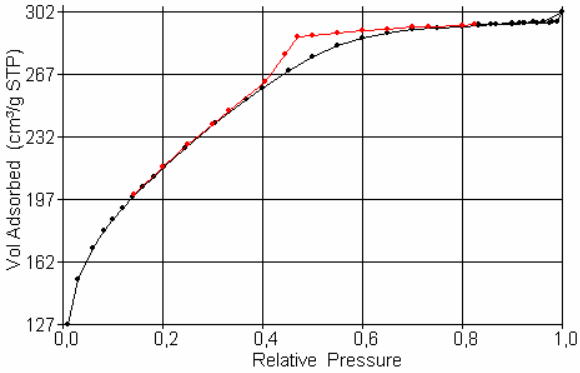

Figure 7. Type I + IV isotherm for material **A**

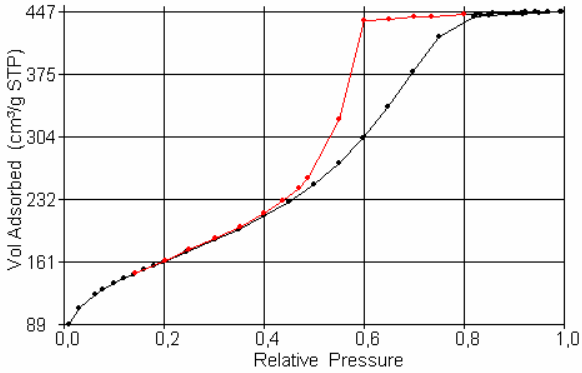

Figure 8. Type IV isotherm for material **B**

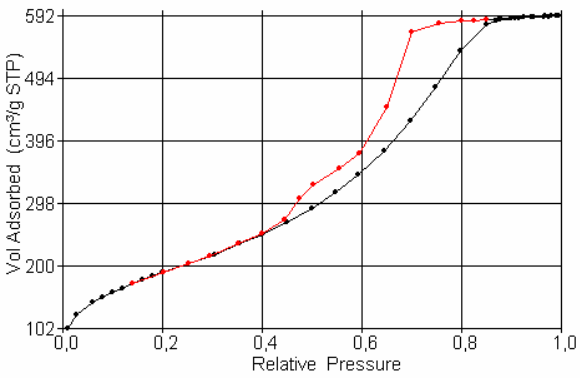

Figure 9. Type IV isotherm for material **C**

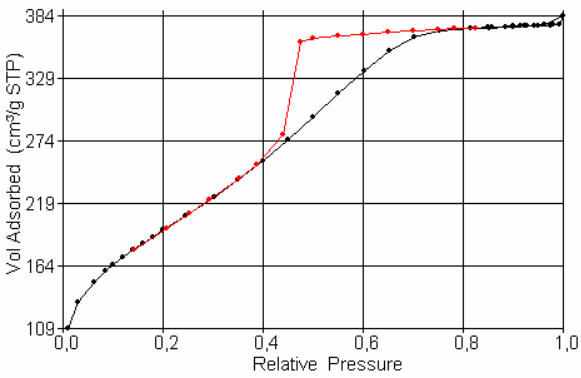

Figure 10. Type I + IV isotherm for material **D**

According to the t-plots (graphical representation of the amount of gas adsorbed vs. the statical thickness of the gas film), material **A** represents a microporous material with mesopores. This is confirmed by $A_{micropore}$ of 127 m^2/g and can be deduced from BJH model and the isotherms (Figure 7 and 11). In Figure 7 the hysteresis loop in the desorption curve (red curve) confirms the presence of mesopores. In Figure 11 the small number of increment pore volume (0.05) for the radius peak and the gradual decay of the curve at the average radius at 2 nm indicate the presence of micro- and mesopores. The BET and BJH data are comparable for **B** and **C** revealing just a small micropore area. From the desorption curves of the isotherms (red curves in Figures 7-10) it can be appreciated that just one pore distribution exists for materials **A**, **B** and **D** whereas in **C** two pore sizes can be distinguished. The larger pores in material **C** are much more abundant than the smaller ones (Figure 13). Thus the pore size of 2.65 nm gives an average number. The hysteresis loops in all isotherms is of type E which is associated with ink-bottle kind of pores. Overall in all four materials the pore distribution is rather narrow as deduced from the isotherms.

The surface areas are rather high, ranging from 586.03 m^2/g (**B**) to 769.13 m^2/g (**A**) (Table 2). The sizes of the pores of the four silicas are between 1.19 and 2.65 (BET) and 1.36 and 2.46 (BJH).

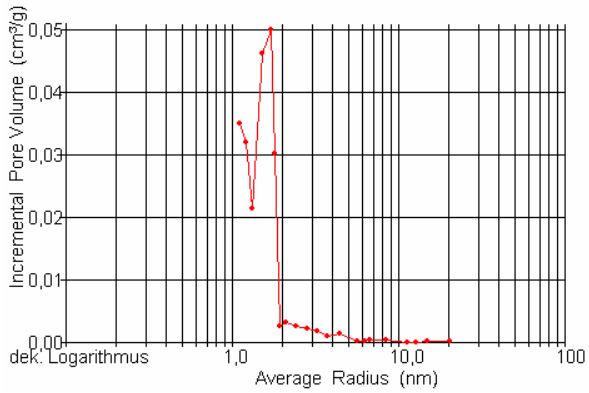

Figure 11. BJH plot of material **A**

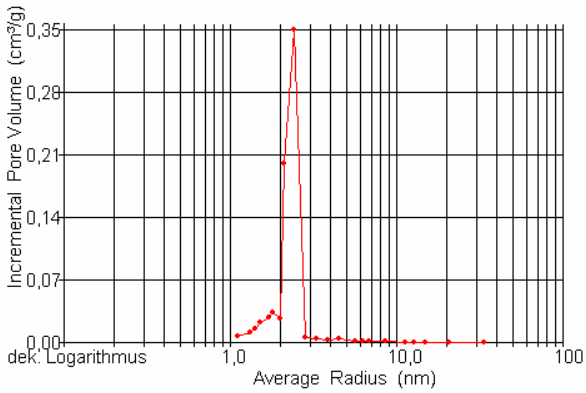

Figure 12. BJH plot of material **B**

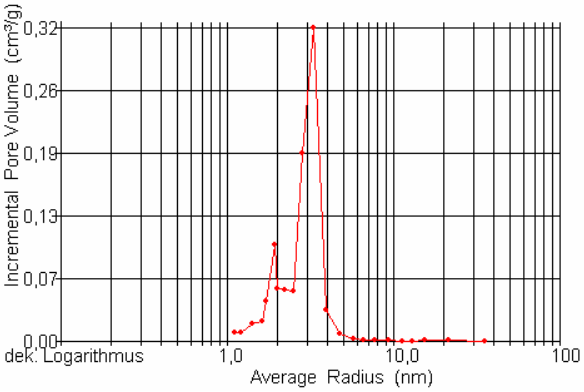

Figure 13. BJH plot of material **C**

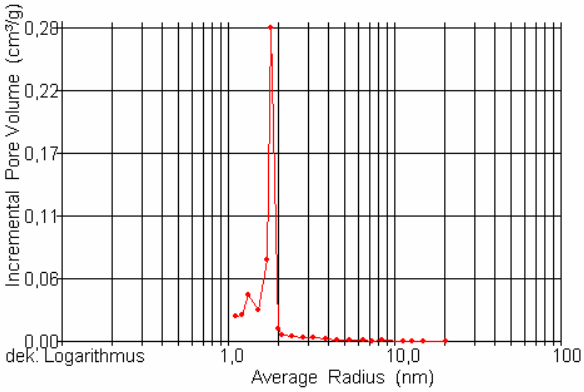

Figure 14. BJH plot of material **D**

Controlling the pH by a buffer systems leads to materials with higher surfaces areas as compared to a sol gel process where the pH was adjusted at the beginning of the reaction and left without further control (Table 2 material **E**).[10] The additional increase of the surface area in **A** compared to that in **B** – **D** is due to the formation of micropores. Obviously the fast evaporation of the solvent in material **A**, does not leave the time to close the micropores by further hydrolysation and condensation processes. This is apparently the case in materials **B** – **D** which were dried at higher temperatures and over a longer period of time.

5.1.4 Synthesis of the nanoparticles

The nanoparticles were synthesized according to the Stöber process.[113] The hydrolysis and condensations are carried out under basic conditions in the presence of ammonia as catalyst. Light scattering measurements [114] showed that the diameter of the particles are 192 ± 8.8 nm and the surface area and porosity obtained by BET

measurements are 29.88 m^2/g and 9.1 nm, respectively (Figure 15). This large value can be attributed to interstitial space between the nanoparticles which are taken as pores.

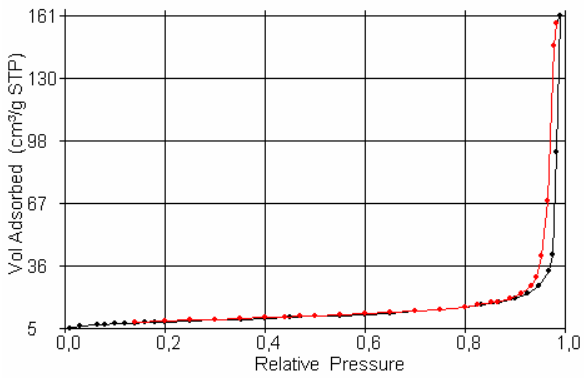

Figure 15. Isotherm of the nanoparticles before the porosity was eliminated

The possible microporosity was eliminated by heating the particles to 600℃ for 16h and subsequent treatment with an HCl solution at 100℃ for 2 h. After that procedure the size of the particles was determined to 175.0 ± 19 nm. The BET measurement showed a smaller surface area and a porosity of 25 m^2/g with 6.2 nm of interstitial space (Figure 16). The reduced interstitial space is in agreement with the smaller sizes of the nanoparticles.

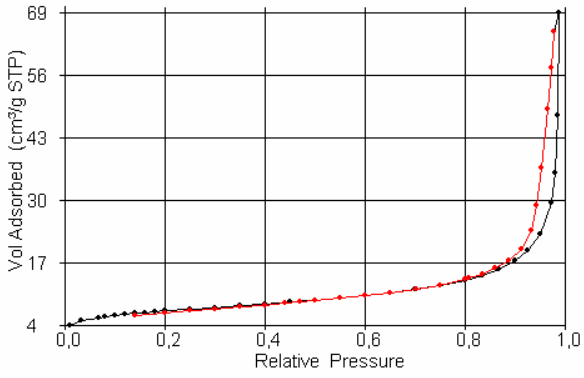

Figure 16. Isotherm of the nanoparticles when the porosity was eliminated

Both fluorophores were attempted to attach to the surface of the nanoparticles. To avoid the formation of excimers the stoichiometry was adjusted to cover only 1% of the SiOH groups, e.g. 344 mg of nanoparticles require 6.8 10^{-4} mmol of **1** or **2**.[115] The nanoparticles were refluxed in a solution of toluene and the appropriate amount of **1** and **2** to give the nanoparticles **1NP** and **2NP**, respectively. Luminescence

measurements with both materials revealed that only the pyrenemethanol has been successfully attached on the surface. The ionic nature of **1** makes it only soluble in very polar solvents like alcohols which hinder the hydrolysis of the ethoxy groups and compete with the ethoxy groups of the fluorophore for the OH groups on the surface of the nanoparticles. An effort to connect **1** to the surface of the nanoparticle in acetone failed due to the low boiling point of acetone which prevents the activation energy of the condensation process to be reached.

5.1.5 Luminescence spectroscopic investigations

5.1.5.1 Luminescence and luminescence excitation spectra of **1** in different materials

Luminescence spectra and luminescence excitation spectra have been recorded for **1** in THF or methanol and for the sol gel material **A** suspended in THF or methanol (Figure 17). The maximum in the Franck-Condon triplet metal to ligand charge transfer excited state (^{3}MLCT) for **1** in THF and methanol solution is found at $\tilde{\upsilon}_{em}^{max} \approx 15530$ cm^{-1} and $\tilde{\upsilon}_{em}^{max} \approx 15740$ cm^{-1}, respectively.

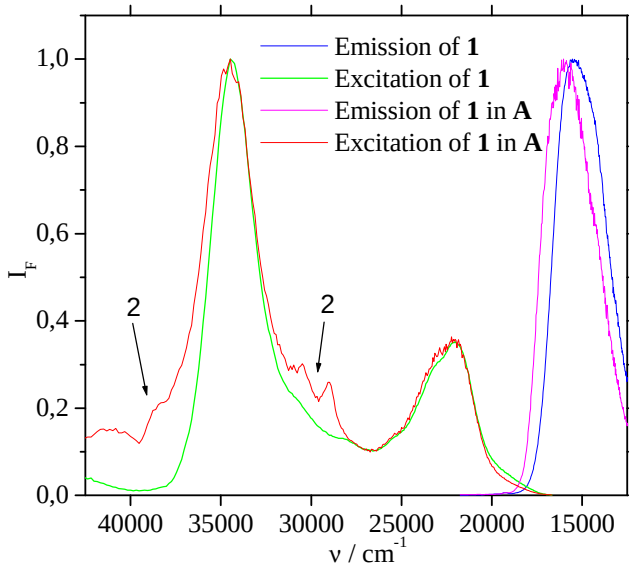

Figure 17. Normalised luminescence and luminescence excitation spectra of **1** in solution and of material **A** suspended in THF, where the excitation signal for the T-pyrenemethanol **2** appears. Emission wavelength λ_{em}=610nm and excitation λ_{ex}=450nm

The transitions are solvent dependent due to the different extents of the stabilisation of the ^{3}MLCT excited state by various solvents (Table 3).The dipole moment of the excited MLCT state is not much different of the ground state. Therefore the solvent-induced shift of the emission maximum is only small.[116] The solvent independent ^{1}MLCT absorption maximum is found at $\tilde{\upsilon}_{abs}^{MCLT} \approx 22050$ cm^{-1}.

Table 3. Spectral positions of the luminescence maxima ($\tilde{\upsilon}$ in cm^{-1}) of **1** and of the sol-gel material **A**

	1	**A**
THF	15530	15910
MeOH	15740	15870

The spectral positions of the luminescence maxima of the ruthenium complex in the sol-gel materials undergo slight (Table 3 and Figure 17), but noticeable changes compared to the values observed for **1** in solution, the $\tilde{\upsilon}_{em}^{\max}$ are found at 15910 cm^{-1}. This blue shift is due to an affect called "*rigidochromism*".[23;24;29;34;117;118] In a fluid solution the excited state of the complex is stabilised relative to the ground state by relaxation of the surrounding solvent dipoles, and the complex emits light from a relaxed excited state. On the other hand, in a rigid matrix, the solvent is not free to reorient and thus the excited state is not completely stabilised or relaxed within its lifetime. Hence, emission occurs from a higher energy level in a rigid state than in a fluid solution.

Two maxima can be observed in the excitation spectrum, the maximum of the absorption at $\tilde{\upsilon}_{abs}^{MCLT} \approx 22050$ cm^{-1} is due to transitions between bipyridine and ruthenium, whereas the maximum at $\tilde{\upsilon}_{abs}^{\max} \approx 34500$ cm^{-1} is due to *intra*-ligand-transitions (Figure 17). The shoulders on both sides of the *intra*-ligand-transitions band correspond to the immobilized pyrenemethanol (See below. Figure 17).

5.1.5.2 Luminescence and luminescence excitation spectra of **2** in different materials

Figure 18 shows the luminescence and luminescence excitation spectra of **2** in different solvents, in material **A** and on nanoparticles. The ratios of the intensities of

the fluorescence peaks I (at 26630 cm^{-1}) and III (at 25910 cm^{-1}) observed are listed in Table 4.

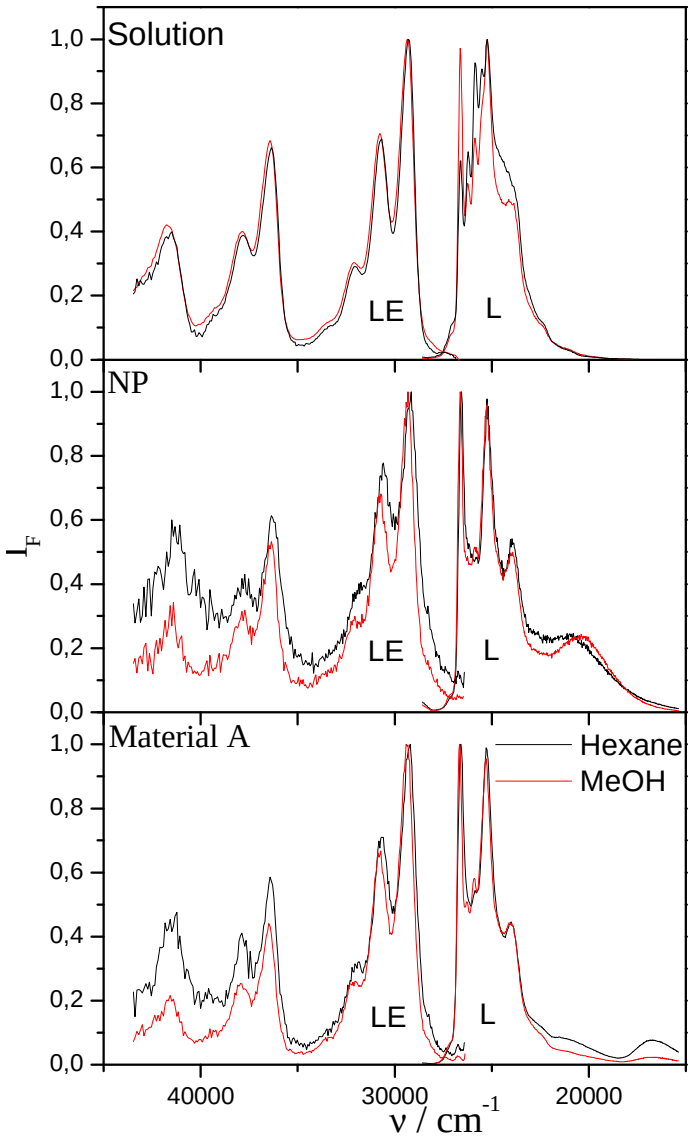

Figure 18. Normalised luminescence (L) and luminescence excitation (LE) spectra of **2** in solution (top panel) **2NP** (middle panel) and material **A** (bottom panel) suspended in methanol (red lines) and in *n*-hexane (black lines). Emission wavelength λ_{em}=396 nm, excitation wavelength λ_{ex}=340 nm

In pyrene,[119] the I/III-ratio depends on the local symmetry of the environment, which changes the selection rules of the transitions contributing to the emission spectrum (Ham effect). Highly symmetric solvation shells lead to small I/III-ratios, whereas environments of low symmetry loosen the selection rule for the transition associated with peak I and hence cause high I/III-ratios. Thus, in solution, the I/III-

ratio serves as a measure of the polarity of the environment, highly polar environments being indicated by large I/III-ratios. Although the symmetry of the fluorophore **2** is reduced to C_s by the CH_2OH-substituent (the symmetry in pyrene is D_{2h}), a similar rule holds true for the I/III-ratio of **2** in solution (Table 4).

Table 4. Spectral positions of the low-energy fluorescence excitation peak (in cm^{-1}) and ratio of the intensities of the peaks I and III (Figure 17) of pyrenemethanol in different environments

		2	**A**	**2NP**
Hexane	Ratio	0.64	1.84	1.9
	Sp. Pos.	29280	29240	29150
MeOH	Ratio	1.37	1.72	1.9
	Sp. Pos.	29325	29370	29330

For **2** anchored to nanoparticles and in material **A**, the ratio is between 1.72 and 1.9 in both solvents. This indicates that the environment of the fluorophores is always of low symmetry, independent of the solvent in which the particles are dispersed. The low symmetry is due to interactions of the probes with the surface. In the case of **2NP** it is not only due to the surface but also by interactions among fluorophores. This can be deduced from Figure 18 which shows a structureless band with a maximum at around 480 nm for the emission of **2NP**. This band indicates the presence of excimers of T-pyrenemethanol on the surface of the nanoparticles. This fluorophore is a fluorescence probe whose excited species can interact with non-excited ones thus forming excited state dimers called excimers. The presence of these excimers is surprising as the quantity of trifunctionalised pyrene methanol has been adjusted to cover only 1% of the surface of the nanoparticles. Obviously a large amount of pyrene molecules condensed in close proximity to each other on the surface. This must be due to the highly polar surface which could provoke a major stability of **2** when they are close together comparable to the formation of micelles. Another explanation may be that the condensation takes place in solution and these aggregates bind to the surface.

The excimer/monomer ratio does not significantly depend on the solvent used for dispersion of the nanoparticles. This might lead to the suspicion that the fluorophores are not well solvated by the solvents which the nanoparticles are

dispersed in. However, the solvent-induced shifts ("Onsager effect") of the fluorescence excitation spectra of **2NP** are pretty much the same as in solution (Table 4), indicating that the fluorophores "feel" the full polarizabilities of the solvents, no matter whether they are attached to silica or not. This solvent shift is also observed for material **A**, suggesting that also in these materials the ratio I/III reflects the low symmetry of the environment induced by interaction of the fluorophores with the surface rather than the polarity of the solvent used for dispersing the materials. To conclude, there seems to be a relatively good solvation of the probes by the solvents but also a substantial interaction with the silica material even in the presence of solvent.

5.1.5.3 Kinetic analysis of luminescence decay curves

An ideal interphase represents a solution-like state.[6] With the simple assumption of such an ideal interphase, the deactivation rate $-d[R^*]/dt$ of photoexcited probe molecules can be described (Eq. 5) by conventional kinetics for homogeneous systems (Scheme 7):

$$-\frac{dR^*}{dt} = \left(k_1 + k_q[S]\right)\cdot[R^*] \qquad (5)$$

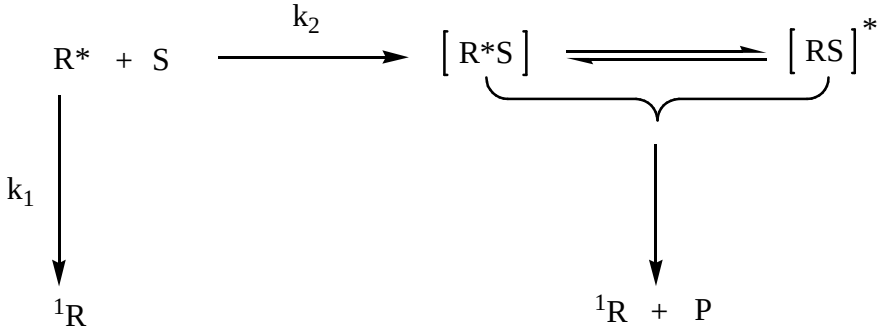

Scheme 7. Schematic presentation of a quenching reaction between a fluorophore R and a quencher S.

Here [R*] is the concentration of excited ^{3}**1** and ^{1}**2** in solution, in the materials **A – D** as well as **2NP,** and [S] is the concentration of a potential reactant that is dissolved in the mobile liquid of the interphase. The rate constant k_1 describes spontaneous deactivation of R* to the inactive electronic ground state, and k_q the deactivation by interaction with S, according to the Stern-Volmer equation:

$$\frac{\tau_0}{\tau} - 1 = k_q \cdot \tau_0 \cdot [S] = 4\pi \cdot N_A \cdot D \cdot R_0 \cdot \tau_0 \cdot [S] = k_{SV} \cdot [S] \quad (6)$$

As model reactions an intermolecular transfer of excitation energy accompanied by double spin flip is chosen, namely:

^{3}**1*** + ^{1}*anthracene* → ^{1}**1** + ^{3}*anthracene** (7)

^{3}**1*** + $^3O_2$ → ^{1}**1** + $^1O_2{}^*$ (8)

^{1}**2*** + $^3O_2$ → ^{3}**2** + $^1O_2{}^*$ (9)

^{1}**2*** + ^{1}*DEA* → ^{1}(**2,** *DEA*) → ^{1}2 + ^{1}DEA (10)

These reactions are possible only by an exchange mechanism after close contact between R* and S or after formation of an exciplex ^{1,3}(RS)* (Scheme 4). In a pulsed laser experiment followed by single-photon counting of R* luminescence, the concentration of R* is always by orders of magnitude lower than that of S, [R*] << [S] ≈ const., so that Eq. 5 can be integrated according to:

$$[R*] = [R*]_0 \cdot e^{-(k_1+k_2)t} \quad (11)$$

where $[R^*]_0$ is the concentration of the excited probe at t = 0 and $k_2 = k_q \cdot [S]$. In a semi-logarithmic plot, Eq. 11 should give a straight line of probe luminescence intensity vs. time. This behaviour is observed for **1** and **2** in homogeneous solution over 2–3 intensity decades and a large range of anthracene, DEA and oxygen concentrations so that k_2 and - if [S] is known - also k_q can directly be determined from Eq. 11. However, in interphases formed from **A** - **D** or **NP** with a variety of liquids, almost all quenching experiments yield nonexponential decay curves. To approximately eliminate the contribution of fluctuations in k_1 to nonexponentionality the decay curves in the presence of S are divided by the decay curves for [S] = 0. As long as Eq. 11 is valid, one obtains for the relative luminescence quenching efficiency at a given time, t, after the laser flash:

$$1 - \frac{[R^*]}{[R^*_{S=0}]} = 1 - e^{-k_2 t} \quad (12)$$

that is, a straight line in the semi-logarithmic presentation. In real systems the curves bend, and very often a constant plateau at t → ∞ is revealed. This type of curve can be approximated with good accuracy by

$$1-\frac{[R^*]}{[R^*_{S=0}]}=\alpha\left(1-e^{-k_2 t}\right) \tag{13}$$

where $0 \le \alpha \le 1$ defines an accessibility factor α, that is, the fraction of excited probe molecules that are able to convert S into P, whereas the fraction (1 - α) is non-reactive ($k_2 \rightarrow 0$). From the product point of view, the accessibility factor α gives the ratio of actual product yield to the maximum possible product yield at $t \rightarrow \infty$:

$$[P]_{max}=\left[R_0^*\right]\frac{k_2}{(k_1+k_2)} \tag{14a}$$

$$\alpha=\frac{[P](t\rightarrow\infty)}{[P]_{\max}(t\rightarrow\infty)}=\frac{1-\frac{[R^*]}{[R^*_{S=0}]}}{1-e^{-k_2 t}} \tag{14b}$$

All time-resolved experiments of this study were evaluated according to Eq. 14b.

In some circumstances where in the case of quenching the decay curves deviate significantly from exponentiality, two different quenching rate constants, k_{q1} and k_{q2} have to be considered

$$[R*]=[R*]_{01}\cdot\left\{\alpha_1\cdot e^{-(k_{11}+k_{21})t}+(1-\alpha_1)\cdot e^{-(k_{11})t}\right\}+[R*]_{02}\cdot\left\{\alpha_2\cdot e^{-(k_{12}+k_{22})t}+(1-\alpha_2)\cdot e^{-(k_{12})t}\right\} \tag{15}$$

where $k_{21}=k_{q1}\cdot[S]_1$, $k_{22}=k_{q2}\cdot[S]_2$

In analogy to Eq. 12, the ratio of quenched and unquenched luminescence decay traces reads:

$$\frac{[R*]}{[R*]_{S=0}}\approx\frac{[R*]_{01}}{[R*]_{S=0}}\cdot\left\{\alpha_1\cdot e^{-(k_{11}+k_{21})t}+(1-\alpha_1)\cdot e^{-(k_{11})t}\right\}+\frac{[R*]_{02}}{[R*]_{S=0}}\cdot\left\{\alpha_2\cdot e^{-(k_{12}+k_{22})t}+(1-\alpha_2)\cdot e^{-(k_{12})t}\right\} \tag{16}$$

where the unquenched luminescence trace is given by:

$$[R*]_{S=0}=[R*]_{01}\cdot e^{-k_{11}t}+[R*]_{02}\cdot e^{-k_{12}t}$$

If the decay times k_{11} and k_{12} are not too different, Eq. 15 simplifies to

$$\frac{[R*]}{[R*]_0}\approx\frac{[R*]_{01}}{[R*]_0}\cdot\alpha_1\cdot e^{-(k_{21})t}+\left(1-\frac{[R*]_{01}}{[R*]_0}\right)\cdot\alpha_2\cdot e^{-(k_{22})t}+\left\{1-\left[\frac{[R*]_{01}}{[R*]_0}\cdot\alpha_1+\left(1-\frac{[R*]_{01}}{[R*]_0}\right)\cdot\alpha_2\right]\right\} \tag{17}$$

where $[R*]_0=[R*]_{01}+[R*]_{02}$

This biexponential quenching time trace is a function of five independent parameters, which makes it impossible to extract a single one individually. However, on the basis of Eq. 17 it is still possible to make some basic statements about the system. The term in brackets in Eq. 17 describes an "average accessibility", i.e., the accessibilities of the two different species, weighted with their concentrations at t = 0. Unless the accessibilities are very different, a value of this term of close to unity means that the majority of all the probe molecules in the system are accessible to the quencher.

5.1.5.4 Luminescence decay curves of **1** in different matrices without quencher

The luminescence decay curves of **1** dissolved in low viscous solutions are single exponential with decay times of τ_F = 670–975 ns. For suspensions of the polysiloxanes **A** - **D** in all investigated solvents, slightly non-exponential decay curves are observed. This type of decay curves is best described by narrow distributions of decay times, but can also be fitted by sums of two exponential functions without loss of accuracy. In all materials, the minor component is slightly shorter than the decay time found in solution, whereas the major component is substantially longer, τ_F = 1.2-1.7 µs, than the corresponding lifetime in solution, and it is due to complexes (**1**) whose primary “solvation shell” is formed by the rigid polymer network.

5.1.5.5 Luminescence decay curves of **1** in different matrices in the presence of oxygen

Quenching of the ruthenium complex[120-122] by energy transfer to dioxygen[123] is a bimolecular process requiring close contact between donor and acceptor. The efficiency of luminescence quenching thus depends on both the mobility of oxygen in the interphase and the accessibility of the transition metal complex.

Table 5. Quenching rate constants k_2 / 10^6 s^{-1} and accessibility factors α (in parentheses) for the luminescence quenching by oxygen of **1** in solution and in suspensions of materials **A** - **D** (Scheme 4) under different quenching conditions

	1	**A**	**B**	**C**	**D**
Hexane	Not Soluble	2.5 (0.40)	4.3 (0.29)	2.4 (0.37)	2.2 (0.35)
THF	3.6 (1)	0.4 (0.43)	0.6 (0.41)	0.5 (0.48)	0.8 (0.38)
MeCN	5.5 (1)	1.5 (0.39)	3.4 (0.30)	3.3 (0.35)	2.6 (0.35)
MeOH	3.9 (1)	1.3 (0.33)	2.5 (0.32)	2.3 (0.33)	1.6 (0.30)

Evaluation of the time-resolved luminescence decay curves according to Eq. 14b yields values for k_2 and α, describing the mobility of oxygen and the fraction of accessible ruthenium complexes (Figure 19 and Table 5).

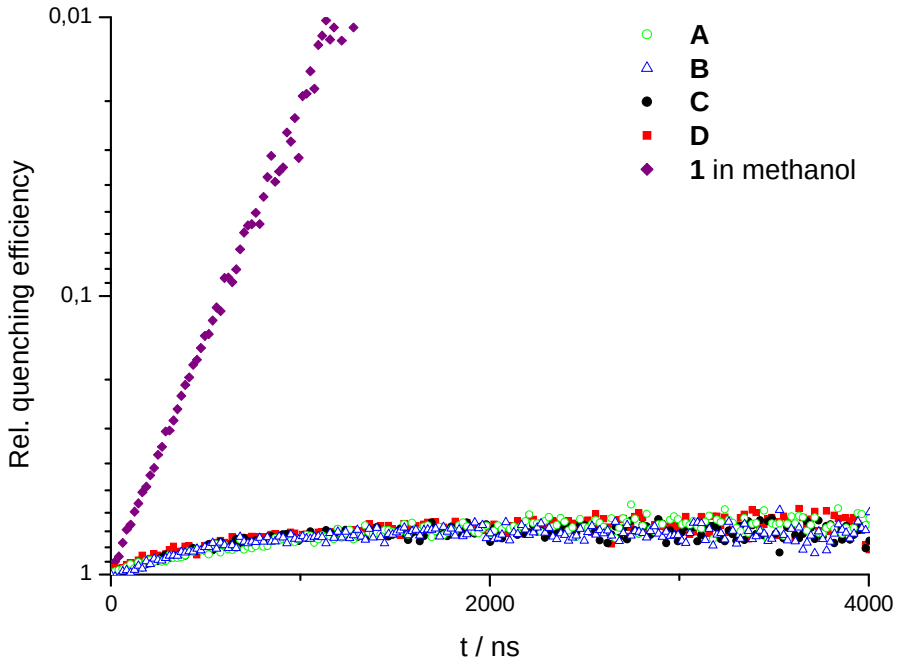

Figure 19. Relative efficiencies for the quenching of the luminescence of **1** by oxygen in methanol and of the materials **A** - **D** suspended in methanol

In homogeneous solutions of **1**, α = 1, that is, all ruthenium complexes are equally accessible by oxygen (Figure 20 and Table 5). The rate constants k_2 are far below the diffusion controlled limit for all solvents.[124]

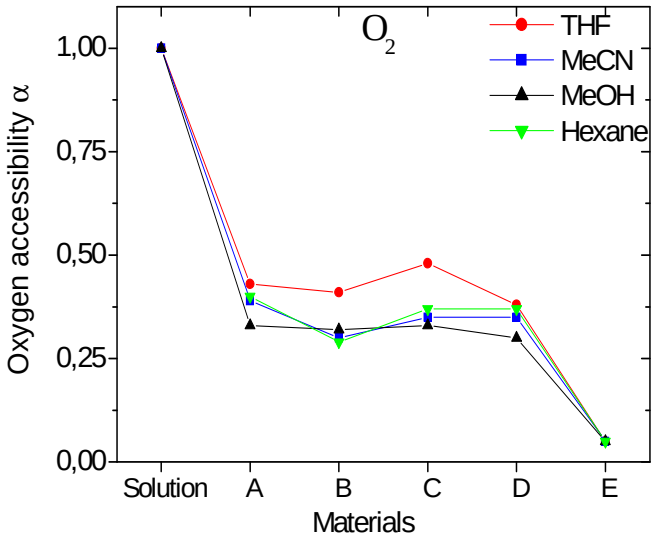

Figure 20. Accessibility factors for luminescence quenching by oxygen in **A** - **D** and **1** in different solvents

In Figure 20 three different ranges of accessibility of the ruthenium complexes in three different environments by oxygen can be identified: 100% for **1** homogeneously dissolved in various solvents, 29 - 48% for **1** in porous materials **A** - **D** and between 0 and 10% of **1** in nonporous **E**. In the materials **A** - **D**, the fraction of accessible ruthenium complexes α varies depending on the solvent (Figure 20). Thus in THF there are up to 60% of the ruthenium complexes better accessible than in MeOH. Only minor changes can be observed which can be related to the different materials. For **A** - **D**, the quenching rate constant k_2 is far from the values observed for **1** in the corresponding solutions (Table 5). This indicates that those ruthenium complexes whose luminescence is quenched by dioxygen are not solvated by the liquid phase as well as **1** in solution. This means that the solvent does not penetrate within the polysiloxane, in other words: the Ru complex is solvated mainly by the sol-gel matrix and not by the liquid. Due to the smaller pore sizes of **A** the values of k_2 are as well smaller than for the other polysiloxanes (Table 5). In summary, two types of ruthenium complexes can be distinguished. The first type is not accessible to oxygen dissolved in the liquid phase. The luminescence of the second type is quenched by oxygen with rate constants that are smaller than those obtained for ruthenium complexes dissolved in solvents.

5.1.5.6 Luminescence decay curves of **1** in different matrices in the presence of anthracene

To determine the accessibility of tethered ruthenium complexes for organic molecules, anthracene is added to the liquid phase of the polymer suspensions. Energy transfer from the ^{3}MLCT excited state of the ruthenium complex to anthracene leads to quenching of the ruthenium luminescence.

Table 6. Quenching rate constants $k_2 / 10^6$ s^{-1} and accessibility factors α (in parentheses) of the luminescence quenching by anthracene of **1** in solution and in suspensions of **A** - **D** under different quenching conditions

	1	**A**	**B**	**C**	**D**
Hexane	Not Soluble	3.2 (0.37)	4.2 (0.37)	4.1 (0.39)	3.4 (0.33)
THF	1.4 (1)	0.06 (0.14)	0.3 (0.12)	0.2 (0.21)	0.1 (0.16)
MeCN	2.7 (1)	1.1 (0.13)	1.9 (0.13)	1.6 (0.16)	0.9 (0.13)
MeOH	3.2 (1)	0.4 (0.10)	1.1 (0.12)	1.1 (0.14)	0.4 (0.10)

In solution, quenching of the ruthenium luminescence results in the reduction of luminescence lifetimes, the decay curves remain single exponential (Figure 21 and Table 6). From the luminescence decay curves the rate constants k_2 and accessibility factors α for the quenching process are calculated according to Eq. 14b. In solutions of **1**, $\alpha = 1$ is obtained, that is, all ruthenium complexes are equally accessible by anthracene (Table 6).

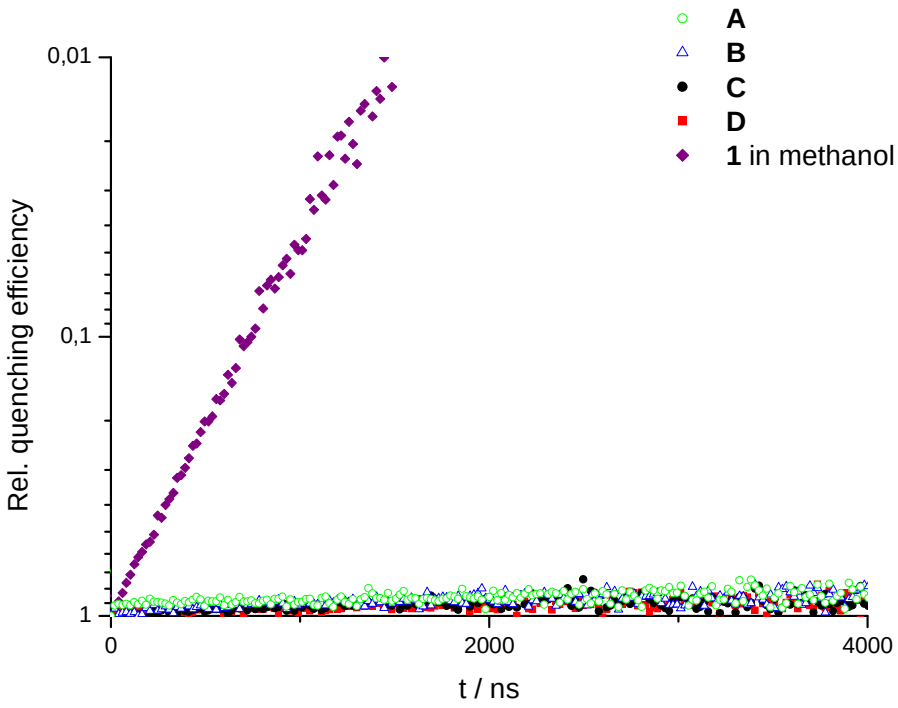

Figure 21. Relative efficiencies for the quenching of **1** luminescence by anthracene in a methanol solution and suspended materials **A** - **D** in methanol

Looking at the values of quenching rate constant k_2, one can observe that they are smaller for **A** – **D** than for **1** in the corresponding solutions (Table 6). This means that the solvation by the liquid phase of those ruthenium complexes whose luminescence is quenched by anthracene is not as good as **1** in solution and therefore one can conclude that the solvent does not penetrate within the polysiloxane network. Interestingly the values of k_2 in hexane are higher for anthracene as a quencher than for oxygen. Two kinds of ruthenium complexes can be distinguished. One of these populations is not quenched by anthracene, whereas the other one is quenched with the rate constant k_2. The absolute values of the accessibility factors α found for anthracene are significantly smaller than those observed for oxygen because the bigger size of ANT partially prevent their penetration into the porous materials. In the case of hexane the accessibilities are in the same order (Figures 20 and 22 and Tables 5 and 6) maybe because the better solubility of the ANT in the non-polar solvent. The values of α in the non-porous material **E** are appreciably smaller.

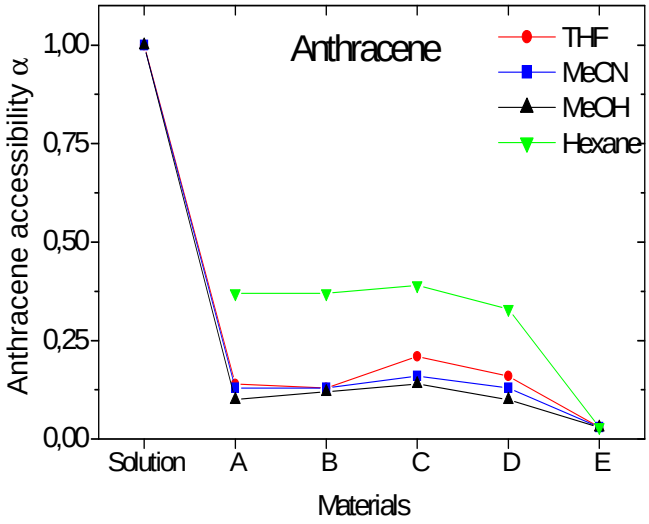

Figure 22. Accessibility factors for luminescence quenching by anthracene of **A** - **D** and of **1** in different solvents

In Figure 22 it can be observed that the accessibility of ruthenium complex quenched by anthracene is 100% for **1** dissolved in various solvents. In materials **A** - **D** two different behaviours can be observed, when the solvent is polar (acetonitrile, methanol and THF) the accessibility ranges between 10-21%, with a slightly better accessibility for materials **C**, whereas in *n*-hexane α increases to 34-39%. Thus in *n*-hexane there are up to three-fold of the ruthenium complexes better accessible than in polar solvents for materials **A** – **D** (Figure 20). One explanation can be the better solubility and diffusion of the anthracene in *n*-hexane. For nonporous material **E** the accessibility is ranged between 0 and 4%.

5.1.5.7 Luminescence decay curves of **2** in different matrices without quencher

The luminescence decay curves of **2** dissolved in low viscous solutions are single exponential with decay times of τ_F = 160–240 ns. For suspensions of the polysiloxanes **A** - **D** in all investigated solvents, slightly non-exponential decay curves are observed. This type of decay curves is best described by narrow distributions of decay times, but can also be fitted by sums of two exponential functions without loss of accuracy. The nonexponentiality of the decay is due to the inhomogeneity of the environment. There are two components, the first decay time, τ_1 = 40-70 ns is shorter than the fluorescence lifetime of **2** in solution and corresponds to the

fluorophore which is in contact ("solvated") with the matrix, whereas τ_2 = 140-240 ns, is about the same order than in solution, which means that **2** is as well solvated in materials **A** - **D** as in solution. Additionally, for suspensions of the nanoparticles, the decay curves are strongly non-exponential, which is due to the strong interaction of the probes, to a minor extent with the surface but mainly with the neighbouring pyrene moieties, which at least partly result in excimer formation. Also in this case, biexponential fits yield sufficient accuracy. Two decay times appear for **2NP**: τ_1 = 10-25 ns and τ_2 = 130-200 ns. The shorter one corresponds to the interaction between neighbouring pyrenes and the explanation for the larger is similar to the one for sol-gel materials **A** - **D**.

5.1.5.8 Luminescence decay curves of **2** in different matrices in the presence of oxygen

Quenching of pyrenemethanol by energy transfer to dioxygen is a bimolecular process requiring close contact between donor and acceptor. The efficiency of luminescence quenching thus depends as in the case of **1** on both the mobility of oxygen in the interphase and the accessibility of the probe.

Table 7. Quenching rate constants $k_2 / 10^6$ s^{-1} and accessibility factors α (in parentheses) for the luminescence quenching by oxygen of **2** in solution, in suspensions **A** - **D** and **2NP** under different quenching conditions

	2	**A**	**B**	**C**	**D**	**2NP**
Hexane	49.3(1)	53.3 (0.38) 7.4 (0.49)	36.0 (0.67) 4.6 (0.18)	36.6 (0.59) 6.8 (0.27)	65.4 (0.48) 7.1 (0.40)	20.1 (0.95)
THF	38.6 (1)	39.1 (0.62) 6.1 (0.29)	40.7 (0.60) 8.6 (0.31)	34.8 (0.63) 8.2 (0.30)	38.9 (0.61) 7.8(0.29)	18.5 (0.95)
MeCN	48.4 (1)	53.6 (0.58) 8.5 (0.30)	47.5 (0.54) 5.0 (0.30)	41.6 (0.53) 9.5 (0.37)	46.6 (0.57) 9.1 (0.35)	20.0 (0.92)
MeOH	40.2 (1)	46.4 (0.61) 7.2 (0.34)	46.4 (0.48) 11.4 (0.43)	42.6 (0.47) 9.6 (0.48)	53.6 (0.46) 12.0 (0.41)	18.4 (0.89)

Evaluation of the time-resolved luminescence decay curves according to Eq. 17 yields values for k_2 and α, describing the mobility of oxygen and the fraction of accessible pyrenemethanol (Figure 23 and Table 7).

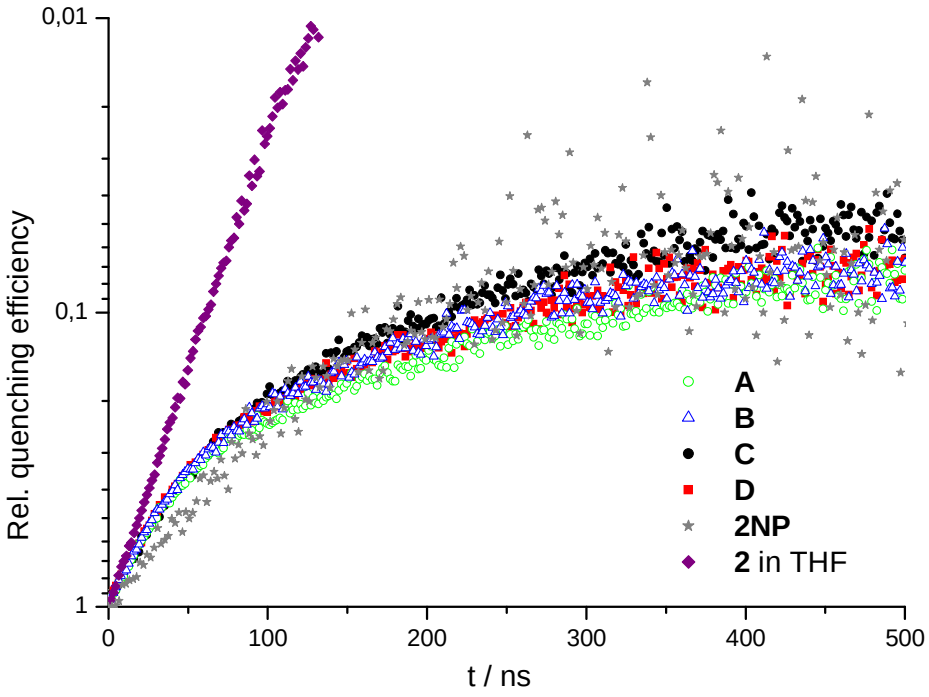

Figure 23. Relative efficiencies for the quenching of the luminescence of **2** by oxygen, of **2** in a THF solution, suspended materials **A** - **D** and **2NP** in THF

In homogeneous solutions of **2**, α=1, that is, all the probe molecules are equally accessible by oxygen (Figure 24 and Table 7). For **2NP**, $\alpha \geq 0.91$ which is comparable to that in solution. This means that more or less all probes are well accessible, almost like in solution, except for the already mentioned small shielding by the silica surface and the adjacent fluorophore.

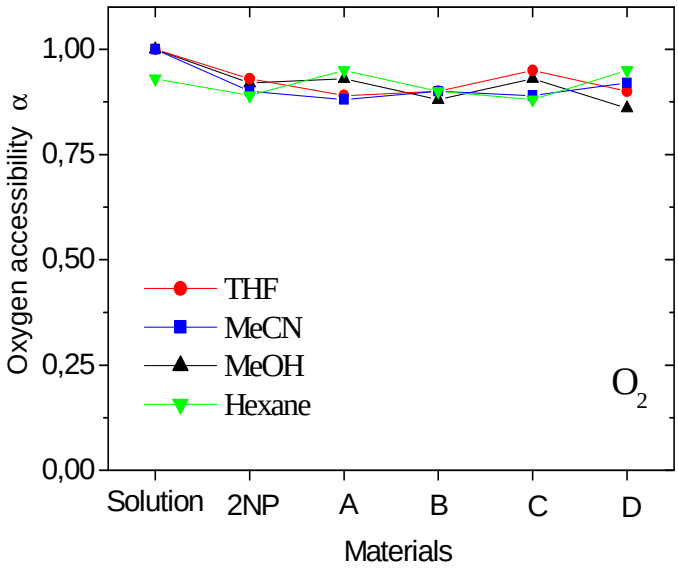

Figure 24. Accessibility factors for luminescence quenching by oxygen in **A** - **D**, nanoparticles and **2** in different solvents

Just two ranges of accessibility are observed (Figure 24). The accessibility of the pyrenemethanol by oxygen is 100% when **2** is on solution. The accessibilities of **2** in sol-gel materials **A** – **D** and in **NP** in suspension of different solvents are of the same range, situated between 86 and 95%. There is no dependence of the accessibility with the solvent or sol-gel materials. The quenching rate constants k_q are around $2 \cdot 10^{10}$ M^{-1} s^{-1} which means that quenching by oxygen is diffusion controlled. The rate constants are thus determined by the diffusion coefficient of oxygen in the respective solvents. For **2** the k_2 values of **2NP** are approximately half of those in solution which means that the fluorophore is not as well solvated as in **2NP**, probably due to the geometrical shielding by the surface of the nanoparticle (Table 7).[125-130] For the sol-gel materials **A** – **D** there are clearly two quenching components. As the decay times of the unquenched samples are very similar, the curves are evaluated according to Eq. 17. Two components are obtained where $k_{21} < k_{22}$ (Table 7). k_{22} is of the same order as k_2 in solution, which means that **2** is as well solvated in materials **A** - **D** as in solution. One may conclude that this population of **2** is located at the surface of materials **A** – **D**. On the other hand k_{21} is smaller than k_2 in solution and corresponds to fluorophores which are more buried into the matrix.

5.1.5.9 Luminescence decay curves of **2** in different matrices in the presence of N,N-diethylaniline

Evaluation of the time-resolved luminescence decay curves according to Eq. 17 yields values for k_2 and α, describing the mobility of N,N-diethylaniline and the fraction of accessible pyrenemethanol in the different materials (Figure 25 and Table 8). The values of the rate constants are smaller than that for oxygen. The smaller rate is quantitatively explained by the smaller diffusion coefficient of DEA vs. the diffusion coefficient of oxygen. The values of the k_2 for **2NP** are approximately of the same order of magnitude as the ones in solution, which means that **2** is well solvated by the liquid (Table 8).

Table 8. Quenching rate constants k_2 / 10^6 s^{-1} and accessibility factors α (in parentheses) for the luminescence quenching by N,N-diethylaniline of **2** in solution, in suspensions of materials **A** - **D** and **2NP** under different quenching conditions

	2	**A**	**B**	**C**	**D**	**2NP**
Hexane	8.6 (1)	7.7 (0.51) 4.7 (0.37)	8.4 (0.23) 5.9 (0.61)	7.9 (0.76) 3.3 (0.16)	7.6 (0.26) 5.8 (0.67)	5.07 (0.88)
THF	5.6 (1)	6.4 (0.58) 4.5 (0.24)	6.0 (0.60) 4.5 (0.18)	5.6 (0.69) 4.2 (0.14)	5.7 (0.64) 4.2 (0.23)	5.90 (0.87)
MeCN	13.1 (1)	13.1 (0.18) 7.1 (0.55)	11.9 (0.75) 6.0 (0.19)	12.6 (0.40) 5.8 (0.43)	12.1 (0.59) 7.5 (0.25)	6.02 (0.85)
MeOH	6.7 (1)	7.7 (0.67) 4.9 (0.27)	6.4 (0.48) 4.5 (0.34)	6.8 (0.29) 4.7 (0.55)	6.7 (0.20) 4.5 (0.51)	8.96 (0.84)

For the materials **A** – **D** there are two different components $k_{21} < k_{22}$, where k_{21} is approximately in the same range as k_2 of **2** in solution which means that the fluorophore is as well solvated as in solution. k_{22} is slightly smaller than k_2 of **2** and corresponds to fluorophores which are more buried into the matrix.

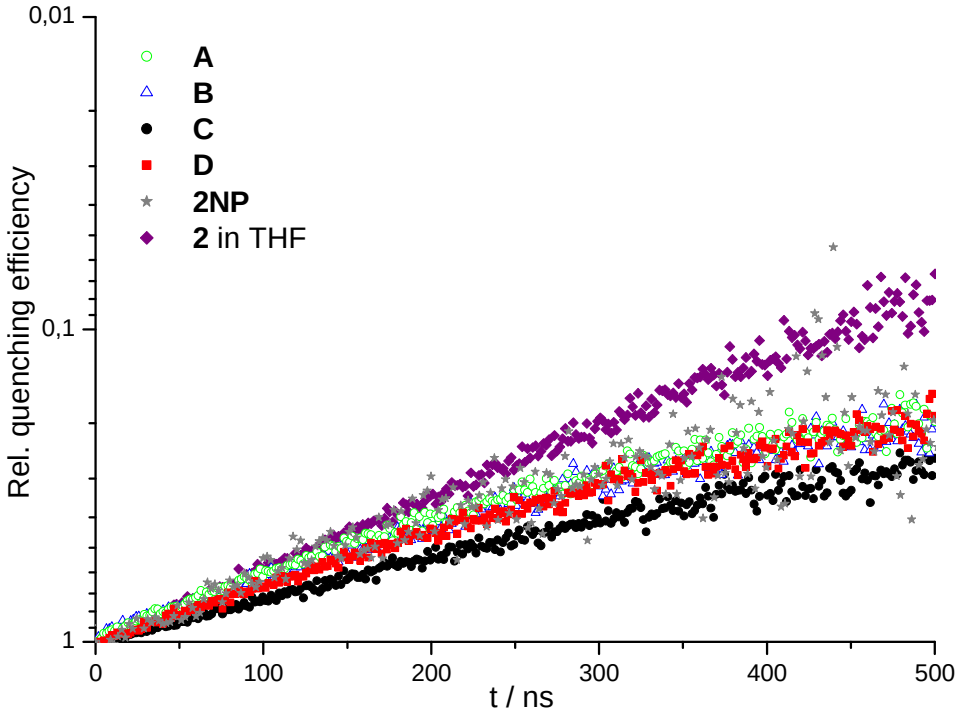

Figure 25. Relative efficiencies for the quenching of **2** luminescence by N,N-diethylaniline. Measured for **2** in a THF solution and suspended materials **A** - **D** and nanoparticles in THF

Just two ranges of accessibility are observed (Figure 26). The accessibility of the pyrenemethanol by N,N-diethylaniline is almost 100% when it is on solution. The

accessibilities of **2** in sol-gel materials **A** – **D** and in **NP** in suspension of different solvents are of the same range, situated between 71 and 93%. No solvent dependence was observed. Moreover there is no dependence of the accessibility with the solvent or sol-gel materials.

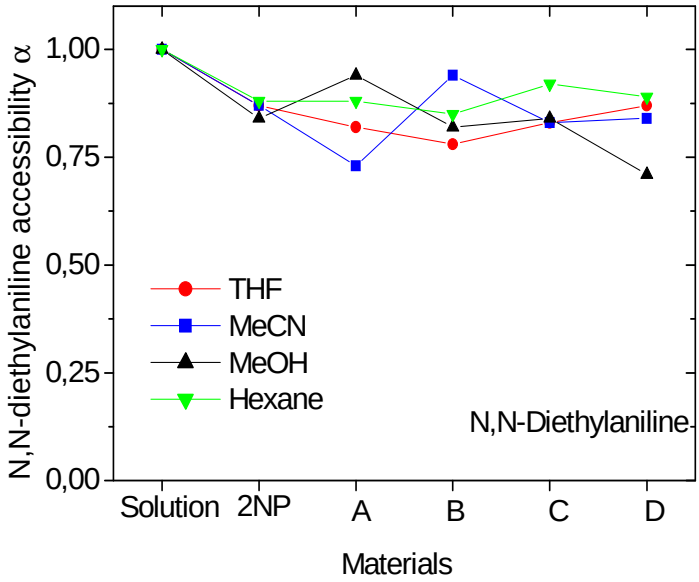

Figure 26. Accessibility factors for luminescence quenching by N,N-diethylaniline in **A** - **D**, nanoparticles and **2** in different solvents

5.1.6 Conclusions

To achieve the chemical incorporation of the two fluorophores **1** and **2** into a polysiloxane network both were added to the reaction mixture of the sol-gel process. The introduction of a buffer system in order to control the kinetics of the hydrolysis and condensation reactions in the sol-gel process has been the key to the successful synthesis of porous sol-gel materials with high surface area and a narrow size distribution. Applying four different drying procedures allowed only slight modification of the surface area and the porosity of the sol-gel materials **A** – **D**. Nanoparticles of approximately 200 nm were synthesised following the Stöber process. Compounds **1** and **2** were tried to covalently attach on the surface of the nanoparticles. While this has been successfully achieved for **2** the poor solubility in the appropriate solvents made it impossible for **1.**

The materials were characterised by solid-state NMR spectroscopy, BET measurements as well as steady-state and time resolved luminescence spectroscopy. The solid-state NMR spectra show that the materials **A** – **D** are

dominated by Q groups and that they have a high degree of condensation (90%). High surface areas between 600-800 m^2/g and pore sizes ranging from 1.19 to 2.65 nm with ink-bottle pore shapes were confirmed by BET measurements. Steady-state and time-resolved luminescence measurements make available a vision of the materials at their molecular level.

The accessibility of **1** by oxygen in the materials **A** – **D** is solvent dependent. In suspension of the slightly polar solvent THF, the accessibility of **1** is increased by around 60% compared with a suspension of the more polar methanol. In material **C** the accessibility is vaguely higher than in materials **A**,**B**,**D**. When the fluorophore **1** is quenched by ANT, the accessibility is smaller than for oxygen which is mainly due to the larger size of the organic molecule which can not reach so many fluorophores as the smaller oxygen. In materials **A** - **D** two different behaviours can be observed. When the solvent is polar (acetonitrile, methanol and THF) the accessibility ranges between 10-21%, with a slightly better accessibility for materials **C**, whereas in *n*-hexane α increases to 34-39%. The values in suspension of polar solvents decrease by about 50% with respect to those when oxygen is the quenching molecule. In contrast to this, for the non-polar *n*-hexane the values of accessibility are maintained constant. The luminescence measurements reveal as well that there are two populations of ruthenium complexes: the first type is inaccessible to the quencher dissolved in the liquid phase. The luminescence of the second type is quenched with rate constants that are smaller than those obtained for **1** dissolved in homogeneous solutions.

The accessibility of **2** quenched by oxygen in the materials **A** – **D** and **2NP** is solvent independent. As **2** is anchored on the surface of **2NP**, the values of their accessibility give the maximal accessibility when the only impediment is the silica shield. Since the accessibility of **2** in the materials **A** – **D** is of the same rate, around 90%, one can conclude that the fluorophore in the silica materials are located at the surface of the pores. In the same way as for **1**, when **2** is quenched by DEA, the accessibility is smaller than for oxygen which is mainly due to the larger size of the organic molecule. The accessibility in the case of DEA goes down to 80-85%. The luminescence measurements reveal as well that there are three populations of **2** in the materials **A** – **D**: the first one is a small population of fluorophores which are inaccessible to the quencher dissolved in the liquid phase. The second type is quenched with rate constants that are smaller than those obtained for **2** dissolved in

a homogeneous solution. These fluorophores are partially “solvated” by the matrix. They are probably located close to the surfaces of the pores and are partially solvated by the matrix. And the third one is quenched with rate constants that are similar to those in homogeneous solution which means that they are as good solvated as in the solution. These are situated at the surface of the materials and are very well solvated by the liquid, which points to a position in large pores or at the circumference of the sol-gel particle.

Moreover, comparing these results with the non-porous material **E**, one can conclude that the accessibility dramatically depends on the surface area of the sol-gel materials. Thus the performance of the sol-gel process already decides about the accessibility of embedded molecules. This is supported also by the strong difference of the accessibility of the cationic ruthenium complex **1** and the nonpolar organic molecule **2**. As the sol-gel process is carried out in a strong polar environment the nonpolar organic molecule **2** is directed more to the surface of the material while the polar complex **1** is incorporated into the silica material.

5.2 SYNTHESIS AND CHARACTERISATION OF FUNCTIONALISED POLYHEDRAL SILSESQUIOXANES (FPOSS)

5.2.1 Introduction

Since their discovery by Sprung and Guenther in 1955 “as a curious white precipitate” during silane polymerisations, the studies and applications of the polyhedral oligomeric silsesquioxanes (POSS) have been exponentially increased.[99;102;131] Nowadays, the investigations of POSS focus on the incomplete condensed silsesquioxanes and the attachment of catalysts and other molecules to them.[56;58-60] The main advantage of POSS over other silica materials is their easier characterization through common analytical measurements like NMR spectroscopy. Moreover, the inorganic nucleus of the silsesquioxanes allows the constructions of one-, two- and even three-dimensional materials nanometer by nanometer under complete control of the periodicity up to the millimetre and even centimetre region.[60] For this the functionalisation of the silsesquioxane is of importance to broaden the scope of their chemistry.

For the synthesis of new functionalised POSS two different methods have been reported (Scheme 8).

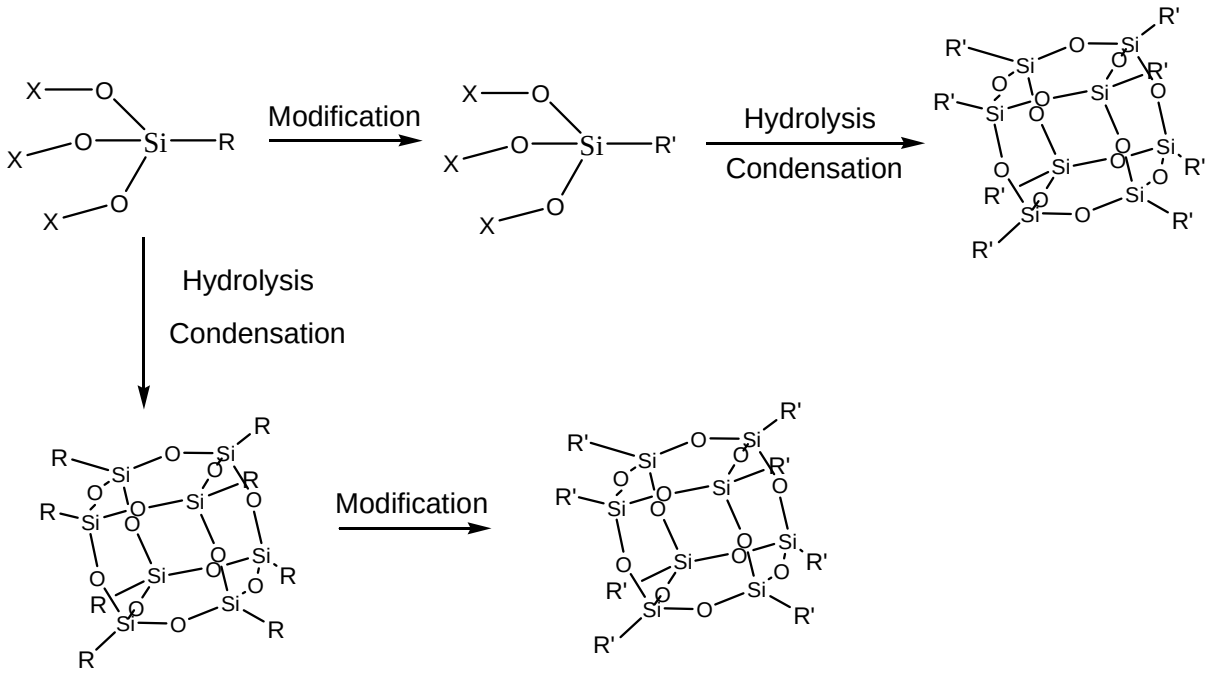

Scheme 8. Synthesis of silsesquioxanes (POSS)

The first one is the modification of T-alkoxysilanes and their subsequent hydrolysis and condensation to generate the caged silsesquioxanes. In the second technique the POSS is synthesised with an organic functional group, which can easily be modified to the desired function. Two examples of the last type of synthesis were performed with the octavinylsilsesquioxane **3**[89] and the octapropylammoniumchloride silsesquioxane **4**. [56;100;132]

Synthesis of octavinylsilsesquioxane **3** is supported by the ion exchanger Amberlite IR-120 which was activated through concentrated HCl. A white powder was obtained after evaporation of the solvent in a yield of 30% (Scheme 9).

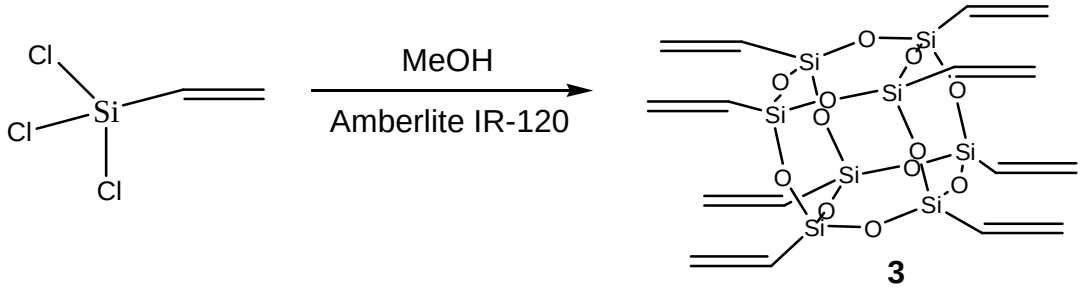

Scheme 9. Synthesis of **3**

The synthesis of compound **4** was first claimed in a 1991 US patent issued to Wacker-Chemie (Scheme 10).

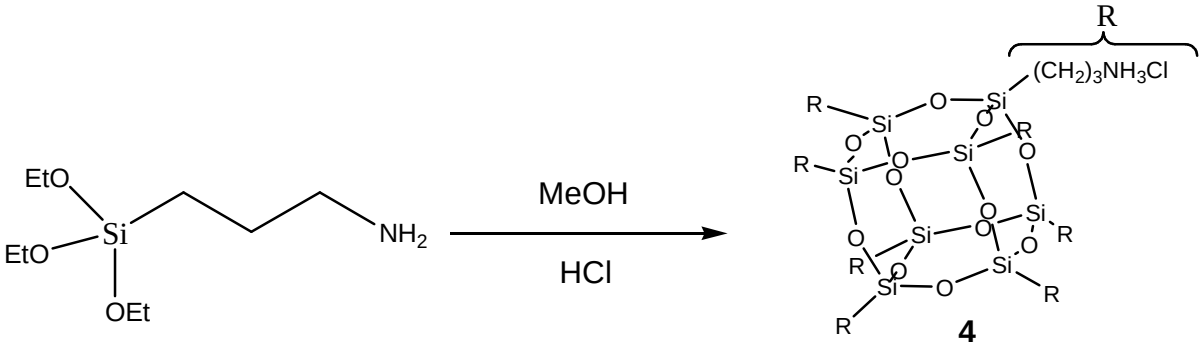

Scheme 10. Synthesis of **4**

The deprotection of the amino groups in **4** to the free amine is difficult to accomplish without compromising the Si_8O_{12} framework. One of the easier methods to achieve the neutralisation was through the ion exchanger Amberlite IRA-400 (Scheme 11).[89] This resin was activated washing it repetitively with water, NaOH solution (1M) and finally with water and methanol to eliminate the sodium chloride.[56]

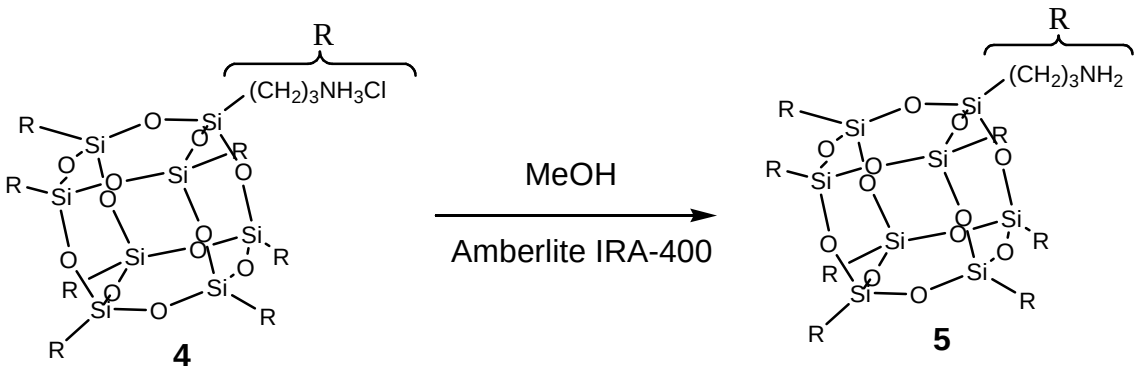

Scheme 11. Synthesis of **5**

The octapropylaminosilsesquioxane **5** is unstable at room temperature because the amine destroys the cage in a self-catalysed process within a few hours (Scheme 12).

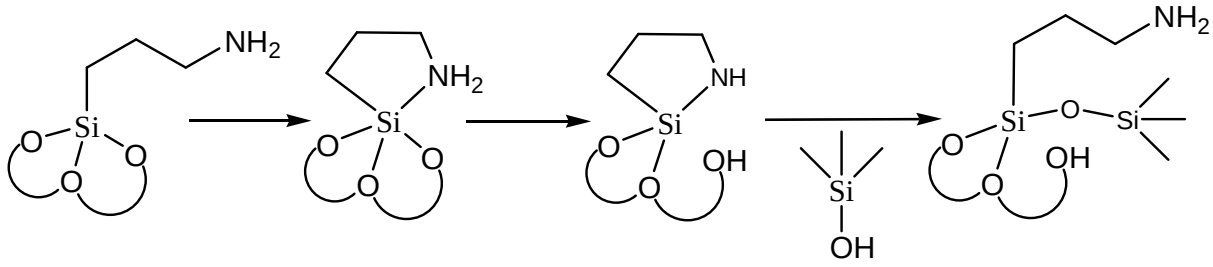

Scheme 12. Self-catalysed decomposition of **5**

The above mechanism shows that the amine acts as a nucleophile which attacks the silicon to form a stable five-membered ring. In a consecutive step a Si-O bond is cleaved which leaves the silicon open for another nucleophilic attack by an SiO^- nucleophile. This leads to a polymerisation of a silica network. Thus the silsesquioxanes are sensitive in basic conditions whereas in acidic environments they are more stable.[56]

5.2.2 Synthesis of octa(3-(ethylmercapto)-propionic acid) silsesquioxane (6)

For the synthesis of **6** two different pathways were developed (Scheme 13). The first one is the radical addition of a thiol to the vinylsilsesquioxane **3** using azoisobutyronitrile (AIBN) as a radical initiator. This reaction was performed with a slight excess of thiol at 80℃ and was applied by S eshadri for silanes[133] other authors have used this reaction for organic synthesis.[134;135]

The second pathway was a catalytic reaction, where the propylamine acts as a catalyst.[136] In a Michael's type addition the thiol groups were added to the vinyl groups of the silsesquioxane **3**. Due to the sensibility of the Si-O-Si bonds towards bases, the amount of the quantity of polyamine must be very carefully adjusted and the reaction has to be performed at room temperature. The white powder of **6** is air stable and easily dissolves in polar solvents. Both methods led selectively to the *anti*-Markovnikov product in good yields.

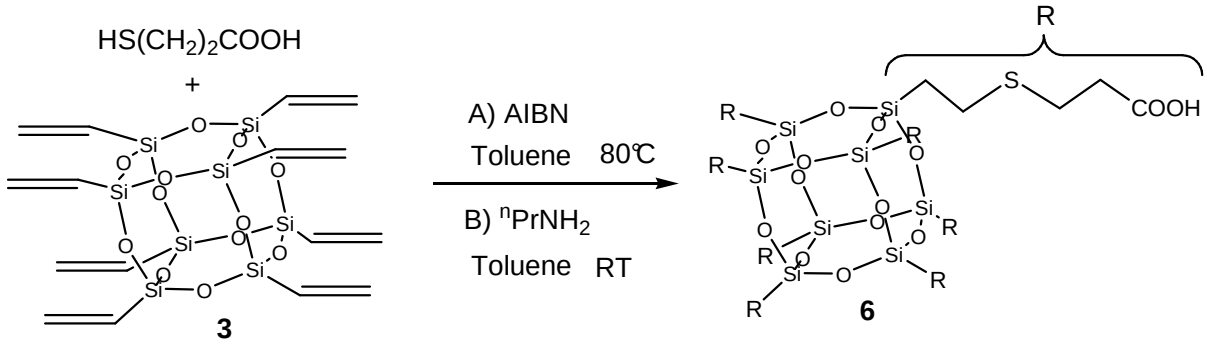

Scheme 13. Synthesis of **6**

5.2.3 Synthesis of octa(3-(ethylmercapto)-propionacyl chloro) silsesquioxane (7)

By treatment of **6** with oxalyl chloride in dichloromethane the carboxylic acids can be transformed into acyl chlorides in quantitative yield (Scheme 14). The new silsesquioxane **7** is tremendously sensitive even to traces of water. This prevents the complete characterisation by MS and NMR spectroscopy. The light yellow powder is difficult to dissolve in polar and non-polar solvents.

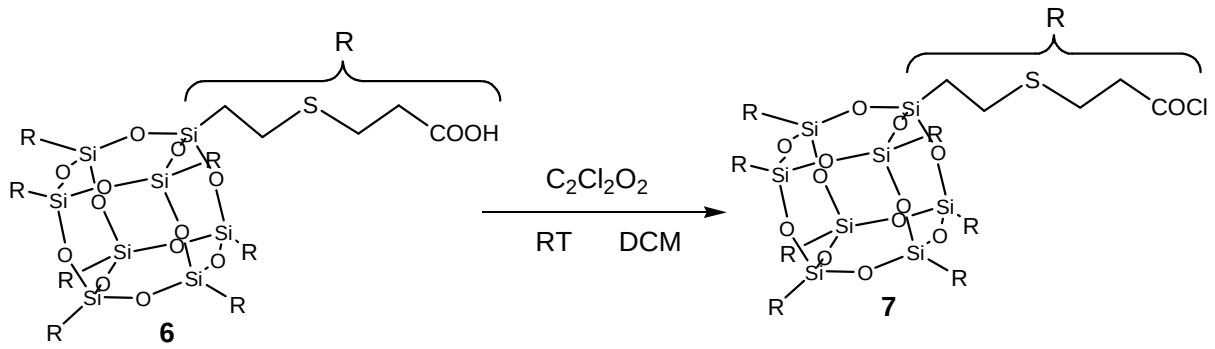

Scheme 14. Synthesis of **7**

5.2.4 Synthesis of octa(ethylbromo) silsesquioxane (8)

The chemistry of octa(ethylbromo) silsesquioxane (**8**) has only poorly been developed due to the synthesis procedure which requires radical initiators and time consuming recrystallisations resulting in yields of around 50%.[137;138] Therefore a new method is reported here which provides an easy access to **8** (Scheme 15). Through a suspension of octavinylsilsesquioxane **3** in dry hexane in a quartz flask is bubbled freshly prepared HBr[139] for two hours and irradiated with UV light. The bright brown octa(ethylbromo) silsesquioxane **8** is obtained exclusively as *anti*-Markovnikov product which is air stable and soluble in a broad range of polar solvents. With this new technique **8** can be produced in quantitative yields and in just two hours. Moreover much smaller quantities of solvents were necessary.

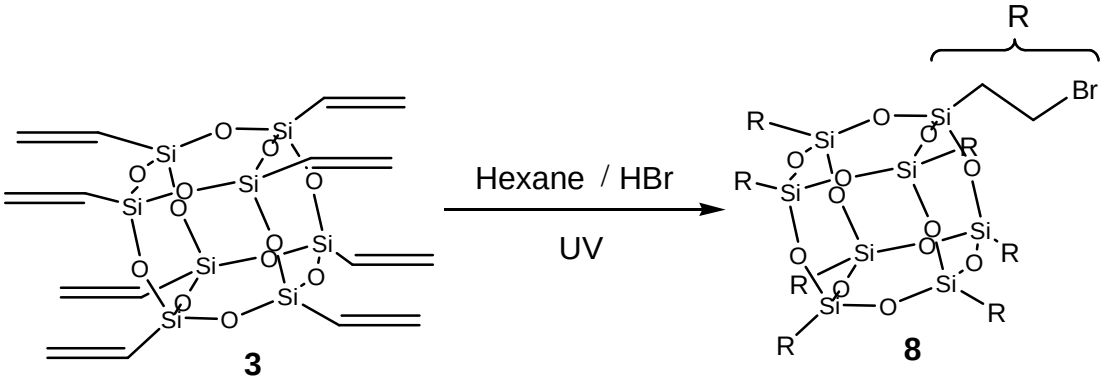

Scheme 15. Synthesis of **8**

5.2.5 Synthesis of octa(ethyliodo) silsesquioxane (9)

This compound was synthesised applying the Finkelstein reaction.[140] Here the treatment of a primary alkyl halide or pseudohalide with an alkali metal halide (e.g. NaI) leads to the replacement of the halogen via an S_{N2} reaction. The equilibrium position of the reaction depends on the nucleophilicity of the anion, whether a good leaving group is present, and whether one anion is better stabilized than the other in a given solvent (Scheme 16).

An excess of sodium iodide was applied to a solution of dry acetone with **8** and heated to reflux for 48 hours. The yellow powder, which was produced in an acceptable yield of 45%, is air stable and soluble in polar solvents.

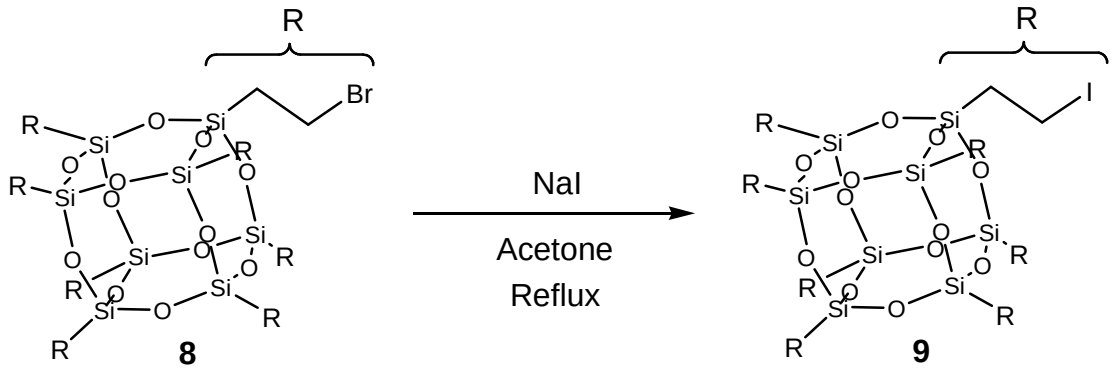

Scheme 16. Synthesis of **9**

5.2.6 Synthesis of ferrocenyl functionalised silsesquioxane (10)

Carefully dried amino silsesquioxane **5** was dissolved in THF together with diisopropylethylamine (DIPEA). The mixture was stirred and a solution of ferrocene acyl chloride in THF was added. The DIPEA works as a base that trapped the HCl resulting from the reaction between the ferrocene acyl chloride and the octapropylaminesilsesquioxane. After 48 hours of stirring at room temperature the solvent was removed and the solid material was washed with chloroform, to eliminate the excess ferrocene acyl chloride and with methanol to remove the partially-reacted silsesquioxane species (Scheme 17).

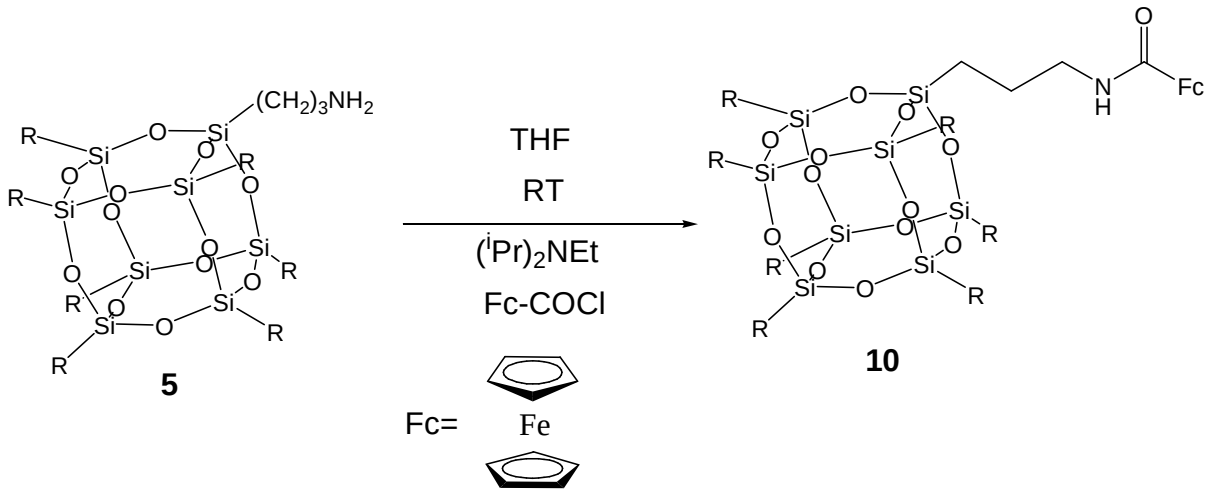

Scheme 17. Synthesis of **10**

The experiment was performed first with the absence of the base DIPEA to know how would be the behaviour of the bands in the ^{1}H NMR when the silsesquioxane was not completely substituted with the ferrocene. In the Figure 27

the two reactions can be compared. One observes that the silsesquioxanes are not completely substituted. They have some arms substituted by ammonium chloride (1,2,3 in Figure 27) and some by ferrocene (a,b,c in Figure 27).

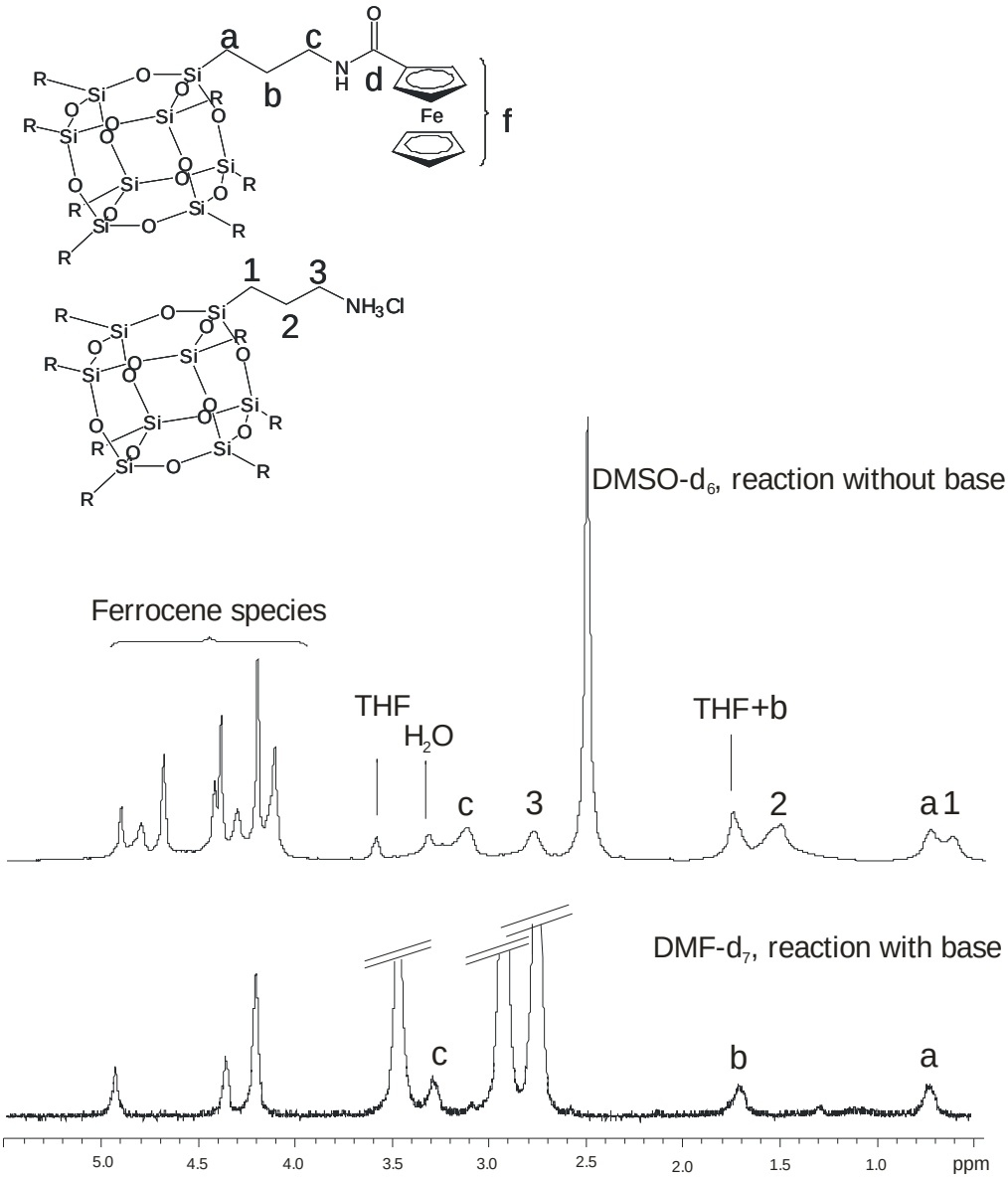

Figure 27. ^{1}H NMR spectra of **10** in absence and presence of base DIPEA in DMSO-d_6 and DMF-d_7

5.2.7 Synthesis of SCS-pincer complex functionalised silsesquioxanes (12, 14)

The reaction of the silsesquioxane precursor **7** with the SCS pincer aniline **11**[141] in dry THF under inert and room temperature conditions resulted in **12** as the

fully condensed T_8 silsesquioxane containing eight SCS pincer ligands (Scheme 18). After purification by flash chromatography this compound was obtained in high purity and moderate yield (33%) as an air stable white crystalline solid. The immense versatility towards solubility resulted in homogeneous solutions in DCM, $CHCl_3$, THF, alcohols, ethers, DMSO and DMF.

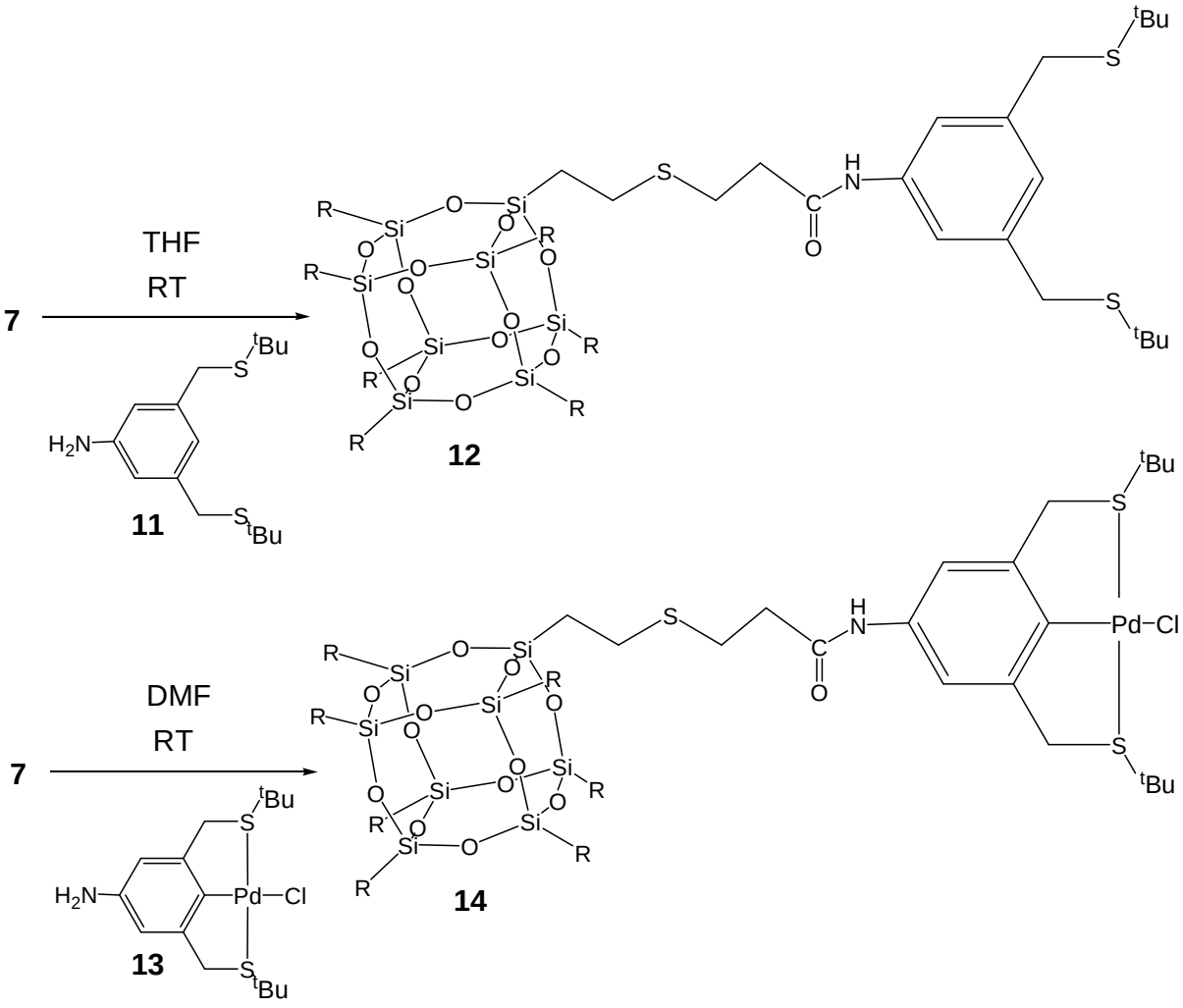

Scheme 18. Synthesis of **12** and **14**

Trials towards palladation of **12** at the pincer ligands were not promising. When the Pd(II) precursor was exposed to a solution of **12** in THF, the immediate formation of an orange polymer was indicated by precipitation from the solution. It could be thought that the coordination of S-Pd-S takes place by affording bigger molecules that decreases the solubility which hinders the further formation of the C-Pd sigma bond.

As a consequence, another approach was undertaken. By stoichiometric reaction of the fully characterised aniline SCS palladacycle **13**[141] to the acyl chloride

end groups of the main silsesquioxane precursor **7** in dry DMF under inert and room temperature conditions during 14 h resulted in **14** in very good yield (100 %) as shown in Scheme 18. This T_8 functionalised polyhedral silsesquioxanes (FPOSS) containing SCS palladacycles resulted in an orange solid and as an air stable compound with good solubility in DMSO and DMF and poor solubility in THF and chlorinated solvents.

5.2.8 Characterization of the silsesquioxanes 6 – 10, 12, 14

The ^{1}H, $^{13}C\{^{1}H\}$ and $^{29}Si\{^{1}H\}$ NMR spectra of the polyhedral silsesquioxanes **6** – **10**, **12**, **14** confirm the structures of the compounds displayed in Schemes 13 - 18. Selected spectroscopic data are summarised in Table 9 while more details are given in the experimental part. Especially the sharp singlets which were observed between δ -67.97 and -70.41 in the solution ^{29}Si NMR spectra of **6** - **9** and **12**, **14** are consistent with a high symmetry of the cage compounds and agree with a complete functionalization at all eight sides of the T_8 cage. This is supported by the elemental analyses of the silsesquioxanes **6**, **8** – **10**, **12**, **14** and by HR ESI mass spectrometry in the cases of **6**, **8**, **10**, **12** which verified the compositions of the compounds and prove that the substances can be synthesised with high purity. The acyl chloride **7** did not give any satisfactory analysis due to its high sensitivity towards even small amounts of moisture. As well for the palladium pincer silsesquioxane **14** no mass spectrum with a molecular peak could be obtained. Moreover the solubility of the ferrocenyl silsesquioxane **10** is too poor to achieve a ^{29}Si NMR spectrum in a reasonable time.

In the IR spectra of **6** – **10**, **12**, **14** the T_8 cages give rise to asymmetric stretching frequencies of the Si-O-Si units between 1124 and 1109 cm^{-1} while the Si-O-Si bending modes are observed between 486 and 466 cm^{-1}.[95] The shift of the ν(CO) from 1708 cm^{-1} in **6** to 1820 cm^{-1} in **7** suggests that the acid has been successfully converted to the acid chloride. Moreover the carbonyl stretching frequencies at 1635 (**10**), 1665 (**12**) and 1727 cm^{-1} (**14**), respectively, provide evidence that the ferrocenyl, the SCS pincer ligand and the palladium complex have been efficiently connected to the amine functions of the silsesquioxane **5**.

The number of multiplets in the ^{1}H NMR spectra and the resonances in the $^{13}C\{^{1}H\}$ NMR spectra of the functionalized silsesquioxanes **6** – **10**, **12**, **14** also

confirm the high symmetry of the compounds. Interestingly the multiplet patterns of the ethylene and the propylene groups in the ^{1}H NMR spectra reflect the mobility of the functional groups attached to the T_8 cage.

Table 9. Selected spectroscopic data of the silsesquioxanes **3**, **4**, **6**-**10**, **12**, **14**

	^{29}Si [ppm]	^{1}H Si-CH_X [ppm]	^{1}H Si-CH_X-CH_Y [ppm]	^{13}C Si-CH_2 [ppm]	^{13}C Si-CH_2-CH_2 [ppm]	IR [cm^{-1}]
Vinyl **3**	79.80	5.7 -6,1		128.70	136.90	1605 ($CH=CH_2$) 1109 ν_{AS}(Si-O-Si)
COOH **6**	68.28	1.08	2.72	13.97	26.81	2915 ν(C-H) 1708 ν(C=O) 1124 ν_{AS}(Si-O-Si) 466 δ(Si-O-Si)
COCl **7**	68.78	0.99	2.60	12.69	26.31	2915 ν(C-H) 1820 ν(C=O) 1120 ν_{AS}(Si-O-Si) 471 δ(Si-O-Si)
Br **8**	70.22	1.52	3.52	18.32	27.39	2922 ν(C-H) 1116 ν_{AS}(Si-O-Si) 470 δ(Si-O-Si)
I **9**	70.41	1.53	3.21	19.34	-2.72	2921 ν(C-H) 1109 ν_{AS}(Si-O-Si) 466 δ(Si-O-Si)
NH_3Cl **4**	66.40	0.71	1.71	8.44	20.61	3023 $\nu(NH_3^+)$ 2903 ν(C-H) 1110 ν_{AS}(Si-O-Si)
Fc **10**		0.79	1.77			2926 ν(C-H) 1635 ν(C=O) 1543 δ(NH) 1116 ν_{AS}(Si-O-Si) 486 δ(Si-O-Si)
SCS **12**	68.52	0.97	2.54	13.17	26.61	3309 ν(NH) 1665 ν(CO) 1121 ν_{AS}(Si-O-Si)
SCS-Pd **14**	67.97	1.12	2.61	12.80	25.54	1727 ν(C=O) 1115 ν_{AS}(Si-O-Si)

In general a hindered internal rotation around the C-C bond in ethylene units is associated with AA'XX' spin patterns while the observation of triplets speaks for a free C-C bond rotation.[142;143] Applying this criteria to compounds **6** - **9**, **12**, and **14** one can show that the C-C bond rotation depends on the size of the functional group

and its distance to the T_8 cage. Thus in **8** and **9** the iodo and bromo ethyl groups freely rotate around the C-C bond (Figure 28).

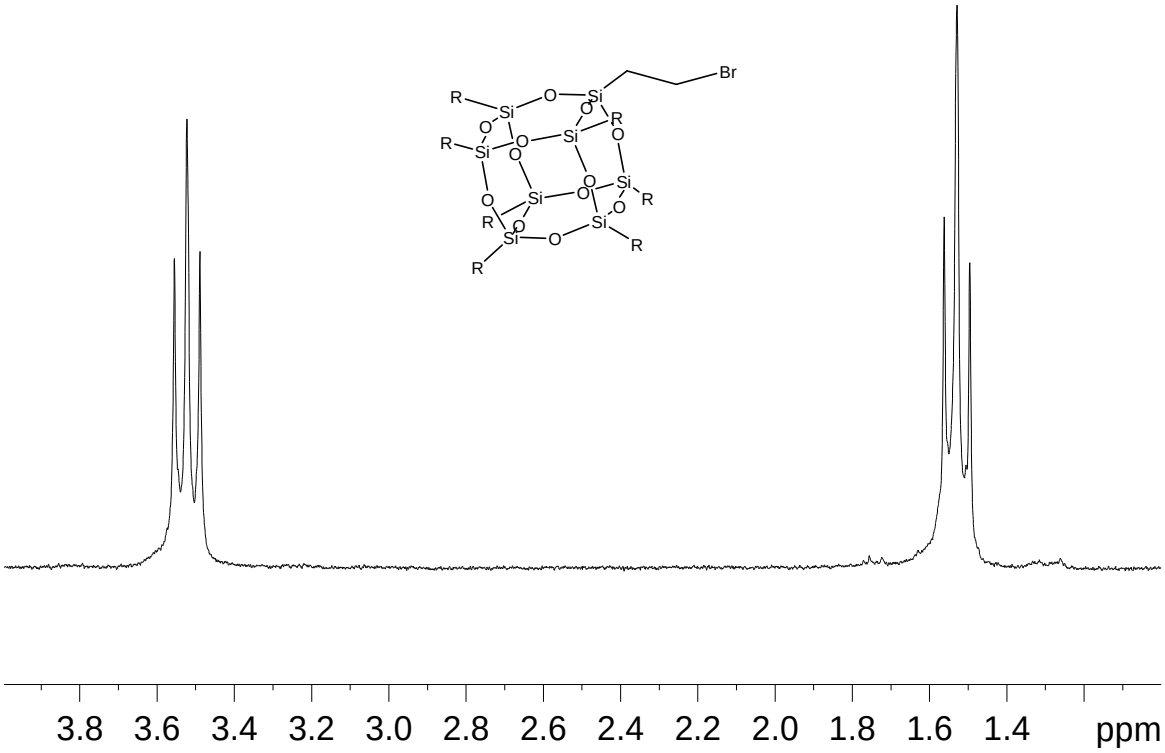

Figure 28. ^{1}H NMR spectrum of **8** in $CDCl_3$

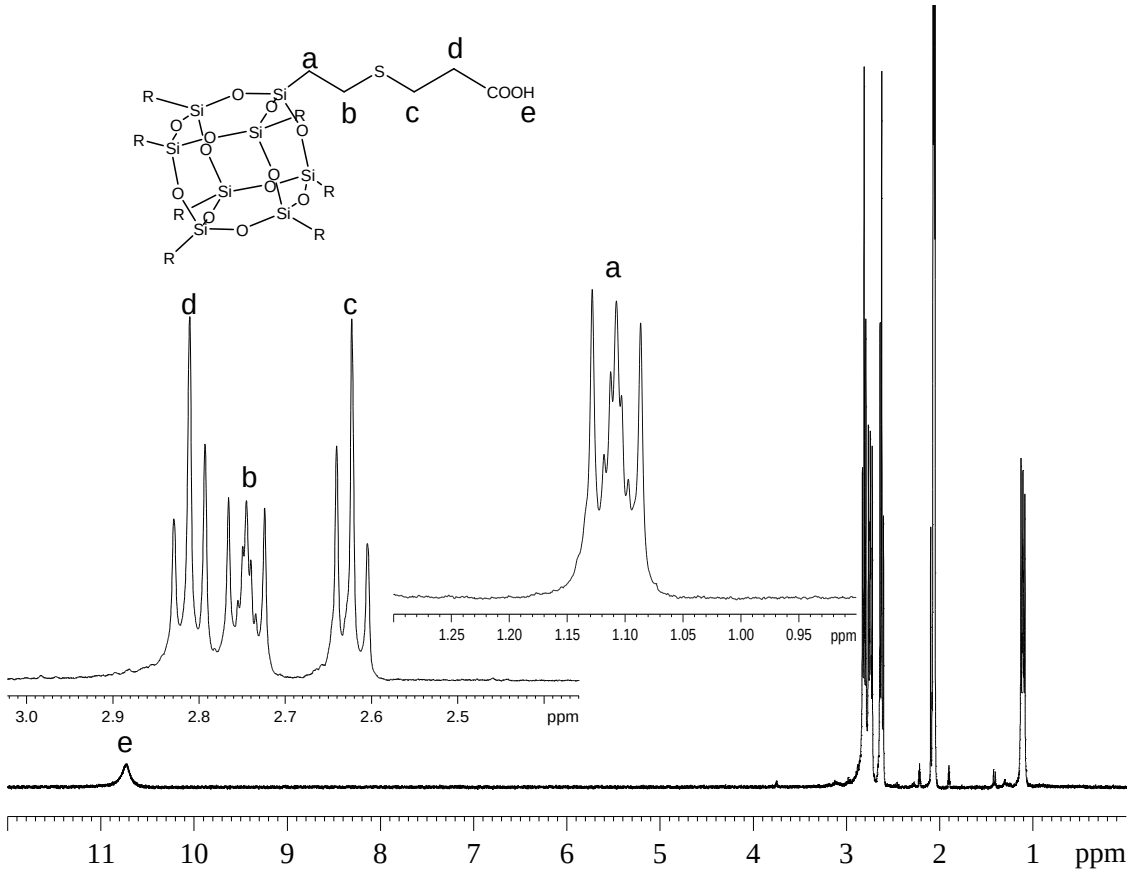

Figure 29. ^{1}H NMR spectrum of **6** in acetone-d_6

The elongation by another ethylene unit in **6** and **7** causes a hindered rotation around the C-C bond of the ethylene moiety directly connected to the silicon atom of the cage while the more distant ethylene unit embedded between the sulphur and carboxyl and acyl groups, still freely rotates (Figure 29).

Further connecting the more bulky SCS pincer ligand and the SCS palladium complex to the chain in **12** and **14**, respectively, induces a hindered rotation around the C-C bonds in both ethylene units (Figure 30). In the ^{1}H NMR spectrum of **10** three broad peaks were detected for the propylene protons at room temperature. Increasing the temperature of the sample up to 100 ℃ gradually leads to a reduced line broadening without a complete resolution of the multiplet structure (Figure 31). Besides the hindered rotation of the functional groups a reduction of the transverse relexation (T_2) is also responsible for the line broadening. This is the case because the octaferrocenyl silsesquioxane (**10**) becomes so large that the slow tumbling of the molecule leads to a small correlation time. This is supported by the fact that it was not possible to detect a ^{13}C NMR spectrum of compound **10** due to the large T_1 and small T_2 relaxation times a typical behaviour for molecules with large molecular weight.

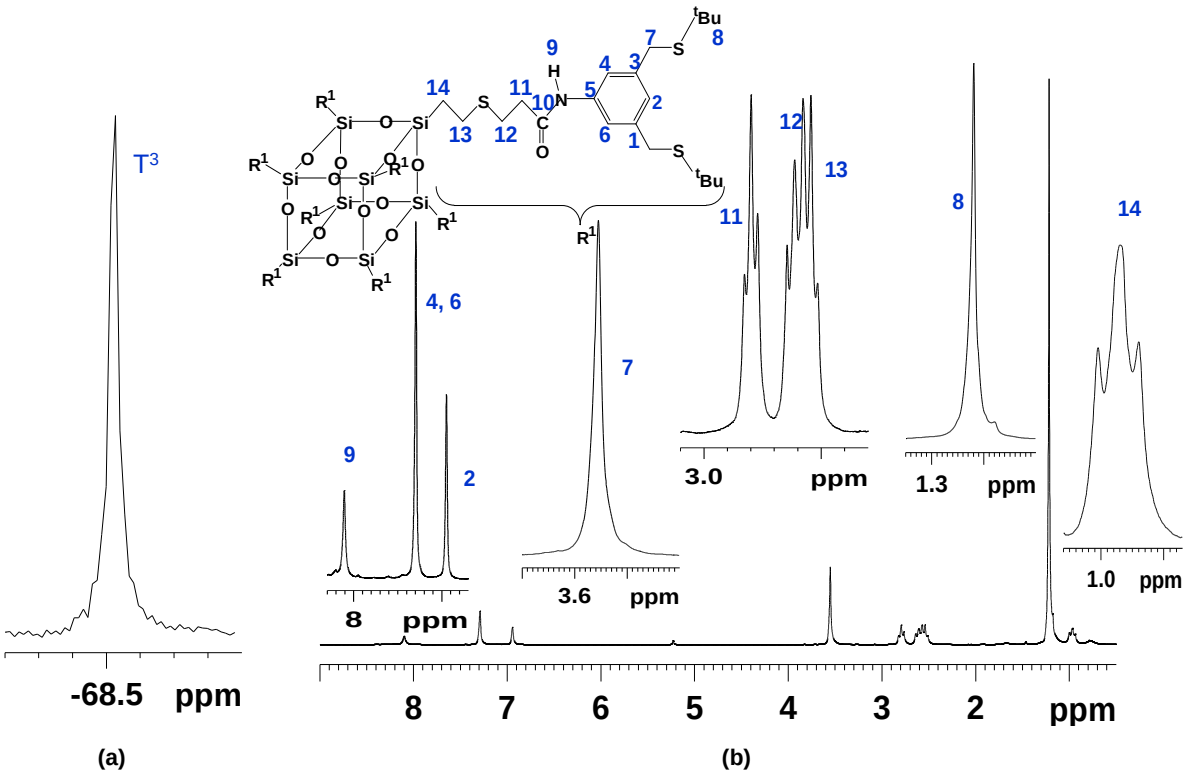

Figure 30. (a) ^{29}Si and (b) ^{1}H NMR spectra of **12** in CD_2Cl_2.

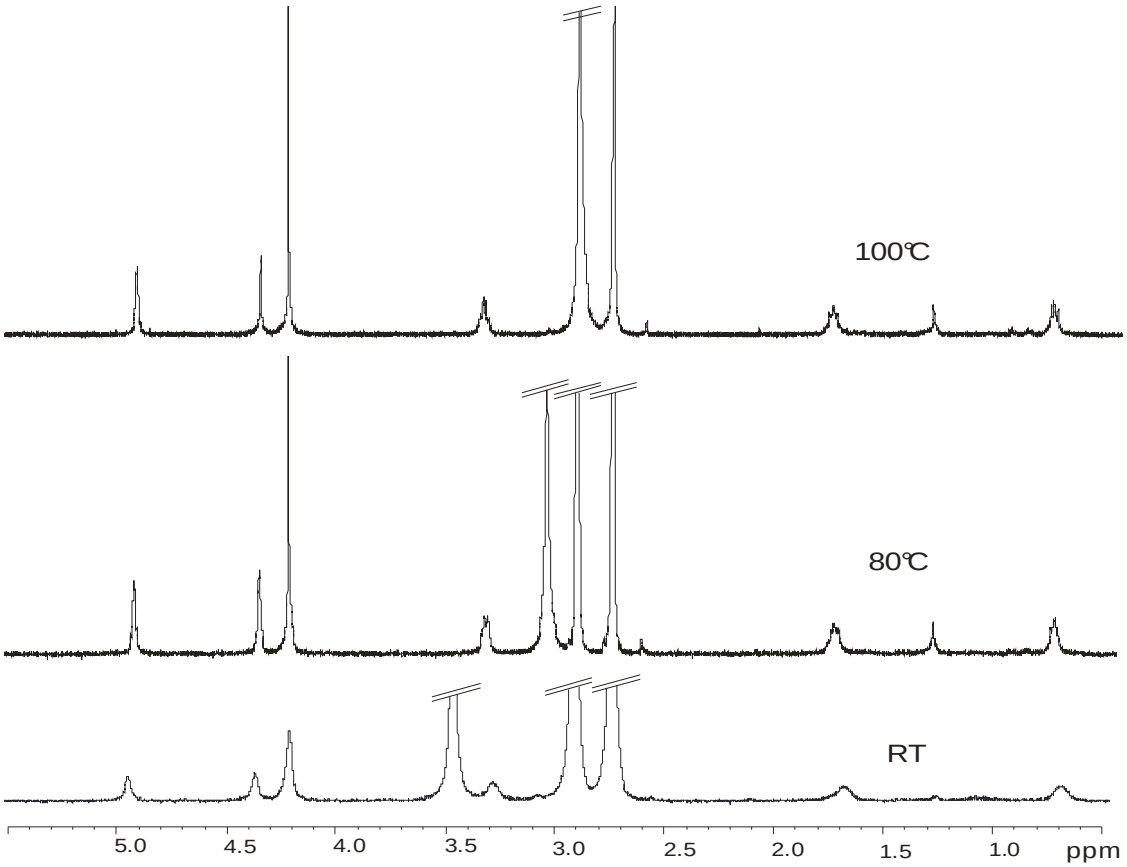

Figure 31. ^{1}H NMR spectra for **10** in DMF-d_7 at different temperatures

The ^{1}H and ^{13}C{^{1}H} NMR spectroscopy of compound **14** revealed that the incorporated SCS palladacycles acquire different types of spatial arrangements which led to a more complicated analysis. The spacer always presented one set of resonances with the correct integration for the eight substituted spacer chains in the ^{1}H NMR spectrum (Figure 32). Apparently, three different arrangements of the palladacycles in a ratio 5 : 4 : 1 were indicated in the ^{1}H and ^{13}C{^{1}H} NMR spectra in solution. The first arrangement (in ratio 5) of the SCS palladacycles was characterised by one set of resonances with broadening of the protons of the methylene groups at the pincer ligand. The second group (in ratio 4) was defined exclusively by broadened signals in all protons from the SCS pincer complex, and the third one (in ratio 1) allowed the observation of one set of resonances with well defined singlets at the pincer complex (Figure 32). The introduction of the metallacycles effect a hindered rotation at the spacers of the system indicated by the increased line broadening of the CH_2 multiplets compared to those on **12**. This is provided by the bulkiness of the metal complex. The spatial nature of these three conformers is due to the syn and anti orientations of the *tert*-butyl groups in the

complex which bulkiness results for hinderness towards rotation. $^{13}C\{^{1}H\}$ solution NMR spectroscopy always revealed three sets of resonances at the pincer fragment and only one set of resonances for the spacer.[141]

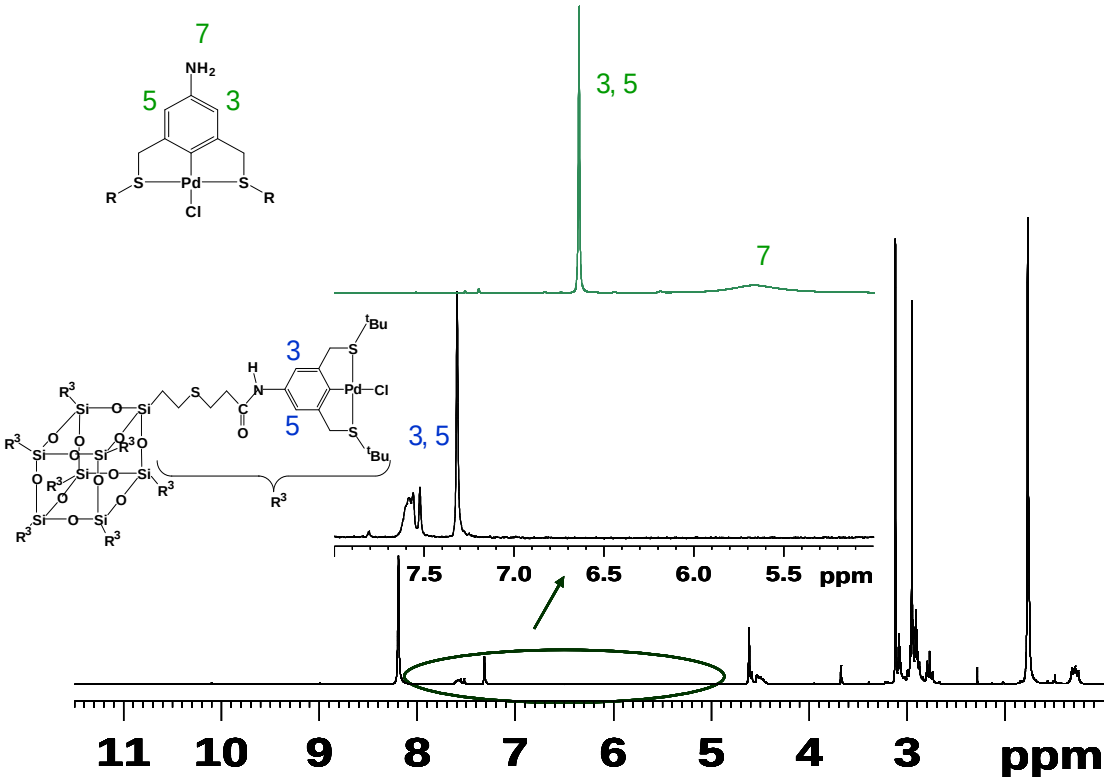

Figure 32. ^{1}H NMR spectra in DMF-d6 of **13** and **14**

In general the molecular symmetry of octahydrosilsesquioxanes in the crystalline phase is reduced from O_h to T_h.[144] This is due to small distortions of the cube which is explained as the result of packing processes. Thus it is not surprising that the successive substitution of the hydride by sterically more demanding groups like in **6** - **9**, **12**, and **14** the distortion of the cube increases. Moreover as with the larger substituents the rotation around the C-C bond is hindered a number of symmetrically independent molecules are generated. This leads to an increase of resonances in the ^{29}Si solid state NMR spectra in the typical region for T^3 groups (Figures 33, 35). For the same reason, the number of resonances for a single carbon side increased in the ^{13}C CP/MAS NMR spectra of **6** - **10** (Figure 34, 35 and 36).

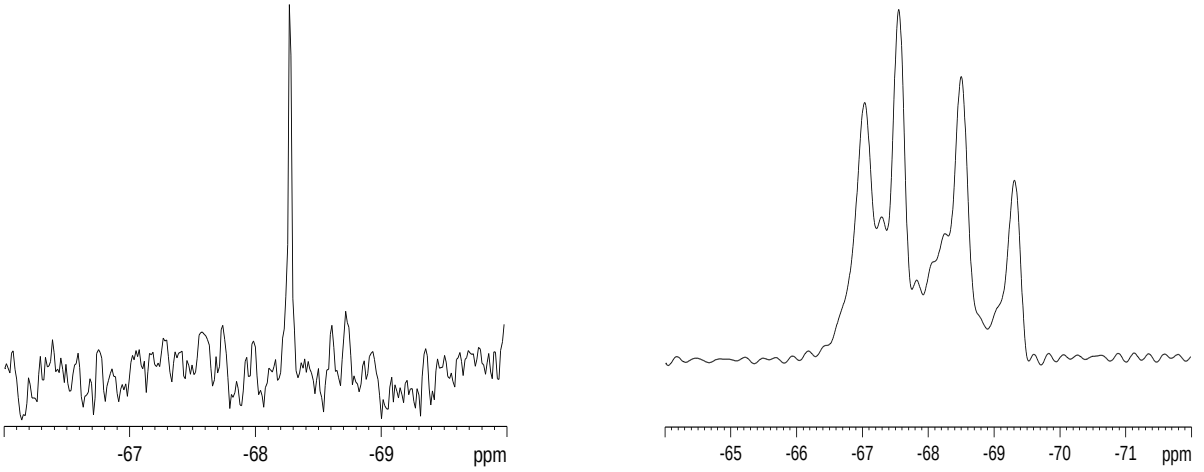

Figure 33. $^{29}Si\{^{1}H\}$ NMR spectrum in acetone-d_6 and ^{29}Si CP/MAS NMR of **6**

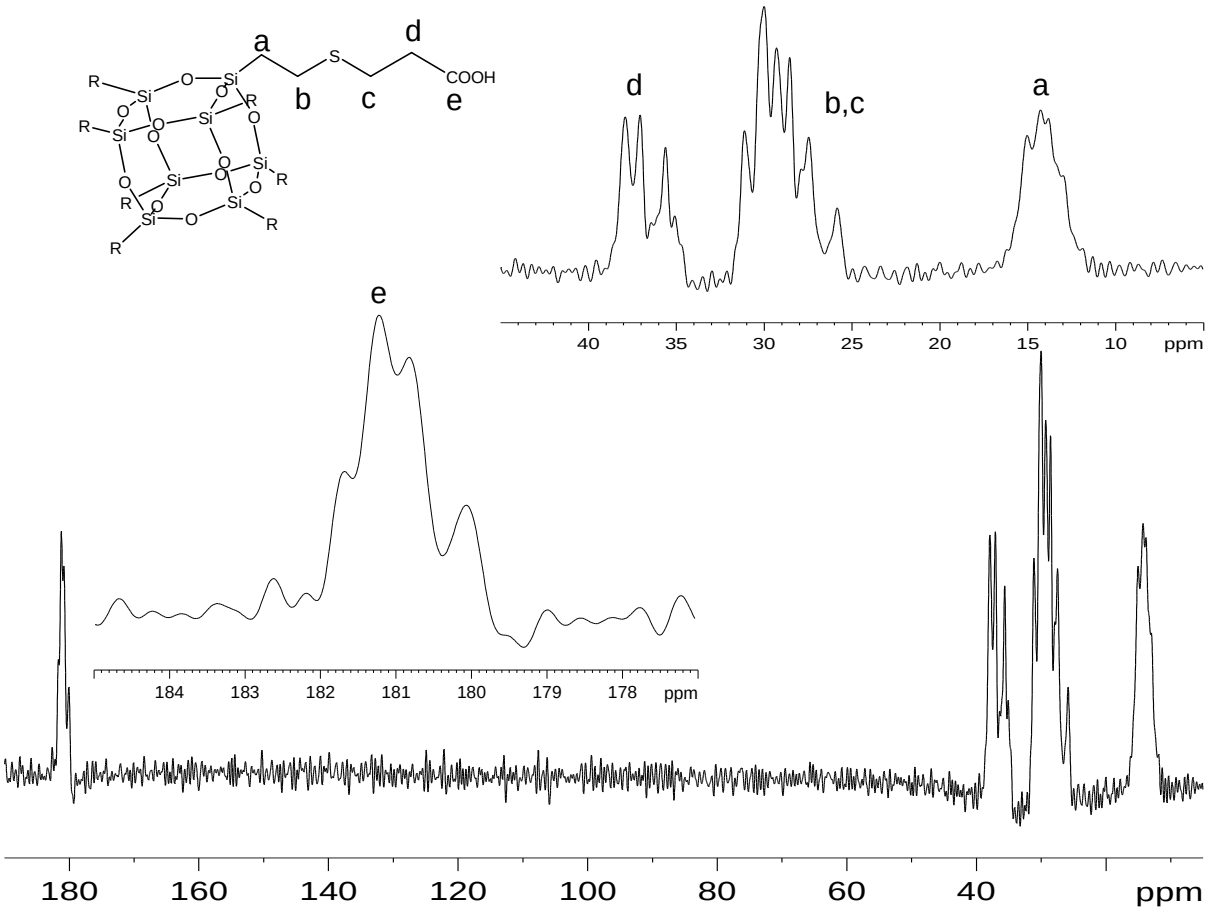

Figure 34. ^{13}C CP/MAS NMR spectrum of **6**

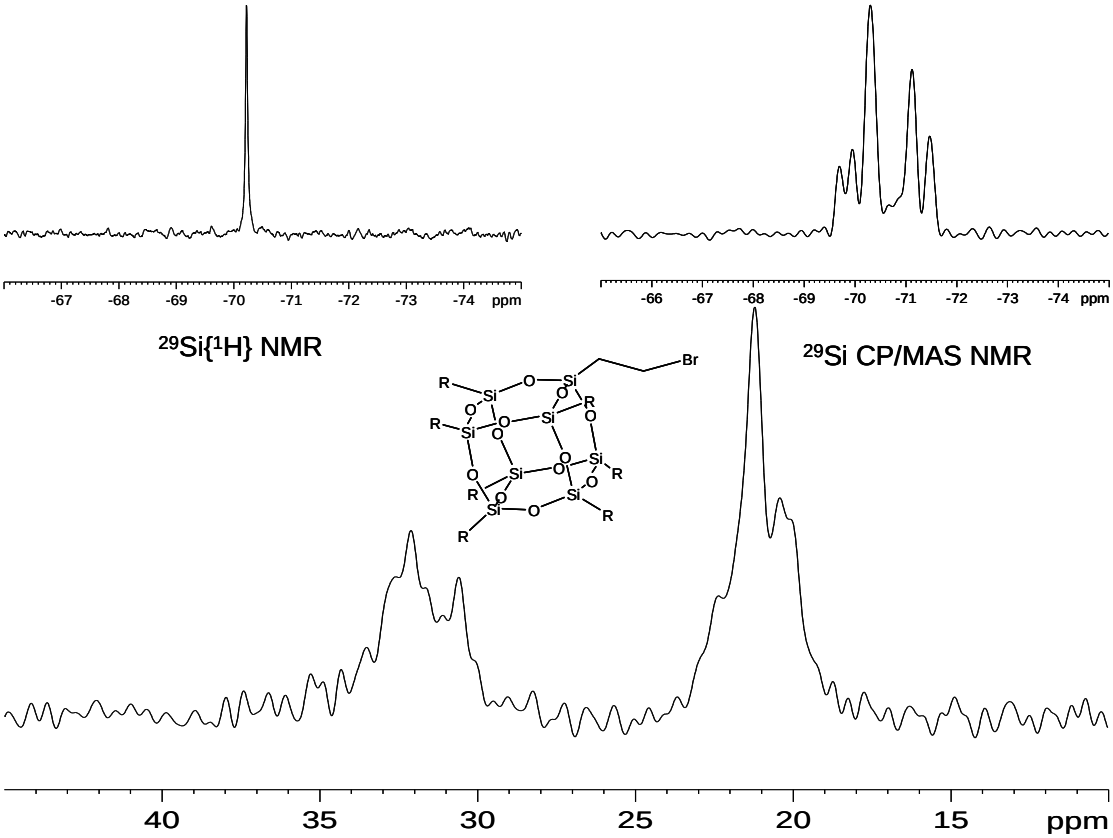

Figure 35. ^{13}C CP/MAS and ^{29}Si CP/MAS NMR spectra and $^{29}Si\{^{1}H\}$ NMR spectra of **8** in $CDCl_3$

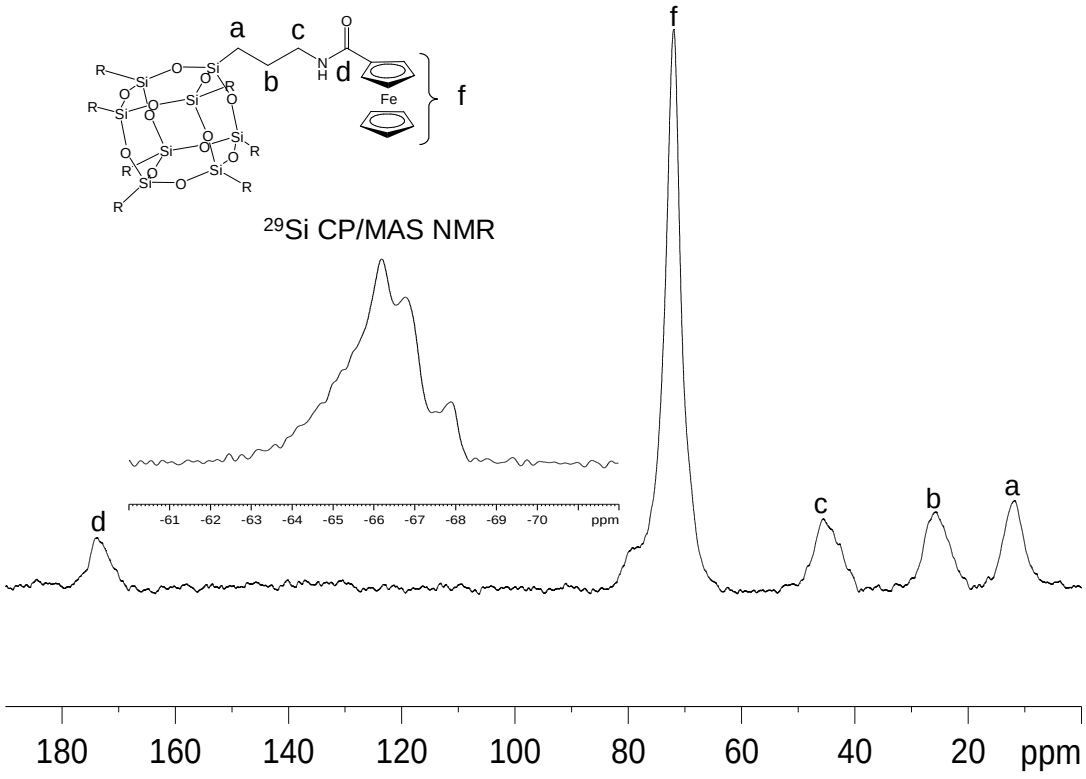

Figure 36. ^{13}C CP/MAS and ^{29}Si CP/MAS NMR spectra of **10**.

5.2.9 Conclusions

POSS with organic functional groups like vinyl and amino groups were first synthesised. These organic groups can easily be modified to the desired function. It must be taken into account that the modifications in silsesquioxanes should not be performed in extremely basic conditions to avoid the destruction of the cage. For the synthesis of **6** two different pathways were developed; A Michael's type addition through an organic catalyst and a radical reaction. As **6** was not reactive enough, it was transformed into the most reactive **7**. Unluckily the complete characterisation of this new material was unsuccessful because of its extraordinary reactivity even with traces of water. Using **7** as precursor, two new FPOSS were synthesised with the attachment of aniline SCS pincer ligands and aniline SCS palladacycle.

The procedure of synthesis of the FPOSS **8** was improved through irradiation with UV light of the octavinylsilsesquioxanes and self-produced HBr. Moreover from **8**, the synthesis of **9** was carried out applying the Finkelstein reaction, resulting FPOSS with a better leaving group. Finally, the new FPOSS **10** was synthesised using as precursors the octaaminosilsesquioxane **5** and ferrocene acyl chloride. The composition and mass of these molecules were characterised by MS, EA. IR spectra of **6** – **10**, **12**, **14** the T_8 cages give rise to asymmetric stretching frequencies of the Si-O-Si units, additionally the carbonyl stretching bands are as well obtained which are a strong indication that the ferrocenyl, the SCS pincer ligand and the palladium complex have been efficiently connected to the FPOSS. All the $^{29}Si\{^1H\}$ NMR spectrum shows a unique peak that together with the number of multiplets in the ^1H NMR spectra are a strong indication of the cage T_8 fully condensed symmetric silsesquioxane. A hindered internal rotation around the C-C bond in ethylene units can be observed in the ^1H NMR spectra with the appearance of multiplets instead of the expected triplets when the size of the functional groups increases. The performance of ^{29}Si solid state NMR spectra gives more peaks than the awaited. This can be explained due to the different conformation that the arms of the FPOSS can achieve in the solid state.

6. EXPERIMENTAL SECTION

6.1 GENERAL ASPECTS AND STARTING MATERIALS

All manipulations were performed under an atmosphere of dry argon employing usual Schlenk techniques. The solvents were dried according to common methods, distilled, and stored under argon.

5,5'-Dimethylbipyridine, 1-pyrenemethanol , 3-(triethoxysilyl)-propylisocyanate, 3-Aminopropyl-triethoxysilane and Amberlite IRA-400 (CI were purchased from Aldrich. Tetramethoxysilane (TMOS), tetraethoxysilane (TEOS), Amberlite IR-120, vinyltrichlorosilane, α,α'-Azo-isobutyronitrile (AIBN), ferrocenecarboxylic acid and ammonia solution ca. 25% were bought from Fluka. 3-chloropropanol, 3,4-dihydro-2H-pyrane, n-butyllithium, TMEDA, triethylamine, diisopropylamine, 2,2'-bipyridine, mercaptopropionic acid, oxalylchloride, propylamine, bromine, 1,2,3,4-tetrahydronaphtalene and sodium iodide were obtained from Merck). Ruthenium(III) chloride hydrate and silverhexafluoroantimonate were purchased from Chempur. The trifunctionalised modified ruthenium trisbipyridine (**1**)[1,7] and octavinylsilsesquioxane[89] were synthesised according to reported procedures.

IR data were obtained on a Bruker Vertex 70 and Bruker Tensor 27 spectrometers. The melting point measurements were performed with a Büchi Melting Point B-540.

Elemental Analyses were performed by the Institut für Anorganische Chemie Universität Tübingen using a Vario EL analyzer. Mass Spectra were recorded on a Bruker Esquire 3000+ mass analyzer equipped with an electron spray ionization (ESI) source. High resolution mass spectroscopy analyses (HR ESI-MS) were applied on a Bruker Daltonics APEX II fourier transform-ion cyclotron resonance (FT-ICR) mass spectrometer. FAB analyses were carried out with the mass spectrometer Thermo Finnigan TSQ70. For the FAB measurements, 3-nitrobenzyl alcohol (NBA) was used as matrix.

The size of the nanoparticles was measured by light scattering COULTER N4 PLUS and scanning electron microscope ZEISS DSC 962.

6.2 STEADY-STATE MEASUREMENTS

All measurements of the sol-gel materials were obtained by suspending 4 mg of the powder in 3 ml of the respective solvent and vigorously stirring the samples with a magnetic stirrer to avoid sedimentation. 12 mg of the nanoparticles were suspended. The measurements were performed under air and as well bubbling nitrogen into the respective liquids. The temperature during the experiments was kept constant at T = 293 K.

Steady-state measurements, excitation and emission spectra, were obtained on a SPEX Fluorolog 222 fluorometer equipped with a xenon source type SUX 1450.

6.3 DECAY TIME MEASUREMENTS

All measurements on the sol-gel materials for the trifunctionalised ruthenium complex were obtained by suspending 4 mg of the powder in 3 ml of the respective liquid and vigorously stirring the samples with a magnetic stirrer to avoid sedimentation. The temperature during the experiment was kept constant at T = 293 K. For quenching experiments, anthracene in concentration of $c \approx \cdot 10^{-4}$ M was dissolved in the liquid phase. Air saturated liquid contain about $c \approx 2 \cdot 10^{-3}$ M of dioxygen were applied for the oxygen quenching experiments.

Luminiscence decay curves were acquired by the single-photon counting method. A picosecond diode laser (PICI QUANT GmbH, Berlin, Model LDH 400) was used for excitation (wavelength 392 nm) and a photomultiplier tube (Hamamatsu) for detection. The signal from the photomultiplier tube was fed into a multichanel analyser via a picosecond amplifier/discriminator and a time to amplitude converter (EG&G ORTEC). The time resolution of this setup is limited to $\Delta t = 0.5$ ns.

For the trifunctionalised pyrenemethanol, 4 mg of the powder in 3 ml of the respective liquid and vigorously stirring the samples with a magnetic stirrer to avoid sedimentation. In the case of the nanoparticles, 12 mg were used. . The temperature during the experiment was kept constant at T = 293 K. For quenching experiments, diethylaniline in concentration of $c \approx 1 \cdot 10^{-3}$ M was dissolved in the liquid phase. Air saturated liquid contain about $c \approx 2 \cdot 10^{-3}$ M of dioxygen were applied for the oxygen quenching experiments.

Luminiscence decay curves were acquired by the single-photon counting method. An IBH Model 5000 F nanosecond flashlamp was used for excitation (wavelength 337 nm) and a photomultiplier tube (Hamamatsu) for detection. The signal from the photomultiplier tube was fed into a multi channel analyser via a picosecond amplifier/discriminator and a time to amplitude converter (EG&G ORTEC). The time resolution of this setup is limited to $\Delta t = 0.5$ ns.

6.4 BRUNAUER-EMMETT-TELLER (BET) MEASUREMENTS

All measurements were obtained after drying about 200 mg of each sample for 12 h at 50℃ under vacuo. The surface area, pore volumes and pore size distributions of the materials will be measured using a Micromeritics ASAP 2010 and the BET method. For the pore size distribution in the mesopore range (2nm – 50nm), nitrogen adsorption has been used. The total pore volume can then be determined from the volume adsorbed at a relative pressure of $\rho/\rho_o = 0.99$. This method allows also an estimate of the micropore volume (< 2nm) by *t*-plot analysis of the nitrogen adsorption isotherm. It is possible as well to obtain the ISOTHERM plots. The pore size distribution in the mesopore range was calculated by Barret-Joyner-Halenda (BJH) method.

As a standard, siliciumoxide-aluminiumoxide was used, which specifications were given from the company: BET surface 216 ± 6 m^2/g, pore volumen 0.61 ± 0.08 m^3/g and the porous size is 11.5 ± 1.5 nm.

6.5 NUCLEAR MAGNETIC RESONANCE (NMR) SPECTROSCOPY

Solution nuclear magnetic resonance spectra (NMR) were recorded on Bruker DRX 250, Bruker Avance II 400 and Bruker Avance II 500 spectrometers at 298 K. Frequencies and standards were as follows: ^{1}H NMR 250.13 and 400.13 MHz; $^{13}C\{^{1}H\}$ NMR 62.90 and 100.62 MHz. $^{29}Si\{^{1}H\}$ NMR 49.66 and 99.36 MHz. Chemical shifts are reported in δ values in ppm relative to external tetramethylsilane (TMS) using the chemical shift of the solvent ^{2}H resonance frequency. All assignments were supported by ^{13}C DEPT135 experiments. For the $^{29}Si\{^{1}H\}$ experiments the DEPT45 puls sequence was applied.

Solid state NMR spectra were recorded on a Bruker ASX 300 multinuclear spectrometer equipped with a wide-bore magnet. Proton high-power decoupling (HPDEC) was applied. Magic angle spinning was performed at 4.5 KHz (^{29}Si) and 10 KHz (^{13}C), respectively. Frequency and standard: ^{29}Si 59.63 MHz, ^{13}C 75.47 MHz. Chemical shifts were reported in δ values in ppm relative to external TMS, using Q_8M_8 (low field peak at 12.05 ppm) and Glycin (176.03 ppm) as secondary reference.

6.6 SYNTHESES

6.6.1 Preparation of triethoxysilylfunctionalised (1-pyrenyl)-methanol (2)

A mixture of 0.939 g of (1-pyrenyl)-methanol (4 mmol) and 1 ml of 3-(triethoxysilyl)-propylisocyanate (4 mmol) was heated to 135℃ for 3 h. Yield: quantitative, m.p. 116 ℃. NMR (400MHz, $CDCl_3$): δ=0.63 (m, 2H, CH_2-Si-O), 1.18 (m, 9H, *CH_3*-CH_2-O-Si), 1.64 (m, 2H, *CH_2*-CH_2-Si), 3.20-3.25 (m, 2H, *CH_2*-CH_2-CH_2-Si), 3.75-3.81 (m, 6H, CH_3-*CH_2*-O-Si), 5.82 (s, 2H, py-CH_2-O), 8.00-8.40 (m, 10H pyrenyl and NH). $^{13}C\{^1H\}$ NMR (400MHz, $CDCl_3$): δ=7.83 (s, CH_2-Si-O), 18.41 (s, *CH_3*-CH_2-O-Si), 23.63 (s, *CH_2*-CH_2-Si), 43.86 (s, *CH_2*-CH_2-CH_2-Si), 58.67 (s, CH_3-*CH_2*-O-Si), 65.06 (s, py-CH_2-O), 123.5-131.8 (m, pyrenyl), 156.65 (s, C=O). IR (KBr, cm^{-1}): ν(NH) 3291, ν(C=O) 1684, δ(NH) 1540[28]. MS (FAB), *m/z*: 479.1 [M^+].

6.6.2 Preparation of the sol-gel materials

5 ml of tetramethoxysilane (TMOS) were dissolved in 20 ml of ethanol. To this solution was added 1.5 ml of a stock solution consisting of 5 ml of acetone and 2.18 10^{-2} mmol of **1** as well a stock solution consisting of 10 ml of THF and 4.37 10^{-2} mmol of **2**. 20 ml of a buffer made of acetic acid and sodium acetate (pH = 4.88) was added to the reaction mixture which was stirred for three days at 30℃ and 852 rpm. The resulting gel was divided into four parts and each one was dried in a different way: in vacuo (**A**), in a water atmosphere at 40℃ (**B**), under reduced pressure (**C**) and in air (**D**).

6.6.3 Preparation of the nanoparticles

A mixture of 15.4 ml of a solution of water and ammonia (25 %), 129.6 ml of distilled water and 330 ml of ethanol was stirred and allowed to achieve a thermal equilibrium at 45° C for 30 min. After this time, 2 2.3 ml of tetraethoxysilane (TEOS) were rapidly added and the reaction mixture was stirred for 3 h. After separation by centrifugation the nanoparticles were washed with water and ethanol and dried in air. To eliminate the porosity, the particles were heated *in vacuo* to 600° C for 16 h. After cooling to room temperature the particles were heated to reflux for 2 h in a 2 M HCl solution. Finally the nanoparticles were washed with water and ethanol and dried. The diameter and the surface area of the particles were determined to 175.0 ± 19 nm and 25 m^2/g, respectively, while no pores were detected by BET.

A suspension of the fluorophore **2** and nanoparticles in dry toluene were heated to reflux for 16 h. Separation of the nanoparticles by centrifugation and washing with toluene and hexane gave clean material. Assuming five Si-OH groups in one square nanometer of the surface,[113] the number of Si-OH groups was calculated for 344 mg of 25 m^2/g surface area. The stoichiometry was adjusted to cover 1%, e.g. 344 mg of nanoparticles and 0.326 mg (6.8 10^{-4} mmol) of **2**. These nanoparticles were dried under vacuo at 50℃ and ne w suspensions of **1** (0.933 mg and 6.8 10^{-4} mmol) with the nanoparticles in different solvents (MeOH, acetone, DMSO) were performed. The coverage of the nanoparticles with **1** remained unsuccessful due to solubility problems of **1**, and low boiling points and competition with the silanol groups of the solvents.

6.6.4 Synthesis of octa(3-(ethylmercapto)-propionic acid) silsesquioxane (6)

For the synthesis of octa(3-(ethylmercapto)-propionic acid) silsesquioxane two different pathways were developed, the first method applies an organic catalyst whereas the second one uses a radical initiator.

First method: 0.094 g (0.149 mmol) of freshly synthesised octavinylsilsesquioxane and 0.129 ml (1.490 mmol) of mercaptopropionic acid were dissolved in 2 ml of dry

toluene. 10 µl of propylamine was added as a catalyst. This solution was stirred for 16 h at 30℃. The solvent was removed at 80℃ in va cuo. Yield: 0.209 g (95%).

Second method: 0.094 g (0.149 mmol) of freshly synthesised octavinylsilsesquioxane and 0.129 ml (1.490 mmol) of mercaptopropionic acid were dissolved in 2 ml of dry toluene. 2 mg of AIBN was added as a radical initiator. This solution was stirred for 16 h at 80℃. The volatile components were removed in vacuo at 80℃. Yield: 0.209 g (95%), m.p.: 142℃.

^{1}H NMR (250MHz, Aceton-d_6): δ=1.10 (m, 16H, Si-*C*H_2-CH_2), 2.62, (m, 16H, S-C*H*$_2$-CH_2), 2.74 (m, 16H, Si-CH_2-C*H*$_2$), 2.81 (m, 16 H, S-CH_2-C*H*$_2$), 10.73 (s, 8H, COOH). ^{13}C{^{1}H} NMR (62.90MHz, Aceton-d_6): δ=13.32 (s, Si-*C*H_2-CH_2), 26.15, 27.00 (s, CH_2-S-CH_2), 34.74 (s, S-CH_2-*C*H_2), 173.14 (s, C*OOH*). ^{13}C CP/MAS NMR (50.32MHz): δ=13.0, 13.8, 14.3, 15.0 (s, Si-*C*H_2-CH_2), 25.9, 27.5, 28.6, 29.3, 30.0, 31.1 (s, CH_2-S-CH_2), 35.1, 35.6, 36.4, 37.1, 37.9 (s, S-CH_2-*C*H_2), 180.1, 180.8, 181.2, 181.6 (s, C*OOH*). ^{29}Si{^{1}H} NMR (49.66MHz, DEPT45, Aceton-d_6): δ=-68.28 (s). ^{29}Si CP/MAS NMR (59.63MHz): δ= -67.0, -67.3, -67.6, -67.8, -68.5, -69.3 (s). IR (KBr, cm^{-1}): ν(C-H) 2915, ν(C=O) 1709, ν_{AS}(Si-O-Si) 1126,. δ(Si-O-Si) 466. Anal. calcd. for ($C_{40}H_{72}S_8Si_8O_{28}$): C, 32.41; H, 4.90; S, 17.31. Found: C, 32.10; H, 4.67; S, 16.65. HR ESI-MS (Negative-Mode), *m/z*: 738.9977 [M-2H]$^{2-}$, calcd for $C_{40}H_{74}S_8Si_8O_{28}$: 738.9992.

6.6.5 Synthesis of octa(3-(ethylmercapto)-propionacyl chloro) silsesquioxane (7)

The carboxylic acid functions in octa(3-(ethylmercapto)-propionic acid) silsesquioxanes can be converted to the more reactive acyl chloride. 366 mg (0.247 mmol) of **6** was suspended in 6 ml of dichloromethane. An excess of oxalylchloride (1.672 ml, 0.020 mol) was added under stirring. The reaction was continued for 16 h at room temperature. The dichloromethane was removed and the bright yellow solid was washed several times with hexane. Yield: 0.382 g (95%).

^{1}H NMR (400MHz, $CDCl_3$): δ=1.03 (m, 16 H, Si-C*H*$_2$), 2.65 (m, 16 H, Si-CH_2-C*H*$_2$), 2.83 (m, 16 H, S-C*H*$_2$-CH_2), 3.17 (m, 16 H, S-CH_2-C*H*$_2$). ^{13}C NMR (100.62MHz, $CDCl_3$): δ=12.69 (s, Si-*C*H_2-CH_2), 26.32, 26.60 (s, CH_2-S-CH_2), 47.32 (s, S-CH_2-

CH_2), 172.53 (s, COCl). ^{29}Si{^{1}H} NMR (49.66MHz, $CDCl_3$): δ=-68.78. IR (KBr, cm^{-1}): ν(C-H) 2915, ν(C=O) 1820, ν_{AS}(Si-O-Si) 1120, δ(Si-O-Si) 471.

6.6.6 Synthesis of octa(ethylbromo) silsesquioxane (8)

250 mg (0.395 mmol) of octavinylsilsesquioxane **3** was suspended in 100 ml of dry hexane in a quartz flask. For 2 h freshly prepared HBr, which was achieved from the reaction between bromine and 1,2,3,4-tetrahydronaphtalene, was bubbled into the suspension and irradiated with UV light. The solvent was removed to give the solid bright brown octa(ethylbromo) silsesquioxane (**8**) in quantitative yield, m.p.: 235℃.

^{1}H NMR (250MHz, $CDCl_3$): δ=1.53 (m, 16H, Si-C*H*$_2$-CH_2-Br), 3.52 (m, 16H, Si-CH_2-C*H*$_2$-Br). ^{13}C{^{1}H} NMR (62.90MHz, $CDCl_3$): δ=18.32 (s, Si-*C*H_2-CH_2-Br), 27.40 (s, Si- CH_2-*C*H_2-Br). ^{13}C CP/MAS NMR (50.32MHz): δ= 20.1, 20.5, 21.2, 22.4 (s, Si-*C*H_2-CH_2-Br), 30.6, 31.1, 31.7, 32.2, 32.6 (s, Si- CH_2-*C*H_2-Br). ^{29}Si{^{1}H} NMR (49.66MHz, $CDCl_3$): δ=-70.22 (s). ^{29}Si CP/MAS NMR (59.63MHz): δ= -69.7, -69.9, -70.3, -70.7, -70.9, -71.1, -71.5 (s). IR (KBr, cm^{-1}): ν(C-H) 2922, ν_{AS}(Si-O-Si) 1116, δ(Si-O-Si) 470. Anal. calcd. for ($C_{16}H_{32}Br_8Si_8O_{12}$): C, 15.01; H, 2.50; Br, 49.94. Found: C, 14.74; H, 2.48; Br, 48.68. HR ESI-MS (Positive-Mode), *m/z*: 1318.3072 $[M+K]^+$, calcd for $C_{16}H_{32}Br_8Si_8O_{12}K$: 1318.3073.

6.6.7 Synthesis of octa(ethyliodo) silsesquioxane (9)

100 mg (0.078 mmol) of **8** was dissolved in acetone and refluxed with an excess of sodium iodide for 48 hours. After the solvent had been evaporated the dark yellow residue was washed with cold acetone. The yellow powder which was produced gave 58 mg (0.035 mmol). Yield: 45%, m.p.:188℃.

^{1}H NMR (250MHz, Acetone-d_6): δ=1.53 (m, 16H, Si-C*H*$_2$-CH_2-I), 3.21 (m, 16H, Si-CH_2-C*H*$_2$-I). ^{13}C{^{1}H} NMR (62.90MHz, Acetone-d_6): δ=-2.72 (s, Si-CH_2-*C*H_2-I), 19.34 (s, Si-*C*H_2-CH_2-I). ^{29}Si{^{1}H} NMR (49.66MHz, Acetone-d_6): δ=-70.41 (s). IR (KBr, cm^{-1}): ν(C-H) 2921, ν_{AS}(Si-O-Si) 1109, δ(Si-O-Si) 466. Anal. calcd. for ($C_{16}H_{32}I_8Si_8O_{12}$): C, 11.60; H, 1.95. Found: C, 12.66; H, 1.94.

6.6.8 Synthesis of ferrocenyl functionalised silsesquioxane (10)

The ion exchanger Amberlite IRA-400 was activated by means of washing successively with water, a solution of NaOH (1 M) and methanol. A part of this ion exchanger was deposited inside a column whereas the rest of it was used to be suspended in ice cold methanol where 0.6 g of **4** was dissolved. This suspension was stirred for 15 minutes and after that it was poured into the column. The column was washed several times with cold methanol and the collected methanol fractions were combined. This solution contained the deprotected octapropylamine silsesquioxane **5**. This material must be stored in methanol and at -30℃ to avoid decomposition. A part of this solution was taken to remove the solvent obtaining 100 mg (0.113 mmol) of octa(propylamine) silsesquioxane which was dissolved in 50ml of dry THF. 0.320 ml of diisopropylethylamine was added to this solution and after that 280 mg (1.13 mmol) of ferrocene acyl chloride. The reaction mixture was stirred for two days and the solvent was removed. The solid part was washed several times with chloroform to eliminate the excess of ferrocene acyl chloride and with methanol to eliminate the non-reacted octapropylamine silsesquioxanes. Yield: 126 mg and 43%. m.p. (dec.) 247°C.

^{1}H NMR (400MHz, DMF-d_7): δ =0.89 (m, 16H, Si-C*H*$_2$), 1.87 (m, 16H, Si-CH$_2$-C*H*$_2$-CH$_2$), 3.46 (m, 16H, Si-CH$_2$-CH$_2$-C*H*$_2$), 4.37 (s, 40H, C_5H_5), 4.53 and 5.10 (m, 32H,). ^{13}C CP/MAS NMR (50.32MHz): δ =11.8 (s, Si-CH$_2$), 25.8 (s, Si-CH$_2$-*C*H$_2$-CH$_2$), 45.6 (s, Si-CH$_2$-CH$_2$-*C*H$_2$), 65.8-82.4 (br, C_5H_4, C_5H_5), 173.9 (s, C=O). ^{29}Si CP/MAS NMR (59.62MHz): δ =-66.2, -66.8, -67.9. IR (KBr, cm^{-1}): ν(C-H) 2926, ν(C=O) 1635, δ(NH) 1543, ν_{AS}(Si-O-Si) 1116, δ(Si-O-Si) 486. Anal. calcd. for ($C_{112}H_{128}Fe_8N_8Si_8O_{20}$): C, 52.19; H, 5.01, N, 4.35. Found: C, 51.31; H, 4.75, N, 3.96. HR ESI-MS (Positive-Mode), *m/z*: 1300.6080 [M+H+Na]$^{+2}$, calcd for $C_{112}H_{129}Fe_8N_8Si_8O_{20}Na$: 1300.6097.

6.6.9 Synthesis of SCS-pincer complex functionalised silsesquioxanes (12, 14)

To a solution of **7** (1 g, 0.60 mmol) in 5 mL THF was added drop wise a solution of **11** (1.78 g, 6 mmol) in 15 mL THF. The reaction mixture was stirred for 4 h under ambient conditions. After reaction completion, the solvent was removed by distillation. Further purification by flash chromatography was performed using ethyl

acetate and hexane as mobile phase in a ratio of 70/30. The solvent was removed to yield 0.74 g of **12** (33 %, 0.10 mmol). DRIFT (KBr, cm^{-1}): ν_{st} (NH) 3309, ν_{st} (CO) 1665, ν_{st} (SiO) 1121. HR ESI-MS (Positive-Mode): *m/z* 3715.460 $[M+2H]^{2+}$, calcd for $C_{168}H_{274}N_8O_{20}Si_8S_{24}$: 3715.210. Elemental analysis obsd (theor): C, 54.50 (54.26); N, 2.96 (3.01); H, 8.65 (7.37); S, 21.52 (20.69). ^{1}H NMR (δ, 400.13 MHz, CD_2Cl_2): 0.97 (m, 8H, $SiCH_2CH_2$); 1.22 (s, 144H, $C(CH_3)_3$); 2.54 (m, 8H, $SiCH_2CH_2$); 2.61 (m, 8H, SCH_2CH_2), 2.80 (m, 8H, CH_2CO); 3.55 (s, 32H, $ArCH_2$), 6.94 (s, 8H, ArH); 7.30 (s, 16H, ArH), 8.18 (br, 8H, NH). $^{13}C\{^{1}H\}$ NMR (δ, 100.58 MHz, CD_2Cl_2): 13.17 (s, $SiCH_2$); 26.61 (s, $SiCH_2CH_2$); 27.69 (s, SCH_2CH_2); 31.09 (s, $C(CH_3)_3$); 33.50 (s, $ArCH_2$), 37.71(s, CH_2CO); 43.14 (s, $C(CH_3)_3$); 119.25 (s, $C^{4, 6}$); 125.73 (s, C^{2}); 138.70 (s, C^{5}); 140.11 (s, $C^{1, 3}$); 170.27 (s, CO); ^{29}Si NMR (δ, 49.62 MHz, CD_2Cl_2)= -68.52 (s, T^{3}).

A suspension of **13** (20 mg, 0.01 mmol) in 5 mL DMF was stirred in an ultra sonic bath for 10 min under inert conditions. Compound **7** (50 mg, 0.11 mmol) was dissolved in 5 mL DMF and further drop wise addition to the suspension was performed within 2 h under room temperature conditions. The reaction was allowed to stir for 12 h and when concluded the reaction time the solvent was removed under reduced pressure distillation to yield 72 mg of **14** (100 %, 0.01 mmol). IR (KBr, cm^{-1}): ν_{st} (CO) 1727, ν_{st} (SiO) 1115. Three different type of compounds are observed in a ratio of 5: 4: 1 by ^{1}H and ^{13}C NMR spectroscopy. ^{1}H NMR (δ, 400.13 MHz, DMF-d6): 1.12 (m, 8H, $SiCH_2$); 1.60 (s, 144H, $C(CH_3)_3$); 2.61 (m, 8H, $SiCH_2CH_2$); 2.75 (m, 8H, SCH_2CH_2); 2.92 (m, 8H, CH_2CO); for **A**: 4.39 (br, 16H, $ArCH_2$); 7.30 (s, 8H, ArH); 10.63 (br, 4H, NH); for **B**: 4.37 – 4.26 (br m, 12H, $ArCH_2$); 7.59 (br m, 6H, ArH); 9.88 – 10.31 (br m, 3H, NH); for **C**: 4.42 (s, 4H, $ArCH_2$); 7.52 (s, 2H, ArH); 10.63 (br, 1H, NH).^{13}C NMR (δ, 100.58 MHz, DMF-d6): 12.80 (s, $SiCH_2$); 25.54 (s, $SiCH_2CH_2$); 26.58 (s, $SiCH_2CH_2$); 29.88, 29.93, 30.37 (s, $C(CH_3)_3$); 42.45, 42.65, 42.56 (s, $ArCH_2$); 51.88, 51.47, 52.07 (s, $C(CH_3)_3$); 113.86, 112.73, 112.81 (s, $C^{3, 5}$); 134.74, 136.30, 135.18 (s, C^{4}); 150.92, 150.08, 151.10 (s, $C^{2, 6}$); 153.97, 153.67, 153.40 (s, C^{1}); 173 (s, CO). ^{29}Si (δ, 49.62 MHz, DMF-d6): -67.97 (s, T^{3}).

7. REFERENCES

Reference List

(1) Arakawa, H.; Aresta, M.; Armor, J.; Barteau, M.; Beckman, E.; Bell, A.; Bercaw, J.; Creutz, C.; Dixon, D. A.; Dixon, D.; Domen, K.; DuBois, D.; Eckert, J.; Fujita, E.; Gibson, D.; Goddard, W.; Goodman, D.; Keller, J.; Kubas, G.; Kung, H.; Lyons, J.; Manzer, L.; Marks, T.; Morokuma, K.; Nicholas, K.; Periana, R.; Que, L.; Rostrup-Nielson, J.; Sachtler, W.; Schmidt, L.; Sen, A.; Somorjai, G.; Stair, P.; Stults, B.; Tumas, W. *Chem. Rev.* **2001**, *101*, 953-996.

(2) Lu, Z.; Lindner, E.; Mayer, H. A. *Chem. Rev.* **2002**, *102*, 3543-3578.

(3) Burkett, S. L.; Soukasene, S.; Milton, K. L.; Welch, R.; Little, A. J.; Kasi, R. M.; Coughlin, E. B. *Chem. Mater.* **2005**, *17*, 2716-2723.

(4) *Applied Honogeneous Catalysis with Organometallic Compounds - A Comprehensive Handbook in Two Volumes*; Wiley-VCH: Weinheim, **1996**.

(5) *Applied Honogeneous Catalysis with Organometallic Compounds - A Comprehensive Handbook in Two Volumes*; Wiley-VCH: Weinheim, **1996**.

(6) Lindner, E.; Schneller, T.; Auer, F.; Mayer, H. A. *Angew. Chem. Int. Ed.* **1999**, *38*, 2155-2174.

(7) Lindner, E.; Baumann, A.; Wegner, P.; Mayer, H. A.; Reinohl, U.; Weber, A.; Ertel, T. S.; Bertagnolli, H. *J. Mater. Chem.* **2000**, *10*, 1655-1662.

(8) Lindner, E.; Salesch, T.; Brugger, S.; Steinbrecher, S.; Plies, E.; Seiler, M.; Bertagnolli, H.; Mayer, H. A. *Eur. J. Inorg. Chem.* **2002**, 1998-2006.

(9) Lindner, E.; Kemmler, M.; Schneller, T.; Mayer, H. A. *Inorg. Chem.* **1995**, *34*, 5489-5495.

(10) Holder, E. Polysiloxanes with luminescence molecular probes: Synthesis, characterization and application of ordered and non-ordered structures. *Thesis* Univ. Tübingen. **2001**.

(11) Holder, E.; Oelkrug, D.; Egelhaaf, H. J.; Mayer, H. A.; Lindner, E. *J. Fluoresc.* **2002**, *12*, 383-395.

(12) Egelhaaf, H. J.; Holder, E.; Herman, P.; Mayer, H. A.; Oelkrug, D.; Lindner, E. *J. Mater. Chem.* **2001**, *11*, 2445-2452.

(13) Schubert, U.; Huesing, N.; Lorenz, A. *Chem. Mater.* **1995**, *7*, 2010-2027.

(14) Khamova, T. V.; Shilova, O. A.; Movchan, T. G.; Saznikov, V. A.; Rusanov, A. I. *Glass physics and chemistry* **2008**, *34*, 63-67.

(15) Bekiari, V.; Lianos, P.; Stangar, U. L.; Orel, B.; Judeinstein, P. *Chem. Mater.* **2000**, *12*, 3095-3099.

(16) Keeling-Tucker, T.; Brennan, J. D. *Chem. Mater.* **2001**, *13*, 3331-3350.

(17) Brusatin, G.; Della Giustina, G.; Romanato, F.; Guglielmi, M. *Nanotech.* **2008**, *19*, 1-7.

(18) Franville, A. C.; Zambon, D.; Mahiou, R.; Troin, Y. *Chem. Mater.* **2000**, *12*, 428-435.

(19) Avnir, D. *Acc. Chem. Res.* **1995**, *28*, 328-334.

(20) Holder, E.; Trapp, G.; Grimm, J. C.; Schurig, V.; Lindner, E. *Tetrahedron: Asymmetry,* **2002**, *13*, 2673-2678.

(21) Sprintschnik, G.; Sprintschnik, H. W.; Kirsch, P. P.; Whitten, D. G. *J. Am. Chem. Soc.* **1977**, *99*, 4947-4954.

(22) Murtagh, M. T.; Shahriari, M. R.; Krihak, M. *Chem. Mater.* **1998**, *10*, 3862-3869.

(23) Maruszewski, K.; Jasiorski, M.; Salamon, M.; Strek, W. *Chem. Phys. Lett.* **1999**, *314*, 83-90.

(24) Innocenzi, P.; Kozuka, H.; Yoko, T. *J. Phys. Chem. B,* **1997**, *101*, 2285-2291.

(25) Ogawa, M.; Nakamura, T.; Mori, J.; Kuroda, K. *J. Phys. Chem. B,* **2000**, *104*, 8554-8556.

(26) Font, J.; De March, P.; Busqué, F.; Casa, E.; Benitez, M.; Teruel, L.; García, H. *J. Mater. Chem.* **2007**, *17*, 2336-2343.

(27) Hui Wei; Yan Du; Jian-Zhen Kang; Guo, B.; Er-Kang Wang *Chinese J. Chem.* **2007**, *25*, 159-163.

(28) Basu, A.; Gafney, H. D.; Perettie, D. J.; Clark, J. B. *J. Phys. Chem.* **1983**, *87*, 4532-4538.

(29) Matsui, K.; Sasaki, K.; Takahashi, N. *Langmuir* **1991**, *7*, 2866-2868.

(30) Kakegawa, N.; Ogawa, M. *Langmuir* **2004**, *20*, 7004-7009.

(31) Huang, X.; Kovaleski, J. M.; Wirth, M. J. *Anal. Chem.* **1996**, *68*, 4119-4123.

(32) Soboleva, I. V.; van Stam, J.; Dutt, G. B.; Kuzmin, M. G.; De Schryver, F. C. *Langmuir* **1999**, *15*, 6201-6207.

(33) Yao, G.; Wang, L.; Wu, Y.; Smith, J.; Xu, J.; Zhao, W.; Lee, E.; Tan, W. *Anal. Bioanal. Chem.* **2006**, *385*, 518-524.

(34) Glomm, W. R.; Volden, S.; Sjoblom, J.; Lindgren, M. *Chem. Mater.* **2005**, *17*, 5512-5520.

(35) Wang, B.; Liu, Y.; Li, B.; Yue, S.; Li, W. *J. Luminescence,* **2008**, *128*, 341-347.

(36) Klein, C.; Nazeeruddin, M. K.; DiCenso, D.; Liska, P.; Gratzel, M. *Inorg. Chem.* **2004**, *43*, 4216-4226.

(37) Chan, M. A.; Lawless, J. L.; Lam, S. K.; Lo, D. *Anal. Chim. Acta,* **2000**, *408*, 33-37.

(38) Lei, Q.; Xiurong, Y. *Adv. Funct. Mater.* **2007**, *19*, 1353-1358.

(39) Samuel, J.; Ottolenghi, M.; Avnir, D. *J. Phys. Chem.* **1992**, *96*, 6398-6405.

(40) McEvoy, A. K.; McDonagh, C.; MacCraith, B. D. *J. Sol-Gel Sci. Technol.* **1997**, *8*, 1121-1125.

(41) Ilharco, L. M.; Santos, A. M.; Silva, M. J.; Martinho, J. M. G. *J. Sol-Gel Sci. Technol.* **1997**, *8*, 877-882.

(42) Samuel, J.; Polevaya, Y.; Ottolenghi, M.; Avnir, D. *Chem. Mater.* **1994**, *6*, 1457-1461.

(43) Deng, Q.; Hu, Y.; Moore, R. B.; McCormick, C. L.; Mauritz, K. A. *Chem. Mater.* **1997**, *9*, 36-44.

(44) Chu, D. Y.; Thomas, J. K. *J. Phys. Chem.* **1989**, *93*, 6250-6257.

(45) Bonzagni, N. J.; Baker, G. A.; Pandey, S.; Niemeyer, E. D.; Bright, F. V. *J. Sol-Gel Sci. Technol.* **2000**, *17*, 83-90.

(46) Liu, J.; Fang, Y.; Chen, C. L. *Langmuir,* **2008**, *24*, 1853-1857.

(47) Yamanaka, T.; Takahashi, Y.; Kitamura, T.; Uchida, K. *Chem. Phys. Lett.* **1990**, *172*, 29-32.

(48) Kaufman, V. R.; Avnir, D. *Langmuir,* **1986**, *2*, 717-722.

(49) Monte, F. d.; Ferrer, M. L.; Levy, D. *J. Mater. Chem.* **2001**, *11*, 1745-1751.

(50) Binnemans, K.; Lenaerts, P.; Driesen, K.; Gorller-Walrand, C. *J. Mater. Chem.* **2003**, *14*, 191-195.

(51) Meneses-Nava, M. A.; Barbosa-Garcia, O.; az-Torres, L. A.; Chavez-Cerda, S.; King, T. A. *Opt. Mater.* **1999**, *13*, 327-332.

(52) Avnir, D.; Levy, D.; Reisfeld, R. *J. Phys. Chem.* **1984**, *88*, 5956-5959.

(53) Levy, D.; Reisfeld, R.; Avnir, D. *Chem. Phys. Lett.* **1984**, *109*, 593-597.

(54) Hungerford, G.; Suhling, K.; Ferreira, J. A. *J. Photochem. Photobiol. A-Chem.* **1999**, *129*, 71-80.

(55) Lin, W. B.; Jaffrezic-Renault, N.; Chovelon, J. M.; Lacroix, M. *Sensors and Actuators B: Chemical* **2001**, *74*, 207-211.

(56) Feher, F. J.; Wyndhanm, K. D.; Soulivong, D.; Nguyen, F. *Dalton Trans.* **1999**, 1491-1497.

(57) Scott, D. W. *J. Am. Chem. Soc.* **1946**, *68*, 356-358.

(58) Feher, F. J.; Wyndhanm, K. D.; Scialdone, M. A.; Hamuro, Y. *Chem. Commun.* **1998**, 1469-1470.

(59) Annand, J.; Aspinall, H. C. *Dalton Trans.* **2000**, 1867-1871.

(60) Asuncion, M. Z.; Laine, R. M. *Macromolecules* **2007**, *40*, 555-562.

(61) Clark, J. C.; Saengkerdsub, S.; Eldridge, G. T.; Campana, C.; Barnes, C. E. *J. Organomet. Chem.* **2006**, *691*, 3213-3222.

(62) Feher, F. J.; Terroba, R.; Ziller, J. W. *Chem. Commun.* **1999**, 2309-2310.

(63) Paolo P.Pescarmona; Jan C.der Waal; Thomas Maschmeyer *Eur. J. Inorg. Chem.* **2004**, *2004*, 978-983.

(64) Pescarmona, P. P.; Maschmeyer, T.; Van Der Waal, J. C. *Chem. Eng. Commun.* **2004**, *191*, 68-74.

(65) Rob W. J. M. Hanssen; Rutger A. Van Santen; Hendrikus C. L. Abbenhuis *Eur. J. Inorg. Chem.* **2004**, *2004*, 675-683.

(66) Carniato, F.; Boccaleri, E.; Marchese, L. *Dalton Trans.* **2008**, 36-39.

(67) Duchateau, R. *Chem. Rev.* **2002**, *102*, 3525-3542.

(68) Olliges, I. Kovalente Anbindung eines SCS-Pincerliganden an Si-H-funktionallisierte Sol-Gel Materialen. *Diplomaarbeit*, Univ. Tübingen. **2007**.

(69) Schubert, U.; Hüsing, N. *Synthesis of inorganic materials*; Wiley-VCH. **2000**.

(70) Wright, J. D.; Sommerdijl, N. A. J. M. *Sol-Gel Materials*; Gordon and Breach Science. **2001**.

(71) Dunn, B.; Zink, J. I. *Chem. Mater.* **1997**, *9*, 2280-2291.

(72) Janotta, M.; Katzir, A.; Mizaikoff, B. *Appl. Spectrosc.* **2003**, *57*, 823-828.

(73) Iler, R. K. *The chemistry of silica*; Wiley-Interscience Publication. **1979**.

(74) Stoeber, W.; Fink, A.; Bohn, E. *J. Colloid Interface Sci.* **1968**, *26*, 62-69.

(75) Szekeres, M.; Toth, J.; Dekany, I. *Langmuir* **2002**, *18*, 2678-2685.

(76) Rossi, L. M.; Shi, L.; Quina, F. H.; Rosenzweig, Z. *Langmuir* **2005**, *21*, 4277-4280.

(77) Beganskiene, A.; Sirutkaitis, V.; Kurtinaitiene, M.; Juskénas, R.; Kareiva, A. *Mater. Sci.* **2004**, *10*, 287-290.

(78) Costa, C. A. R.; Leite, C. A. P.; Galembeck, F. *J. Phys. Chem. B* **2003**, *107*, 4747-4755.

(79) Nozawa, K.; Gailhanou, H.; Raison, L.; Panizza, P.; Ushiki, H.; Sellier, E.; Delville, J. P.; Delville, M. H. *Langmuir* **2005**, *21*, 1516-1523.

(80) Bogush, G. H.; Zukoski, C. F. *J. Colloid Interface Sci.* **1991**, *142*, 1-18.

(81) Bogush, G. H.; Zukoski, C. F. *J. Colloid Interface Sci.* **1991**, *142*, 19-34.

(82) Matsoukas, T.; Gulari, E. *J. Colloid Interface Sci.* **1988**, *124*, 252-261.

(83) Matsoukas, T.; Gulari, E. *J. Colloid Interface Sci.* **1989**, *132*, 13-21.

(84) Matsoukas, T.; Gulari, E. *J. Colloid Interface Sci.* **1991**, *145*, 557-562.

(85) Pozdniakova, Y. A.; Lyssenko, K. A.; Korlyukov, A. A.; Blagodatskikh, I. V.; Auner, N.; Katsoulis, D.; Shchegolikhina, O. I. *Eur. J. Inorg. Chem.* **2004**, 1253-1261.

(86) Baney, R. H.; Itoh, M.; Sakakibara, A.; Suzuki, T. *Chem. Rev.* **1995**, *95*, 1409-1430.

(87) Loy, D. A.; Shea, K. J. *Chem. Rev.* **1995**, *95*, 1431-1442.

(88) Shea, K. J.; Loy, D. A.; Webster, O. W. *Chem. Mater.* **1989**, *1*, 572-574.

(89) Dare, E. O.; Liu, L.-K.; Peng, J. *Dalton Trans.* **2006**, 3668-3671.

(90) Bornhauser, P.; Calzaferri, G. *Spectrochimica Acta Part A: Molecular Spectroscopy* **1990**, *46*, 1045-1056.

(91) Brown, J. F. *J. Am. Chem. Soc.* **1965**, *87*, 4317-4324.

(92) Hoebbel, I. P. *Z. anorg. allg. Chem.* **1990**, *583*, 133-144.

(93) Vogt, L. H.; Brown, J. F. *Inorg. Chem.* **1963**, *2*, 189-192.

(94) Mori, H.; Lanzendorfer, M. G.; Muller, A. H. E.; Klee, J. E. *Macromolecules* **2004**, *37*, 5228-5238.

(95) Frye, C. L.; Collins, W. T. *J. Am. Chem. Soc.* **1970**, *92*, 5586-5588.

(96) Voronkov, M. G.; Lavrent'yev, V. I. *Top. curr. chem.* **1982**, *102*, 199-236.

(97) Harrison, P. G. *J. Organomet. Chem.* **1997**, *542*, 141-183.

(98) Feher, F. J.; Newman, D. A.; Walzer, J. F. *J. Am. Chem. Soc.* **1989**, *111*, 1741-1748.

(99) Sprung, M. M.; Guenther, F. O. *J. Am. Chem. Soc.* **1955**, *77*, 3990-3996.

(100) Feher, F. J.; Budzichowski, T. A.; Blanski, R. L.; Weller, K. J.; Ziller, J. W. *Organometallics* **1991**, *10*, 2526-2528.

(101) Paolo P.Pescarmona; Jan C.van der Waal; Ian E.Maxwell; Thomas Maschmeyer. *Angew. Chem. Int. Ed.* **2001**, *40*, 740-743.

(102) Sprung, M. M.; Guenther, F. O. *J. Am. Chem. Soc.* **1955**, *77*, 3996-4002.

(103) Lakowicz, J. R. *Principles of fluorescence spectroscopy.* **1999**.

(104) Sharma, A.; Schulman, S. G. *Introduction to fluorescence spectroscopy.* **1999**.

(105) Valeur, B. *Molecular fluorescence. Principles and applications.* **2001**.

(106) Habib Jiwan, J.-L.; Robert, E.; Soumillion, J.-P. *J. Photochem. Photobiol. A-Chem.* **1999**, *122*, 61-68.

(107) Rampazzo, E.; Bonacchi, S.; Montalti, M.; Prodi, L.; Zaccheroni, N. *J. Am. Chem. Soc.* **2007**, *129*, 14251-14256.

(108) Marzini, M. Automatisierung und Optimierung des Sol-Gel Prozesses. *Thesis* Univ. Tübingen. **2006**.

(109) Lin, H. P.; Mou, C. Y. *Acc. Chem. Res.* **2002**, *35*, 927-935.

(110) Brunauer, S.; Emmett, P. H.; Teller, E. *J. Am. Chem. Soc.* **1938**, *60*, 309-319.

(111) Barrett, E. P.; Joyner, L. G.; Halenda, P. P. The determination of pore volume and area distributions in porous substances. I, *Computations from nitrogen isotherms*. 373-380. **1951**.

(112) Gregg, S. J.; Sing, K. S. W. *Adsorption, surface area and porosity*; Academic Press. **1982**.

(113) Zhuravlev, L. T. *Colloids Surface A* **2000**, *173*, 1-38.

(114) Green, D. L.; Lin, J. S.; Lam, Y. F.; Hu, M. Z.; Schaefer, D. W.; Harris, M. T. *J. Colloid Interface Sci.* **2003**, *266*, 346-358.

(115) Elings, J. A.; Ait-Meddour, R.; Clark, J. H.; Macquarrie, D. J. *Chem. Commun.* **1996**, 2707-2708.

(116) Kim, H. B.; Kitamura, N.; Tazuke, S. *J. Phys. Chem.* **1990**, *94*, 7401-7405.

(117) Castellano, F. N.; Heimer, T. A.; Tandhasetti, M. T.; Meyer, G. J. *Chem. Mater.* **1994**, *6*, 1041-1048.

(118) Matsui, K.; Sasaki, K.; Takahashi, N. *Langmuir,* **1991**, *7*, 2866-2868.

(119) Dominska, M.; Krysinski, P.; Blanchard, G. J. *J. Phys. Chem. B* **2005**, *109*, 15822-15827.

(120) Hartmann, P.; Leiner, M. J. P.; Lippitsch, M. E. *J. Fluorescence* **1994**, *4*, 327-330.

(121) Murtagh, M. T.; Kwon, H. C.; Shahriari, M. R.; Krihak, M.; Ackley, D. E. *J. Mater. Res.* **1998**, *13*, 3326-3331.

(122) Draxler, S.; Lippitsch, M. E.; Klimant, I.; Kraus, H.; Wolfbeis, O. S. *J. Phys. Chem.* **1995**, *99*, 3162-3167.

(123) Garcia-Fresnadillo, D.; Marazuela, M. D.; Moreno-Bondi, M. C.; Orellana, G. *Langmuir* **1999**, *15*, 6451-6459.

(124) Timpsom, C. J.; Carter, C. C.; Olmsted, J. *J. Phys. Chem.* **1989**, *93*, 4116-4120.

(125) Shoup, D.; Lipari, G.; Szabo, A. *Biophys. J.* **1981**, *36*, 697-714.

(126) Samson, R.; Deutch, J. M. *J. Chem. Phys.* **1978**, *68*, 285-290.

(127) Solc, K.; Stockmayer, W. H. *Int. J. Chem. Kinet.* **1973**, *5*, 733-752.

(128) Schmitz, K. S.; Schurr, J. M. *J. Phys. Chem.* **1972**, *76*, 534-545.

(129) Johnson, D. A.; Yguerabide, J. *Biophys. J.* **1985**, *48*, 949-955.

(130) Somogyi, B.; Lakos, Z. *J. Photochem. Photobiol. B: Biol.* **1993**, *18*, 3-16.

(131) Sprung, M. M.; Guenther, F. O. *J. Am. Chem. Soc.* **1955**, *77*, 4173-4175.

(132) Weidner, R., Zeller, N., Deubzer, B., and Frey, V. *Patent*, **1991**.

(133) Seshadri, T.; Haupt, H. J. *Anal. Chem.* **1988**, *60*, 47-52.

(134) Leydet, A.; Jeantet-Segonds, C.; Bouchitte, C.; Moullet, C.; Boyer, B.; Roque, J. P.; Witvrouw, M.; Este, J.; Snoeck, R.; Andrei, G.; De Clercq, E. *J. Med. Chem.* **1997**, *40*, 350-356.

(135) Moraes, M. A. R.; Moreira, A. C. F.; Barbosa, R. V.; Soares, B. G. *Macromolecules,* **1996**, *29*, 416-422.

(136) Pan, B.; Clark, T.; Hoyle, C. E.; Lichtenhan, J. D. *Technical Conference Proceedings - UV & EB Technology Expo & Conference, Charlotte, NC, United States, May 2-5,* **2004**, 643-649.

(137) Drylie, E. A.; Andrews, C. D.; Hearshaw, M. A.; Jimenez-Rodriguez, C.; Slawin, A.; Cole-Hamilton, D. J.; Morris, R. E. *Polyhedron* **2006**, *25*, 853-858.

(138) Lücke, S.; Stoppek-Langner, K.; Krebs, B.; Läge, M. *Z. anorg. allg. Chem.* **1997**, *623*, 1243-1246.

(139) Becker, H.; Berger, W.; Domschke, G.; Fanghänel, E.; Faust, J.; Fischer, M.; Gentz, F.; Gewald, K.; Gluch, R.; Mayer, R.; Müller, K.; Pavel, D.; Schmidt, H.; Schollberg, K.; Schwetlick, K.; Seiler, E.; Zeppenfeld, G. *Organikum* **1976**.

(140) Dittmar, U.; Hendan, B. J.; Fl÷rke, U.; Marsmann, H. C. *J. Organomet. Chem.* **1995**, *489*, 185-194.

(141) Toledo Rodríguez, F. Pd(II)- and Rh(III)- XCX pincer complexes and their inmobilisation into silica-gel, nanoparticles and silsesquioxanes. *Thesis.* Univ. Tübingen. **2008**.

(142) Ault, A. *J. Chem. Educ.* **1970**, 812-817.

(143) Günther, H. *Angew. Chem.* **1972**, 907-920.

(144) Agaskar, P. A. *Inorg. Chem.* **1991**, *30*, 2707-2708.

8. SUMMARY

The necessity of reducing costs and the stricter environment laws has provoked an increment in the sources that are dedicated to the investigations of new synthetic pathways which can save energy and reduce the amount of dangerous waste. With more efficient catalysts and with the development of new matrices where the catalysts are attached one can approach to the previous aims. The catalysts in these new matrices (heterogeneous catalysts) must be as accessible as in solution (homogeneous catalysts), in this way the heterogeneous catalysis can reach the efficiency and selectivity of the homogeneous catalysis and they become easily separable from the reaction mixture. For the combination of the advantages of homogeneous and heterogeneous catalysis, several concepts have been established. With the aim to develop high-performance heterogenised catalysts, the idea of chemistry in interphases has recently been introduced. Major drawbacks of conventional supported catalysts can be overcome with this principle. An interphase is defined as a region within a material in which a stationary and mobile component penetrate each other on a molecular level. In an ideal interphase, the reactive center is uniform, well-defined, and highly mobile. Therefore, an interphase is able to simulate homogeneous reaction conditions, and at the same time it has the advantage of a heterogeneous catalyst.

In this work several matrices were synthesised by means of sol-gel process. A buffer system was used in this process to control the kinetics of hydrolysis and condensation and has been the key to the successful synthesis of porous sol-gel materials with high surface area. To accomplish the chemical incorporation of the two fluorophores, the ionic triethoxysilyl functionalised modified $[Ru(bpy)_3]^{2+}$ (**1**) and the non-ionic triethoxysilyl functionalised pyrenemethanol (**2**), into the polysiloxane network both were added to the reaction mixture of the sol-gel process. To this gel four different drying procedures were applied which allowed only slight modification of the surface area and the porosity of the sol-gel materials **A** – **D**. The materials were characterised by solid-state NMR spectroscopy, BET measurements as well as steady-state and time resolved luminescence spectroscopy. The solid-state NMR spectra show that the materials **A** – **D** are dominated by Q groups which confer high degree of condensations. As it was awaited, no presence of T groups was found due to the small amount of triethoxyfunctionalised fluorophores added for the synthesis of

the sol-gel materials. High surface areas and pore sizes ranging between meso- and microporous with ink-bottle pore shapes were confirmed by BET and BJH measurements. Nanoparticles of approximately 200 nm were synthesised following the Stöber method. The BET measurements of the nanoparticles verify that this is a non-porous material with a reduced surface area of 25 m^2/g. These nanoparticles were used to attach the fluorophores on their surface, although due to solubility problems of **1**, just **2** was anchored.

Steady-state and time-resolved luminescence measurements make available a vision of the materials at their molecular level. The steady-state measurements for the ruthenium complex **1** shows a blue shift when the fluorophore is attached in a sol-gel material with respect to the measurements of **1** in solution. This is given because in a fluid solution the excited state of the complex is stabilised relative to the ground state by the surrounding solvent dipoles, and the complex emits light from a relaxed excited state. On the other hand, in a rigid matrix, the solvent is not free to reorient and thus the excited state is not completely stabilised or relaxed within its lifetime. Hence, emission occurs from a higher energy level in a rigid state than in a fluid solution. The steady-state measurements of **2** anchored to nanoparticles and material **A** show solvent-induced shifts. The fluorescence excitation spectra of material **A** and **2NP** are pretty much the same as in solution, indicating that the fluorophores "feel" the full polarizabilities of the solvents. Moreover the I/III-ratio is between 1.72 and 1.9. This indicates that the environment of the fluorophores is always of low symmetry due to interactions of the probes with the surface and in the case of **2NP** it is not only due to the surface but also by interactions among fluorophores. There seems to be a relatively good solvation of the probes by the solvents but also a substantial interaction with the silica material even in the presence of solvent. Additionally the fluorescence measurements confirm the presence of excimers in **2NP**. This fact is surprising taking into account that the quantity of trifunctionalised pyrenemethanol has been adjusted to cover only 1% of the surface of the nanoparticles. Obviously a large amount of pyrene molecules condensed in close proximity to each other on the surface. This must be due to the highly polar surface which could provoke a major stability of **2** when they are close together. Taking into account that the quenching processes between the fluorophores, **1** and **2** and the quenchers, respectively, occurs when they are in close contact with the time-resolved luminescence measurements for **1** and **2** in **A** – **D** and

on the nanoparticles, the accessibility of the fluorophores to different quencher molecules like oxygen, anthracene and N,N-diethylaniline and in solvents of different polarities (MeOH, MeCN, THF and *n*-hexane) was obtained. The accessibilities for the case of **1** depend on the size of the quencher and are as well solvent dependent. The smaller values of k_2 for the ruthenium complexes in the silica materials than in solution indicate that **1** are not solvated by the liquid phase as good as **1** in solution which is in agreement with the steady-state measurements. Two different population of the ruthenium complexes were found, the first type is inaccessible to the quencher dissolved in the liquid phase. The luminescence of the second type is quenched with rate constants that are smaller than those obtained for **1** dissolved in homogeneous solutions.

In the case of **2** their accessibilities depend too on the size of the quencher but are solvent independent. The accessibility is of the same range in the sol-gel materials and in **2NP**. As **2** was attached on the surface of the nanoparticles one can conclude that in the materials **A** – **D** this fluorophore is as well situated on the surface. Three different populations can be distinguished in materials **A** – **D**, the first one is inaccessible to the quencher, the second type has k_2 of the same order than in solution which means that they are equally solvated and the third one has a k_2 smaller than in solution which indicate that is “solvated” by the matrix. In **2NP** just two populations are observed, the first one is not accessible and the second in almost as solvated as in solution.

In the second project of this thesis the synthesis of different functionalised polyhedral silsesquioxanes (FPOSS) was treated. The polyhedral silsesquioxanes are acquiring more importance every year due to their versatility to be anchored with different molecules like catalysts. Four silsesquioxanes were provided with interesting functional groups (carboxylic acid, acyl chloride, bromine and iodide) for the anchor of new molecules. Michael’s type additions, radical reactions, photoreactions and Finkelstein reactions were performed to obtain octa(3-(ethylmercapto)-propionic acid) silsesquioxane (**6**), octa(3-(ethylmercapto)-propionacyl chloro) silsesquioxane (**7**), octa(ethylbromo) silsesquioxane (**8**) and octa(ethyliodo) silsesquioxane (**9**). Moreover three new FPOSS were synthesised with the attachment of aniline SCS pincer ligands, aniline SCS palladacycle and ferrocenyl acyl chloride. The composition and mass of these molecules were characterised by mass spectroscopy and elemental analysis. The IR was used to confirm the attachment of the functional groups through

the bands of the carbonyl stretching frequencies in the case of ferrocenyl functionalised silsesquioxane (**10**) and SCS-pincer complex functionalised silsesquioxanes (**12**, **14**), and as well to confirm that the T_8 cage was not destroyed. $^{29}Si\{^1H\}$ NMR, $^{13}C\{^1H\}$ NMR, ^1H NMR, and ^{29}Si, ^{13}C solid state NMR spectra were performed. The NMR spectra provide information about the high symmetry of the cage where the eight arms are identical and as well provide information about hindered internal rotation around the C-C bond with the biggest substituents.

Meine akademischen Lehrer waren:

K. Albert, H. Bertagnolli, F. Castaños, C. Cesteros, H.-J. Egelhaaf, J. M. Gutierrez Zorilla, I. Katime, L. M. León, E. Lindner, A. Luque, H. A. Mayer, K. Müller, C. Ochsenfeld, J. L. Pizarro, W. Rosenstiel, I. Ruiz Larrea, M. N. Sanchez, V. Schurig, M. J. Sodupe Zurbano, B. Speiser, R. Valenciano, J. Veguillas, L. Wesemann, K.-H. Wiesmüller.

LEBENSLAUF

Name:	David Ruiz Abad
Geboren:	17. November 1976 in Barakaldo
Eltern:	Francisco Ruiz Maldonado
	Antonia Abad Fraga
Staatsangehörigkeit:	Spanisch

Ausbildung

09/2004-10/2008	Bearbeitung der vorliegenden Doktorarbeit unter der Leitung von Prof. Dr. Hermann A. Mayer am Institut für Anorganische Chemie, Eberhard Karls Universität Tübingen, Tübingen.
07/2003-08/2004	Praktikum in organischer Spurenanalytik. IFA-Tulln (Forschungsinstitut für Agrarbiotechnologie Tulln) Österreich.
01/2003-06/2003	Englischkurs in “Camara de Comercio de Bilbao“ (Spanien).
06/2002-12/2002	Englischkurs in England (First Certificate).
07/2001-05/2002	Arbeit als Fahrer in Spanien.
10/1994-06/2001	Chemiestudium an der “Universidad del País Vasco“. Spanien.
1990/1994	Dolores Ibarruri-Gymnasium. Abanto y Zierbana (Spanien).
1982/1990	Otxartaga Grundschule. Ortuella (Spanien).